

**THE ELASTIC-PLASTIC STABILITY OF STANCHIONS
BENT ABOUT TWO AXES**

A Thesis presented for the Degree of Ph. D. (Engineering)
in the University of London

by

H. R. Milner, B.E., M. Eng. Sc.

Imperial College of Science & Technology,
London

December 1965

ABSTRACT

The work reported in this thesis is concerned with research into the behaviour of elastic-plastic elastically restrained H-section columns which are restrained against sway. The thesis is sub-divided into chapters. Chapter 1 is a review of previous allied work. Chapter 2 presents the results of experimental work and Chapter 3 gives a theoretical treatment of the problem and discusses the correlation between experiment and theory. Chapter 4 shows how the theoretical equations of Chapter 3 can be presented to form the basis of a suitable design approach and Chapter 5 summarises the findings of the investigation as a whole.

The experimental work was concentrated on a series of exploratory tests in which significant parameters were varied from one experiment to the next and the theoretical work investigated the influence of unloading, strain hardening, and torsion.

ACKNOWLEDGEMENTS

The Author wishes to thank the following people.

Professor Sparkes, in his capacity as my supervisor.

Dr. Gent, for drawing attention to the problem and actively supervising it.

Fellow students, with whom a variety of topics were discussed.

Various members of Staff of Imperial College, who assisted in the preparation of both the experiments and the thesis.

CONTENTS

	Page
ABSTRACT	1
ACKNOWLEDGEMENTS	2
CONTENTS	3
CHAPTER 1: INTRODUCTION	
1.1 An Outline of the Problem	5
1.2 Previous Work	7
1.3 Summary of Previous Work and Its Relationship to this Thesis	13
CHAPTER 2: EXPERIMENTAL WORK	
2.1 Introduction	15
2.2 Details of Experimental Rig	20
2.3 Preparation of Specimens	26
2.4 Measurement Technique	29
2.5 Experimental Procedure	32
2.6 Material Properties	34
2.7 Experimental Results	35
2.8 Conclusions on Column Performance	50

CHAPTER 3: THEORETICAL STUDY	
3.1 Notation	52
3.2 Aims of Theoretical Study	54
3.3 Introduction	56
3.4 General Principles of Calculation Procedure	58
3.5 General Equations for Inelastic Biaxial Bending of Columns	62
3.6 Calculation of the Deflected Shape	81
3.7 Details of the Calculation Procedure	84
3.8 Discussion of the Computation Procedure	92
3.9 Discussion of the Theoretical Results and their Comparison with the Experimental Results	97
3.10 Conclusions on Theoretical Results	112
CHAPTER 4: A DESIGN APPROACH	
4.1 Introduction	114
4.2 Principle of the Method	117
4.3 Use of the Curves	127
CHAPTER 5: CONCLUSIONS AND NOTES RELEVANT TO FUTURE WORK	129
APPENDIX A	136
APPENDIX B	149
REFERENCES	158
FIGURES A1 to A20	161

CHAPTER 1

INTRODUCTION

1.1 AN OUTLINE OF THE PROBLEM

1.1.1 The purpose of this thesis is to study the behaviour of steel H-section columns stressed into the elastic-plastic range whilst subject to restraint about both axes from elastic beams. The loading is applied axially to the columns and laterally to the beams. Attention is restricted to the no-sway case and in particular to the loading conditions shown in Figure 1.2(a) where the beam loads cause symmetrical single curvature. This condition represents an important loading case which can arise in an office type building frame where the beams have been designed to remain elastic and the columns elastic-plastic.

1.1.2 Interest in the problem was occasioned by recent publications due to Heyman⁽¹⁾, Stevens⁽²⁾⁽³⁾ and Gent⁽⁴⁾ where an alternative approach to conventional structural design, based on assuming a suitable deflection configuration and force distribution, has been outlined. In the elastic range this consists of selecting members capable of supporting all loads in the deformed state so that strength, stability and deflection requirements are satisfied simultaneously. A further paper by Gent⁽⁵⁾, awaiting publication, extends these general ideas in a modified form to cover a design approach for office type buildings in which elastic beams and elastic-plastic columns are

used. By this approach the necessity for a designer to analyse a column largely disappears and many of the difficulties which were perceived in the past⁽⁶⁾ in the design of this class of member no longer exist. It was because of the enhanced prospects of finding a suitable design method by this approach that this investigation was undertaken.

1.1.3 In considering the possibility of deriving suitable design methods for elastic-plastic columns, it was realised that there were several research problems which might receive attention. Some of these are extremely difficult and can only properly be solved by a rigorous theoretical approach; others are simpler and their solution is a much more mechanical process. These are enumerated and discussed below and the particular problems considered in this thesis are pointed out. They are as follows:

1. An examination of the chief parameters affecting column behaviour when the irreversible nature of plastic strains and residual stress effects are not considered. In this thesis this particular aspect was the main problem investigated although within the limits set out in paragraph 1.1.1. It is also the problem to which the vast majority of present literature is devoted.
2. An examination of the effects of unloading after yield. The precise effect of this is unknown although the available evidence indicates its influence will be to strengthen a column rather than weaken it. In the current literature calculations on only one particular column have been reported⁽⁶⁾ which show in a straightforward manner this strengthening effect. A general proof covering all columns is not available. In this thesis

calculations on particular members have also been performed and can be compared with calculations which ignore unloading.

3. An examination of the effects of residual stress. Recent work ⁽⁷⁾ on the behaviour of pin-ended columns has indicated that this is the most serious column imperfection. It is possible however, that in restrained columns, subjected to primary moments, the effect is quite small.

4. An examination of whether shakedown will occur. No solution to this problem has ever been attempted even in particular cases and since only an approximate solution is available in the absence of axial load a solution for elastic-plastic columns seems far off.

1.2 PREVIOUS WORK

1.2.1 Previous work on the whole field of elastic-plastic stability is extensive, going back to the end of the last century. To restrict the field somewhat attention in this thesis is focussed mainly on that dealing with elastically restrained, elastic-plastic columns. However, since most of this previous work is concerned with single axis bending, a review of the literature dealing with bi-axially bent but unrestrained members is also included as this indicates how geometry and internal and external force distributions can be related.

1.2.2 The first work on the restrained elastic-plastic column appears to have been done in 1937 by Chwalla; his work has been reported by Bleich ⁽⁸⁾. Chwalla presented a highly involved

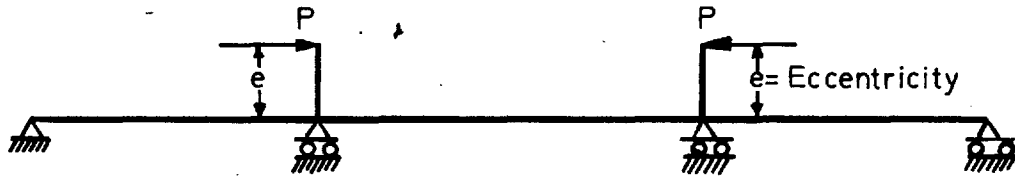


FIG. 1.1

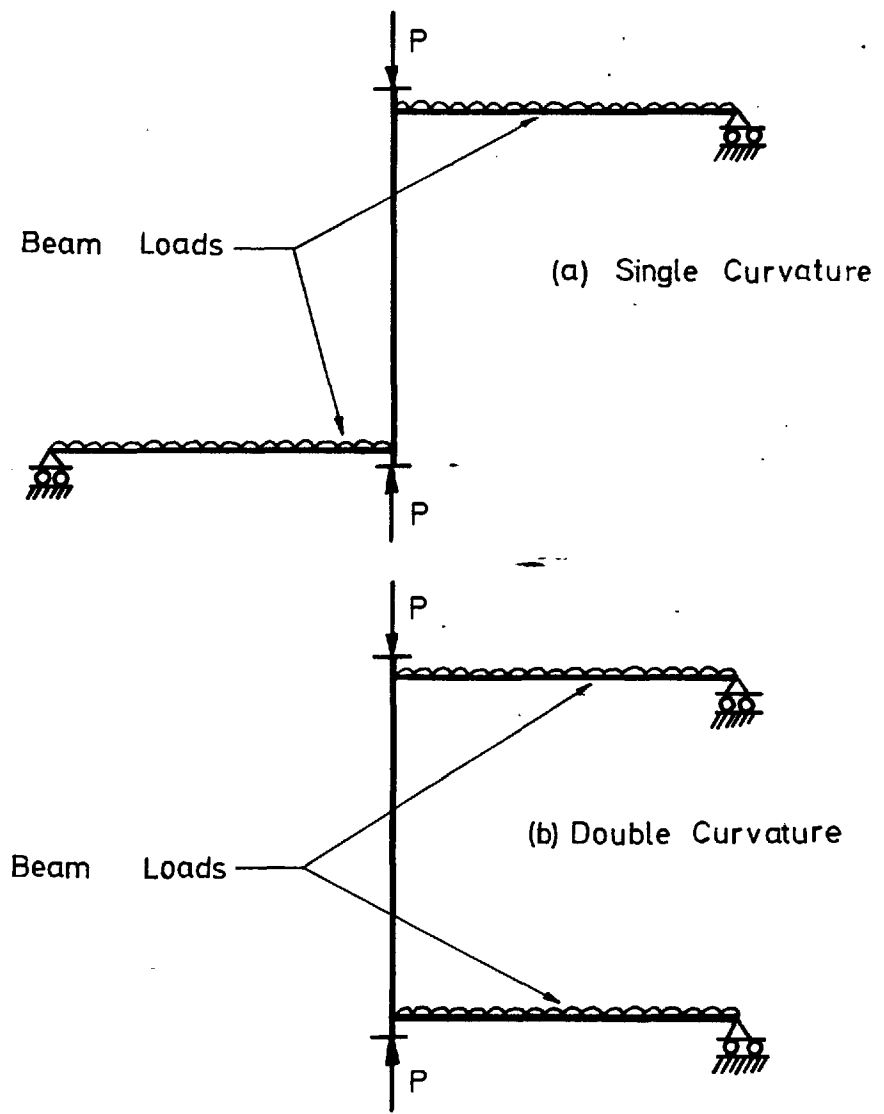


FIG. 1.2

grapho-analytical procedure to calculate equilibrium configurations for the structure shown in Figure 1.1 The method, as presented, was restricted to columns bent in one plane.

1.2.3 Further and rather more extensive work was carried out in Britain by Baker and his associates who conducted a series of experimental and theoretical studies chiefly on restrained rectangular columns. This work was reported in "The Steel Skeleton", Vol. II ⁽⁶⁾ where the important aspects of several papers were summarised. The method of experimental investigation differed from the one shown in Figure 1.1 in that moment was applied by loading the beams of the structure shown in Figures 1.2(a) and (b) and this was followed by the application of axial load to failure. Both symmetrical single curvature and symmetrical double curvature cases were investigated, taking unloading into account where necessary, and the work was extended to H-section columns bent about the minor axis. Agreement between the experimental and theoretical results was excellent, the errors on the collapse loads being generally less than 5 per cent. One notable exception occurred in a case where a column had been bent in double curvature. By ignoring unloading a theoretical collapse load was computed which was 12 per cent low. Inclusion of the unloading effect produced a result which was then 7 per cent too high. This discrepancy was attributed to the possibility of a column unwinding from the double curvature

condition into a single curvature failure mode, a factor which was ignored in the theory. However, the importance of this result is that it is the only one available where the influence of unloading has been clearly demonstrated. Some approximate methods of calculating collapse loads were also given.

1.2.4 In the British work the theoretical solution of the non-linear differential equation for deflection was reduced to evaluating a series of elliptic integrals, i. e. the integration was performed analytically. In a recent paper by Hauck and Lee⁽⁹⁾ this process of analytical integration has been extended to H-section members bent about their major axis. This has been done by idealising the member cross-section as being composed of a series of thin-walled elements.

1.2.5 Subsequent to the British work further research was undertaken in the U. S. A. by Bijlaard, Fisher and Winter⁽¹⁰⁾. The work consisted of a presentation of two computational methods for restrained columns of any cross-sectional shape, bent in symmetrical single curvature, together with corroborating experimental work. The first computational method was described by the authors as exact and was an extension of work on pin-ended columns. It consisted of finding a hypothetical, pin-ended, concentrically loaded column of length less than the length of the real column such that it behaved in the same manner as a portion of the original member. The second method, described as approximate, was based on certain

assumptions which were not completely justified. The method, however, was the one by which most of the theoretical results were computed. Several assumptions were involved and these were debated at some length in the discussion to the paper by various contributors. Experimental work was carried out for both rectangular columns and H-section columns bent about the minor axis using the loading arrangement shown in Figure 1.1. Agreement between experiment and theory was satisfactory.

1.2.6 Further work by Bijlaard ⁽¹¹⁾ extended the theoretical treatment mentioned above to deal with unsymmetrical bending, i. e. cases with unequal end eccentricities and equal and unequal end restraints. The basis of the calculations was the same although the work did represent a significant extension of the theory. The methods overcame a defect of the British work in that for the symmetrical double curvature case allowance was made for the unwinding mentioned previously.

1.2.7 A further extension along the same lines was made by Ojavlo ⁽¹²⁾ who described how nomographs could be developed to design columns with one end hinged and also columns with equal applied end moments and equal rotational restraints. Methods of performing graphical research type calculations with non-linear rotational restraints and unequal end eccentricities were also given.

1.2.8 Research into the behaviour of bi-axially bent columns

has not been extensive but two recent publications on the topic, discussed below, are particularly interesting. Before discussing these, however, it should be mentioned that a standard textbook on elastic stability such as Timoshenko and Gere⁽¹³⁾ provides useful background information since it is a fairly easy matter to extend their derivation of the elastic flexural-torsional equations to the inelastic case.

1.2.9 Work on the elastic-plastic problem has been done by Klöppel and Winkelmann⁽¹⁴⁾ who studied experimentally and theoretically a large number of eccentrically loaded pin-ended columns of H and \square shaped sections. Their theory ignored unloading and the contribution made to torsional resistance by flange warping. The solution was based on assuming polynomial expressions for u and v displacements* and satisfying equilibrium at a sufficient number of points to determine the coefficients, i. e. a power series solution. Twist was found later in a separate operation.

1.2.10 A more philosophically accurate theoretical solution to this problem was given by Birnstiel and Michalos⁽¹⁵⁾. Their solution allowed for all possible contingencies so far as stress distribution at a cross-section was concerned. Warping strains and unloading were considered and allowance was made for residual stresses although this effect was not included in the

* These are defined in Chapter 3.

one calculated example given. The solution itself involved a computer and graphical solution of a set of simultaneous non-linear algebraic equations in which the displacements at selected points along the column were adjusted.

1.3 SUMMARY OF PREVIOUS WORK AND ITS RELATIONSHIP TO THIS THESIS

1.3.1 From the previous work mentioned above it can be seen that two distinct broad theoretical approaches to the restrained column problem have been attempted. The first, used by the British team, determines the column shape without reference to solutions obtained for various end moment values and axial loads for pin-ended members whilst the second, used by Bijlaard and Ojavlo, does. This latter approach cannot be extended to biaxial bending because of the infinity of end moment combinations possible nor can it be used when strain reversal is considered. The first broad approach has therefore been adopted in this thesis.

1.3.2 The experimental problem has likewise been approached in two different ways, viz. by the loading conditions represented by Figures 1.1 and 1.2. The second was chosen for use in this thesis as it was felt that it was more directly representative of the loading conditions to which an elastically end restrained column in an actual building frame would usually be subjected.

1.3.3 In considering the relationship of this thesis to previous work it is possible to regard it as an extension of two different aspects, depending on the point of view. Firstly, it can be regarded as an extension of the work of Chwalla or the British team to bi-axial bending or, secondly, as an extension of the work of Klöppel and Winkelmann or Birnstiel and Michalos to the case of elastically restrained members. In either case, there are considerable differences in the details of the theoretical calculations, e.g. the concepts involved in calculating torsional displacements are different from those used by Birnstiel and Michalos and the method has been fully "computerised." Many other detailed differences also exist. However, despite the fact that considerable work has been performed on restrained columns bent about a single axis and pin-ended columns bent bi-axially, this appears to be the first theoretical and experimental study of restrained and bi-axially bent H-section columns.

CHAPTER 2

EXPERIMENTAL WORK

2.1 INTRODUCTION

2.1.1 The experimental work consisted of loading model H-section columns axially and through elastic beams framing into their ends. This loading was restricted to that causing single symmetrical curvature as explained previously in paragraph 1.1.1. Whilst restricting attention to this particular loading case considerably reduced the scope of the investigation it was realised at the outset that a vast amount of work would still be required if a comprehensive experimental programme were to be undertaken. Consequently attention was restricted even further to the extent of conducting a series of pilot tests for which corresponding theoretical results were obtained. By obtaining the theoretical and experimental results conjunctively it was reasoned that the significant parameters affecting column behaviour could be determined. The full test programme that was ultimately undertaken is summarised in the table given as Figure 2.6. In this table the slenderness ratio values are computed on the basis of the length of the column between beam centre lines and the ratio of beam to column stiffness is the moment of inertia of the beam divided by that of the column.

2.1.2 The work divides itself naturally into two parts; firstly three tests in which major axis beam loads and axial load only

were applied, and a second series of tests with both the major and minor axis beams loaded and axial load applied. Test specimens were accurately machined from annealed solid bars so as to minimise imperfections and beams were welded to the column to provide rigid joints.

2.1.3 The loading system that was used in the experiments is shown diagrammatically in Figure 2.1. Firstly moment was applied to the column to produce a preselected amount of beam-column joint rotation by pulling the beam ends together with turnbuckles, see Figures 2.2(a) and (b). This action is indicated in Figure 2.1 by the loads W_1 and W_2 . The distance between the beam ends was then fixed by tightening locking nuts in the turnbuckles, see Figure 2.2(a), and this was followed by the application of axial load, P , until failure. (Note: For convenience the moments, joint rotations and curvatures present after the application of the loads W_1 and W_2 will be known as the initial values, i. e. the ones present at the commencement of the axial load application.)

2.1.4 In considering the application of the loading described above it is important to realise that it corresponds exactly to that applied to the structure shown in Figure 1.2(a). The loads W_1 and W_2 correspond to the distributed beam loads and can be arranged to produce the same joint rotation exactly. Also the ratio of beam moment to beam shear can be adjusted by changing the beam length and changes in the beam stiffness can be effected by alteration of the cross-sectional dimensions,

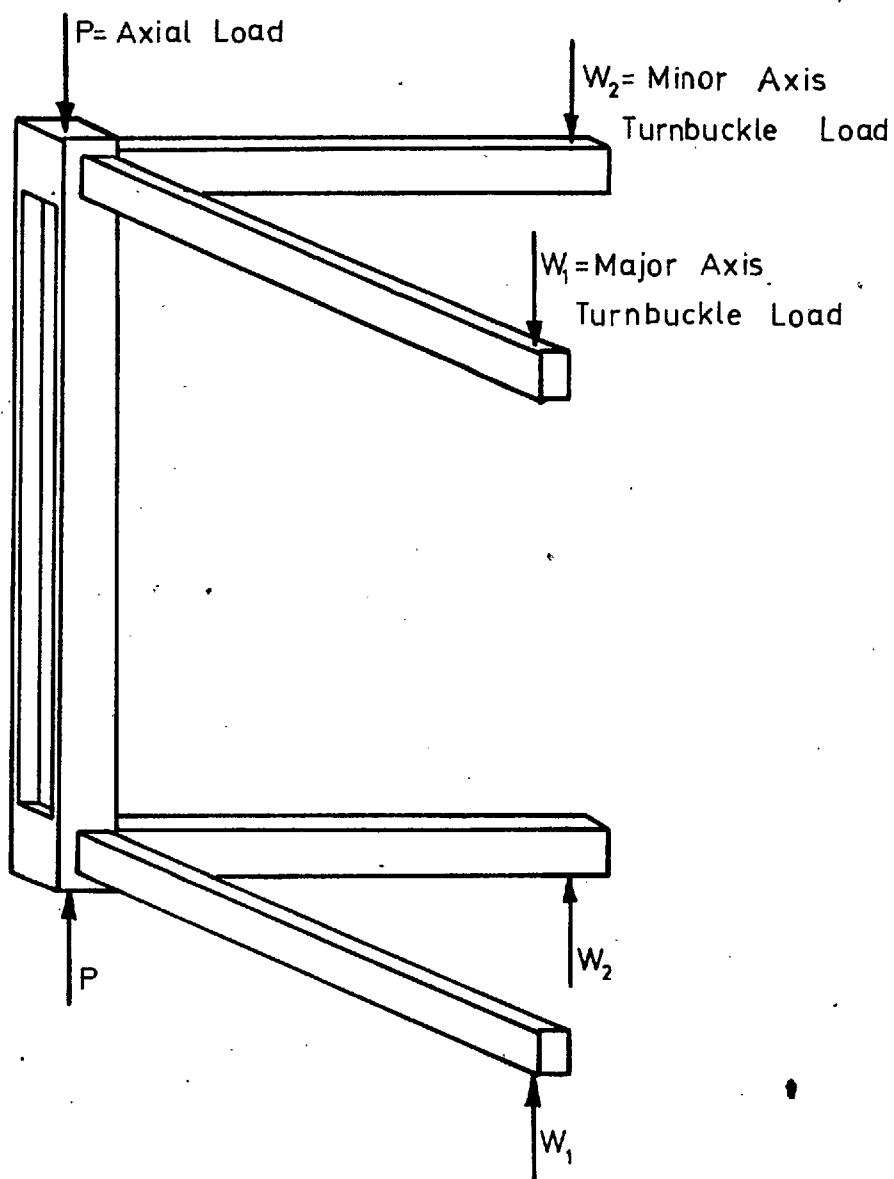


FIG. 2.1

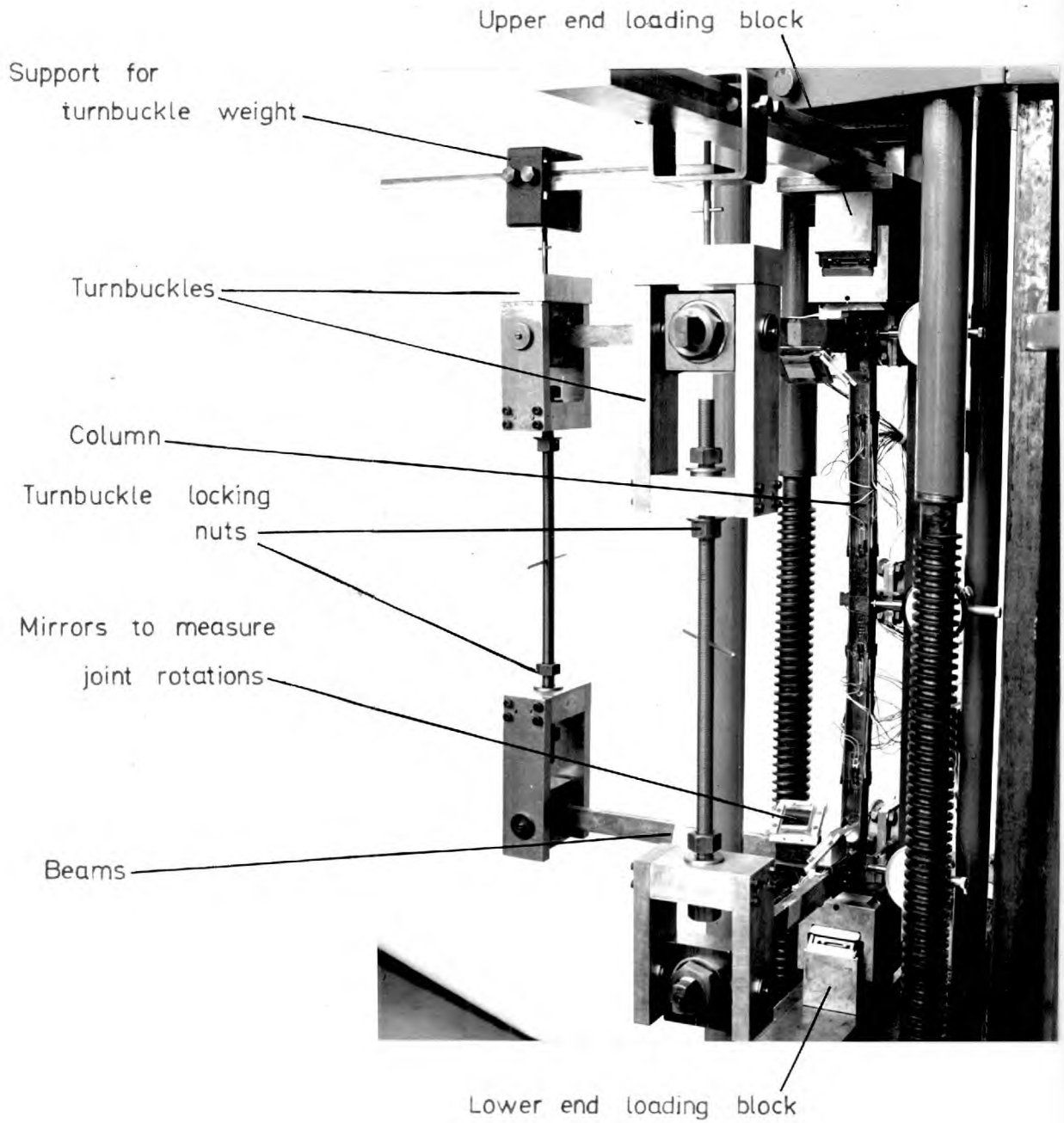


FIG. 2.2 (a)

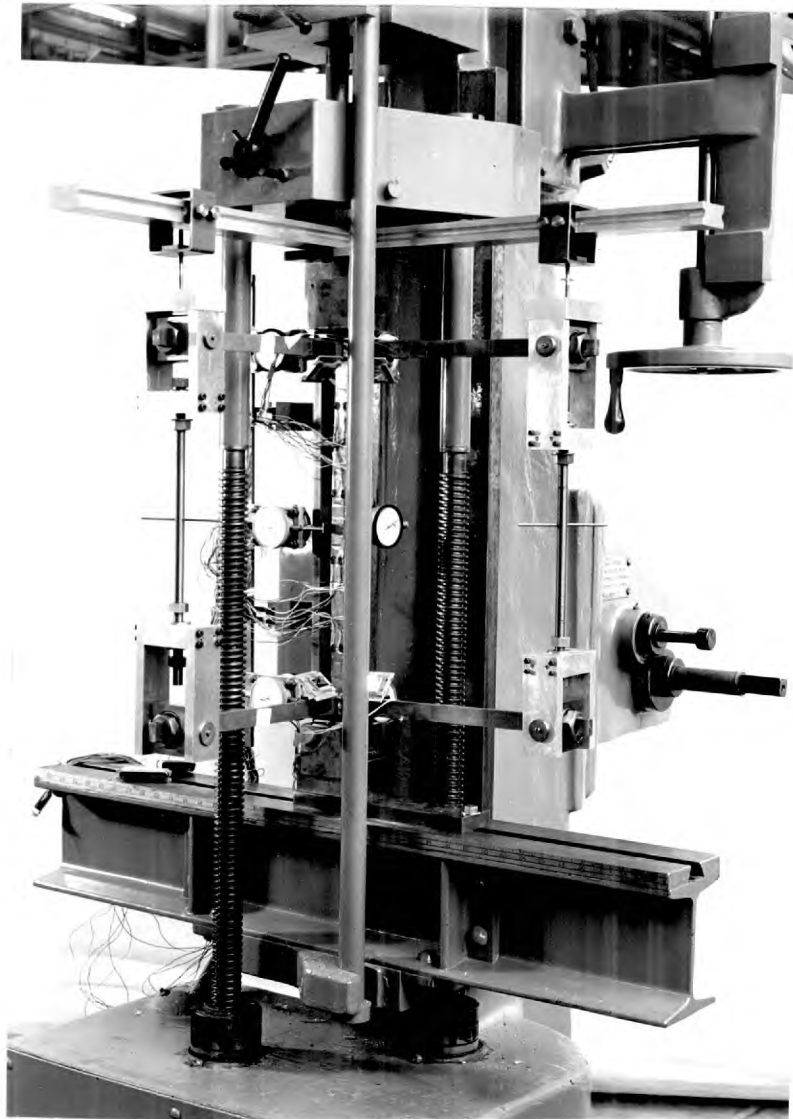


FIG. 2.2 (b)

2.1.5 A further matter requiring consideration is the irreversible nature of the plastic strains which can cause variations in the collapse load depending on the order of load application. Despite this the loading sequence described in paragraph 2.1.3 was used throughout. This was because it was difficult to predict sequences whereby strain reversal could be avoided to any large extent. It was concluded that any changes which might be induced in this way would be very small.

2.2 DETAILS OF EXPERIMENTAL RIG

2.2.1 The full experimental rig is shown in the photographs, Figures 2.2(a) and (b). These are two views of the apparatus and a specimen, column 3.1, at the completion of a test. Important pieces of the apparatus which are not part of the loading machine are labelled.

2.2.2 The major design problem was the provision of end bearings capable of applying a concentric load whilst retaining free joint rotation in both major and minor axis directions. (The question of torsional conditions is deferred until a later section). This was solved using two sets of mutually perpendicular and concentric roller bearings whose common rotational centre, C, was nominally coincident with the intersection of the beam centre lines. Therefore provided the column was placed between the centres of the upper and lower end bearings no eccentricities could exist, and provided the

bearings neither jammed nor became affected by significant friction no unaccounted rotational restraint could occur.

The principle of operation of the bearings is easily understood by referring to Figure 2.3.

2.2.3 It should be obvious from Figure 2.3 that the bearings must have certain clearances between the sides of their lower and middle sections and again between their middle and upper sections. These were quite small, being 0.003 inch on either side in the former case and 0.005 inch on either side in the latter case. The clearances were necessary to prevent friction on the sides but they did allow the possibility of small end eccentricities being applied. However, by moving the column bodily across on the bearings, the clearances could be used to advantage to remove any eccentricities due to machining errors.

2.2.4 Positioning of the column on the end bearing was by means of a 3/8 inch diameter pin located accurately in the centre of the column end and the final loading surface of the bearing itself. The bearing block as a whole was positioned by a pin entering the base plate and a hole provided in the loading machine for centralising purposes. This did not need to be located accurately, however.

2.2.5 The action of the turnbuckles has been described previously in paragraph 2.1.3 and labelled photographs have also been given, Figures 2.2(a) and (b). Two important details

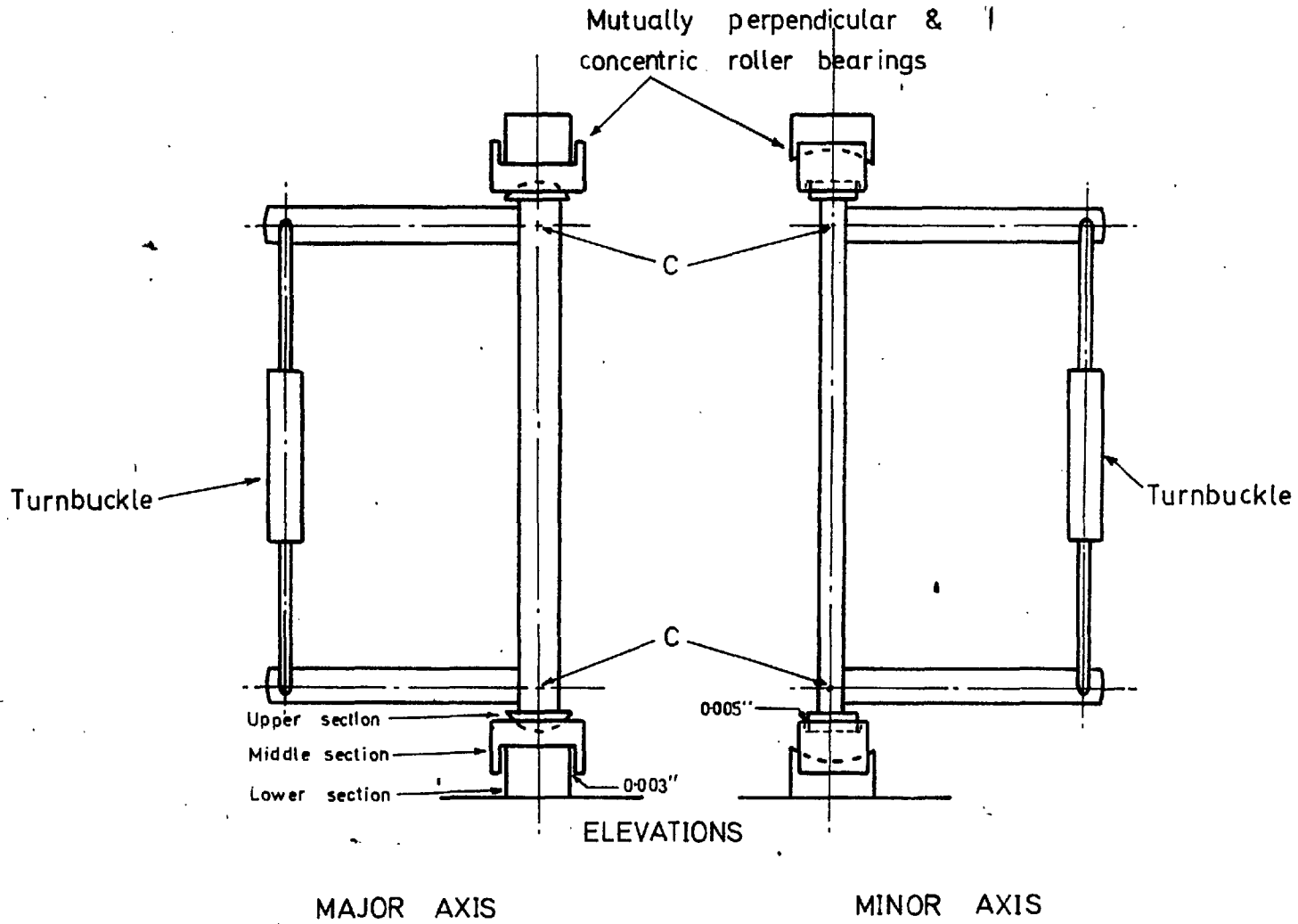


FIG. 23

of the turnbuckles not mentioned previously, however, are two sets of roller bearings, one of which allowed free rotation of the beams about their major axes, i. e. provided a simply supported condition, and a second set which prevented the application of twisting moments to the beams. The ends of the beams were specially machined to slide neatly into bushes of this first set of bearings.

2.2.6 A problem encountered with the use of turnbuckles was their own self-weight. The adjustment for this was by means of the screw device shown and labelled in Figure 2.2(a). The screwed thread was right-hand-left-hand, enabling rapid adjustment to be made. The use of this and the process of adjustment are deferred to paragraph 2.5.3.

2.2.7 The turnbuckles in conjunction with their supports performed a further function by supplying torsional restraint once the turnbuckle locking nuts had been tightened. Minor axis beam stiffnesses were quite high in comparison with the torsional rigidity of the column so that torsional restraint depended largely on the lateral resistance at the beam ends. But since the adjusting screws of the turnbuckle supports were sufficiently rigid to prevent the top U piece of the turnbuckle from rotating significantly the rather rigid turnbuckles were then able to prevent relative rotation of the column ends. Evidence that the ends were restrained was supplied by deflection data recorded in the experiments. In no case were relative rotations greater than 2×10^{-3} radians recorded, this

value being within the accuracy of the readings.

2.2.8 A solid end section, see Figure 2.5(b), at the beam column junction ensured complete restraint against torsional warping at both ends of the column.

2.2.9 Central displacement measurements only were taken and were made by dial gauges throughout. The frame to which both major and minor axis gauges were attached was bolted to the base plate of the top end bearing and cantilevered the full column length, see Figure 2.4. The frame was ~~obviously~~ of sufficient rigidity for its purposes and the fact that it and the column could move and rotate as rigid bodies was irrelevant with the three dial gauge system used. Central deflection was found using the formula,

$$\Delta_c = d_c - \frac{1}{2} (d_t + d_b)$$

where d_t , d_c , d_b are reduced top, central and bottom dial gauge readings. Minor axis dial gauges were used in pairs and column twist was the difference of these readings divided by the distance between dial gauges.

2.2.10 In the photographs, Figures 2.2(a) and (b), mirrors mounted on the beams can be seen. The intention was to take readings of the average end rotations, by double reflection, to provide information concerning the relative amounts of moment relaxation due to joint rotation and column shortening. However, although the initial rotations, i. e. with beam loads alone, could be measured accurately, subsequent joint

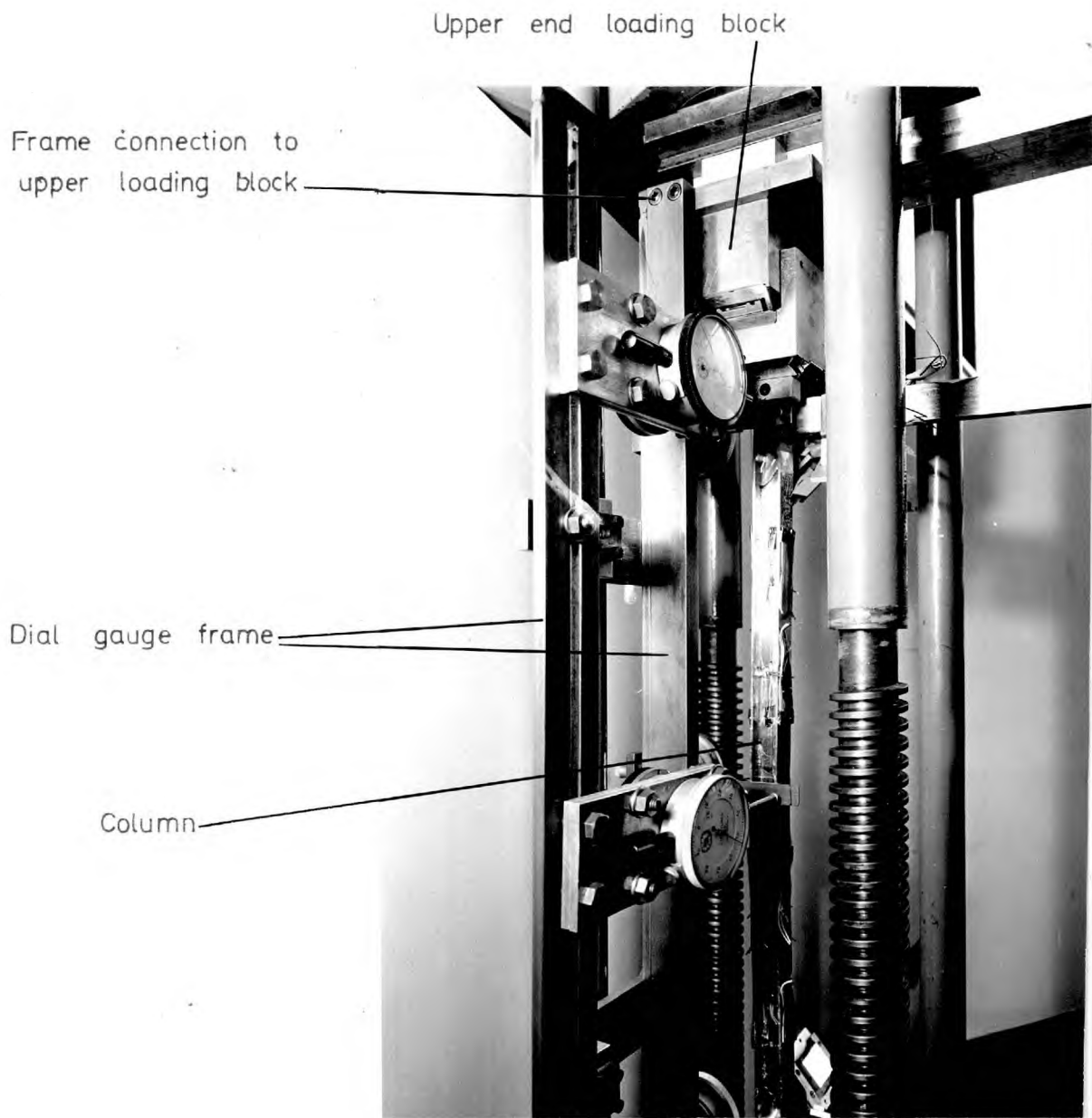


FIG. 2.4

rotations were so small that little useful information was obtained. To provide more reflections and thus magnification would have been impossibly complicated for various reasons so that the use of the mirrors was discontinued in later column tests.

2.3 PREPARATION OF SPECIMENS

2.3.1 The theoretical analysis of the columns contained no allowance for either residual stress or initial deflections. To fulfill these assumptions experimentally the specimens were cut from solid bars that had been annealed. This treatment was not given to the three columns subjected to major axis bending alone, viz. 1.1, 2.1, 2.2.

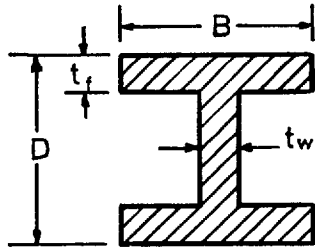
2.3.2 Lengths of $1\frac{1}{4}$ inches by $1\frac{1}{4}$ inches commercial black bar were heated to 840°C for $1\frac{1}{2}$ hours and subsequently cooled to room temperature in the furnace entry chamber. Since the largest column specimens cut were 1 inch square and since only the top $1/8$ inch is usually considered decarburised in a natural atmosphere no purging gas was used.

2.3.3 The heat treatment given to the specimens was regarded as lying somewhere between a normalising and full-annealing treatment. This was because the cooling in the entry chamber was considered to occur at a moderately slow rate due to the reasonably high temperature in this confined region. This was done to reduce the drop in yield stress that occurs with a full-annealing process and so produce an experimental

series related to the unannealed columns. The treatment could only have left small temperature gradients.

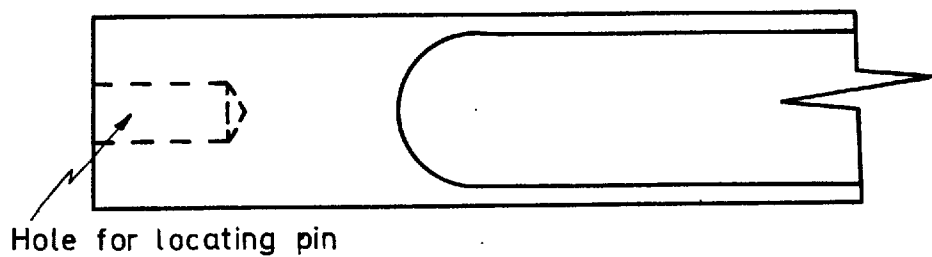
2.3.4 The machining of the columns was a lengthy and difficult operation. Firstly, specimens were roughly and fairly rapidly machined to within 0.01 inches of their finished size. Sufficient care was taken at this stage, however, to ensure parallel and constant width flanges. Next they were laid aside for two weeks to "settle". Outside dimensions were then finished to size by grinding and the flange and web thicknesses by a milling operation. In this final machining, particularly for the long slender columns, packing was required to ensure that bends were machined out rather than clamped out. This often required approaching the final sizes more gradually with further "settling" periods between the grinding and milling operations.

2.3.5 In designating machining tolerances for the column specimens it was specified that the correct cross-sectional shape be maintained, i. e. the flanges of equal thickness (to within ± 0.001 inches) and parallel and the web centrally placed (to within ± 0.001 inches). Liberal tolerances were allowed on the actual values of web and flange thickness, however (± 0.005 inches). The columns shown in the table, Figure 2.6, are in three groups, each group having nominally the same dimensions. The actual finished sizes are given in Figure 2.5(a). Columns were generally straight to almost undetectable amounts.



COLUMN	B	D	t_f	t_w
1.1	1.000"	1.000"	0.100"	0.060"
1.2	1.000"	1.000"	0.100"	0.060"
1.3	1.000"	1.000"	0.101"	0.060"
1.4	1.000"	1.000"	0.101"	0.060"
2.1	0.500"	1.000"	0.075"	0.060"
2.2	0.500"	1.000"	0.075"	0.060"
3.1	0.750"	0.750"	0.060"	0.050"
3.2	0.750"	0.750"	0.055"	0.054"
3.3	0.750"	0.750"	0.055"	0.054"
3.4	0.750"	0.750"	0.055"	0.054"

(a)



(b)

FIG. 2.5

A maximum bend of between 0.001 inches and 0.002 inches was recorded on one of the 18 inch long columns.

2.3.6 Welding of the beams to the columns was facilitated by the solid end section mentioned previously, see paragraph 2.2.9 and also Figure 2.5(b). Direct attachment to the thin flanges would have only resulted in them burning away. The solid section was needed, in any case, as a platform for the application and transmission of the axial load. Squareness of the beams to the columns was ensured by machining the beam ends square and clamping both beam and column during the welding process.

2.4 MEASUREMENT TECHNIQUE

2.4.1 The quantities recorded during the course of an experiment were,

- (i) axial load,
- (ii) major and minor axis deflections and column twist,
- (iii) beam moments,
- (iv) column strains.

2.4.2 Axial load was read directly off the Buckton 10-ton loading machine used. This was a dead load device with a scale capable of being read to 0.001 ton. However, the accuracy of the actual load applied was not commensurate with this reading as a comparison with a proving ring indicated errors of up to + 0.01 ton.

2.4.3 The measurement of deflections and rotations has been discussed previously, see paragraph 2.2.9.

2.4.4 Beam moment measurement was by means of electrical resistance wire strain gauges. Beam steel was chosen to prevent yielding and the moment gauges glued near the beam-column junction slightly away from the weld area. Calibration charts were prepared by plotting electrical resistance change, measured on a Peekell strain gauge bridge, against moment. Care was exercised in positioning the strain gauges since it was desirable to have the calibration factors the same for the two beams on any one axis, see paragraph 2.5.3.

2.4.5 Column strain measurements were taken principally to provide approximate post-mortem data for columns where experimental and theoretical results were not agreeing. They also provided an independent check on the initial moment present and by applying a nominally axial load in a preliminary test the existence of accidental eccentricities. Gauges were arranged symmetrically in four sections as shown in Figures 2.7(a) and (b) so that additional data which indicated the assumed symmetry of the loading in the experiment was also available. The limitations on absolute measurements were due to both placing and measuring the position of strain gauges with large strain gradients present and to the gauge size (10 mm by 2 mm grid), a limitation imposed by economic reasons. Strains were recorded on a Solartron automatic high-

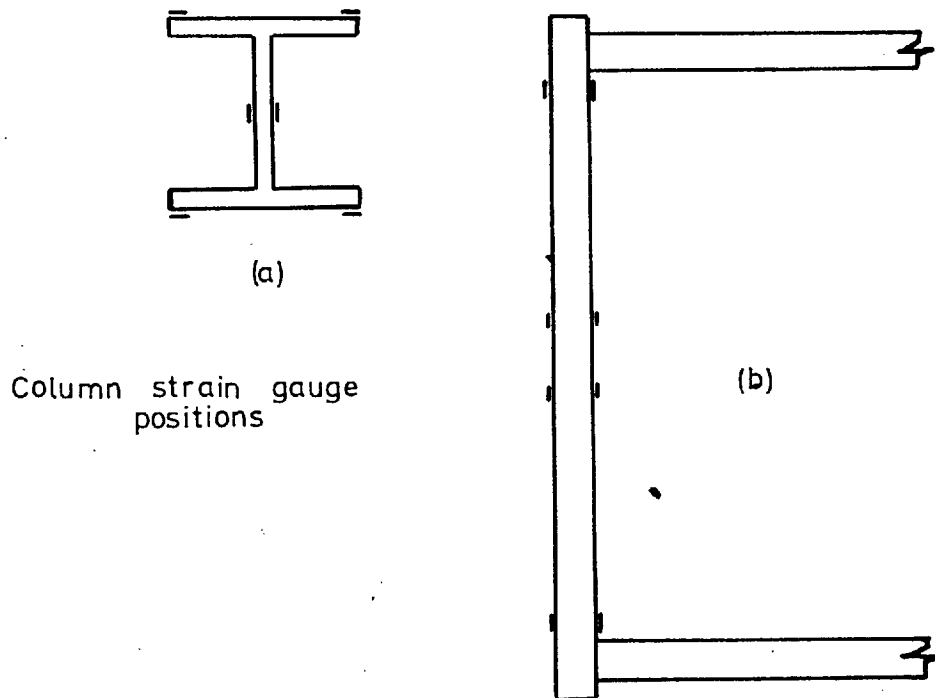


FIG. 2.7

speed recorder.

2.5 EXPERIMENTAL PROCEDURE

2.5.1 The experimental procedure consisted of preliminary tests, designed to eliminate faulty functioning of any component and errors in the preparation of the calibration charts, followed by the test to failure. The details of this are given below.

2.5.2 Firstly, all bearings were cleaned and oiled. Next the column was positioned and a small holding load applied. After checking the bearing clearances a safe axial load was applied to the column as the first part of the preliminary testing. Column strain readings were taken to check on accidental eccentricities, as mentioned in paragraph 2.4.5, and the beam ends flexed lightly with the fingers to check that the bearings were running freely. Provided all strain gauge readings were the same to ± 20 micro-strain and no residual deflections remained after the beam flexing, the stage was considered satisfactory. The effectiveness of the end bearings in avoiding frictional restraint was demonstrated with loads up to 3 tons.

2.5.3 A second preliminary test consisted of applying moment about each axis in turn keeping all stresses below the yield point values. During this application adjustment was made to correct for turnbuckle self-weight by making use of the equal moment-strain gauge calibration factors for the beam arms, see paragraph 2.4.4. Firstly, the strain gauge readings were equalised with the

turnbuckles off by using variable balancing resistors in a switchbox. Thus by subsequently manipulating the turnbuckle support to keep these readings the same, equal moments on the column ends were ensured. During this loading column deflection and strain readings were taken and required to be within ± 0.002 inch and ± 5 per cent respectively of the theoretical values.

2.5.4 The test to failure began with a recheck of all bearing clearances and a rereading of all strain and dial gauges. Beam loads were then applied to produce the preselected beam-column joint rotation, as described in paragraph 2.5.3, and the locking nuts tightened as described in paragraph 2.1.3. During the locking process the moment induced in the column by the beam loads usually decreased slightly and it is this value which is plotted in the graphical presentation of the results and which was used in the corresponding theoretical calculations.

2.5.5. Increments of axial load were then applied until failure, the turnbuckles supports being continuously adjusted to equalise the beam moments. Deflection and strain gauge data were recorded throughout. Near collapse the increment was decreased and up to 20 minutes was allowed for the column to creep. If at the end of this period the column was still supporting its load, readings were taken and a further load increment applied. Periodic checks were made of the bearing clearances to ensure their free running.

2.6 MATERIAL PROPERTIES

2.6.1 The properties required for correlation of theory with the experimental results and general identification of the column material were the upper and lower yield points and Young's modulus E. Further tests were conducted to indicate the extent of the plastic plateau and to obtain strain hardening data.

2.6.2 All the material used for the columns was originally purchased in one batch and could therefore be assumed similar. However, column tests 1.1, 2.1, 2.2 were of unannealed material whilst that of 1.2, 1.3, 1.4 and 3.1, 3.2, 3.3, 3.4 was annealed in two separate batches due to limitations imposed by available furnace sizes. Upper and lower yield point tests were conducted on samples from each of the three batches, three specimens from each batch, whilst the Young's modulus value was obtained by testing two samples, one each of annealed and unannealed material.

2.6.3 Upper and lower yield point values were the result of Hounsfield tensometer tests. In the order of the grouping of paragraph 2.6.2, the upper yield point values recorded were 18, 16, 16 tons per square inch respectively and lower yield point values were 15.5, 14.6, 14.6 tons per square inch respectively.

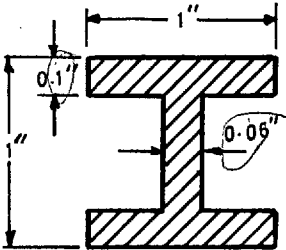
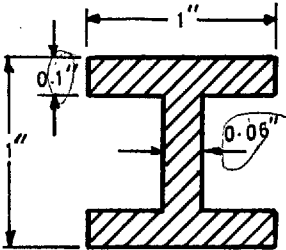
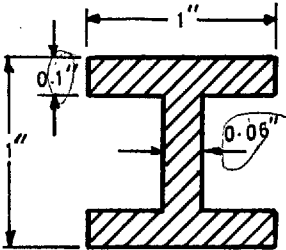
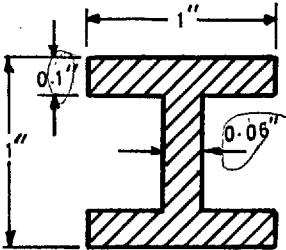
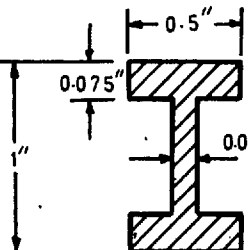
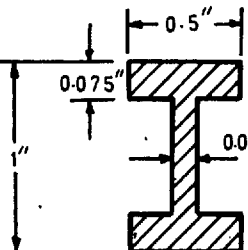
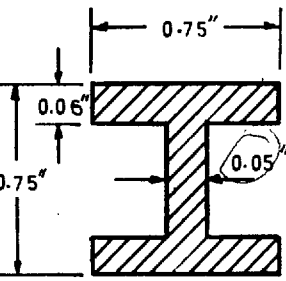
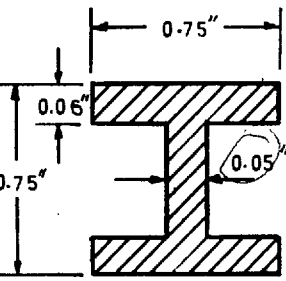
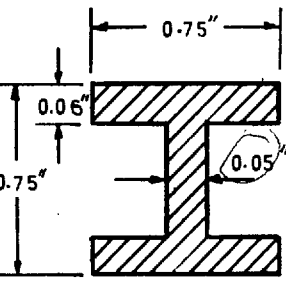
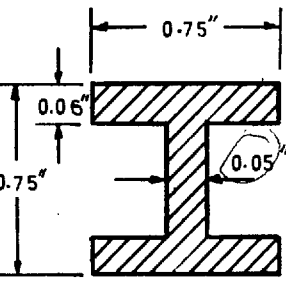
2.6.4 Young's modulus was determined by loading a specimen with a hydraulic machine and recording strains with electrical

resistance strain gauges. Results were obtained for the first and third batches of material indicated in paragraph 2.6.2; the values recorded were 13.3 and 13.7 tons per square inch respectively.

2.6.5 Although both the tensometer tests and the Young's modulus test showed that some plastic yielding was occurring neither indicated the extent of the plastic plateau or the initial strain-hardening modulus. The tensometer test was not capable of doing so and the use of strain gauges and a hydraulic loading machine was found to be unsuitable for the purpose. Consequently a test was run using a 10 ton Dennison hydraulic testing machine with load and strain recorded on a revolving drum. Results were obtained only for the last batch of annealed material and these are shown in Figure 2.8. A lower yield stress of 15.5 tons per square inch is indicated, together with a plastic plateau extending to 3.8 times the yield strain, and a strain hardening modulus of 1.08 tons per square inch.

2.7 EXPERIMENTAL RESULTS

2.7.1 As stated previously, the experimental programme consisted of three tests involving major axis beam loads only and a further seven with both beams loaded. The details of each test are discussed below, the order of discussion corresponding to the chronological order of testing. The major axis tests were conducted first and have been reported elsewhere by Gent ⁽⁵⁾ but the essential details are included here as part of the more

CHRONOL. ORDER	COLUMN	CROSS-SECTION	COLUMN LENGTH	SLENDERNESS RATIO	BEAM STIFFNESS / COLUMN STIFFNESS		INITIAL MAJOR AXIS	MOMENT MINOR AXIS	COLLAPSE LOAD	COLLAPSE LOAD / SQUASH LOAD
					MAJOR AXIS	MINOR AXIS				
1	1.1		12"	46.5	2.73	0	3080	0	8300	0.956
4	1.2		12"	46.5	2.73	7.01	1370	620	8400	0.967
9	1.3		16.5"	63.9	0.61	1.57	1400	540	7800	0.953
10	1.4		16.5"	63.9	0.12	1.57	500	510	7400	0.904
2	2.1		13"	112.6	6.87	0	1250	0	1430	0.351
3	2.1		13"	112.6	6.87	12.08	1100	0	3630	0.892
5	3.1		18"	98.8	2.56	7.36	470	179	3210	0.761
6	3.2		18"	98.8	2.56	7.36	670	101	3430	0.843
7	3.3		18"	98.8	2.56	7.36	210	160	3350	0.811
8	3.4		18"	98.8	2.56	0.29	670	25	2240	0.550

ALL FORCES IN INCH-POUND UNITS

FIG. 2.6

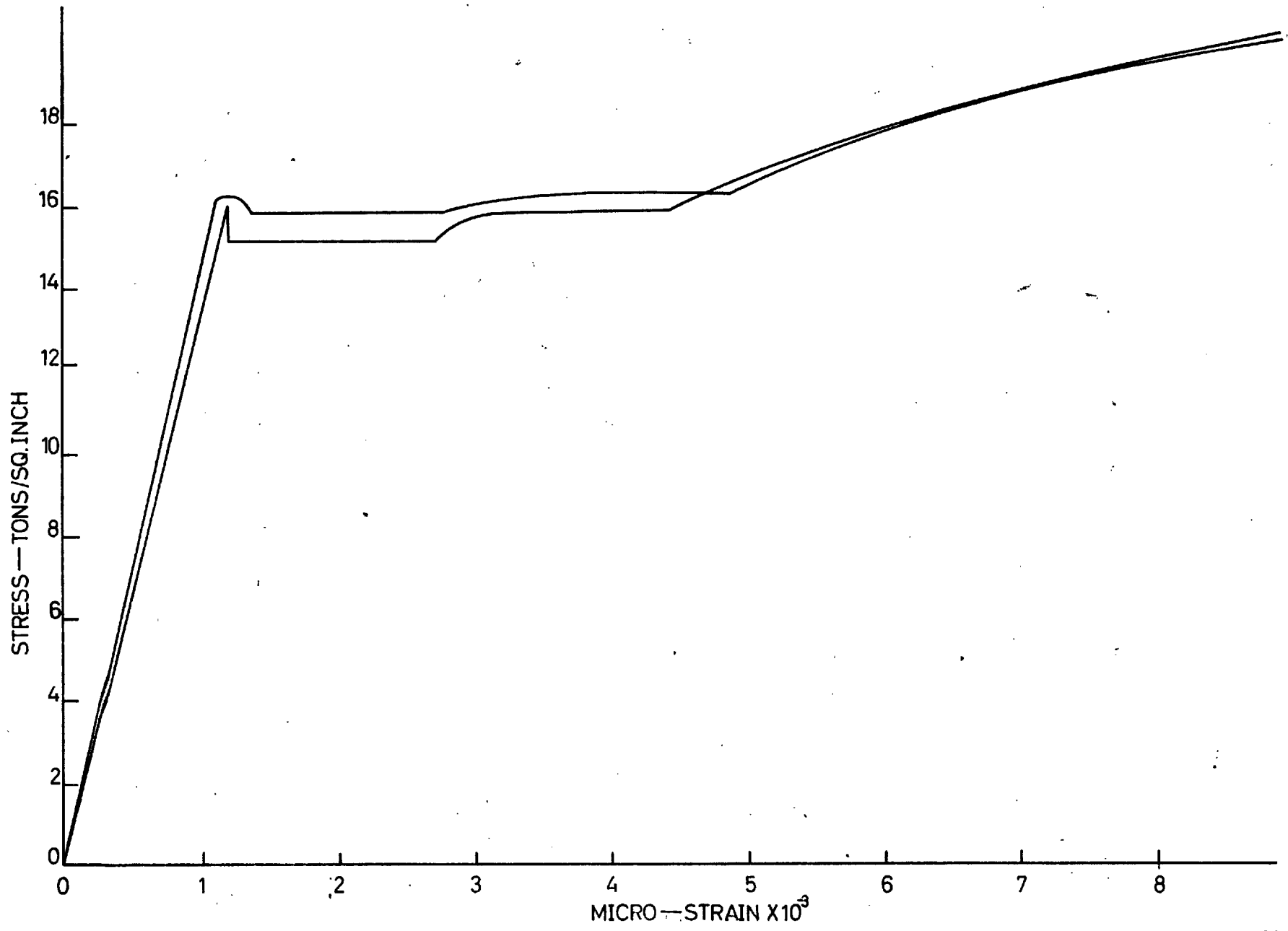


FIG. 2.8

general experimental programme. A discussion of the biaxial tests then follows. Experimental results for axial load versus central displacements (a deflection and in some cases an angle of twist) and axial load versus beam moment are given for all columns in Figures A. 1 to A. 20 along with the summary mentioned previously, Figure 2. 6.

2. 7. 2 The purpose of conducting the major axis tests was to investigate the question of lateral stability under these particular loading conditions. Little previous work was available, the only tests which appear in the literature seeming to be those reported in "The Steel Skeleton". These indicated that columns of this type fail by lateral bending with little twist. The same tendencies were noted in the tests reported in this thesis. In his discussion of the latter test series Gent ⁽⁵⁾ reasoned that torsion was a minor effect and could, for practical purposes, be ignored so that a simple application of the deterioration of stability concept, i. e. in this context, that material which becomes plastic no longer contributes to the stiffness of the member, would allow lateral stability to be checked. As it can be arranged that no tension yield occurs during the loading process ^{*} the elastic critical load of one flange will be a lower limit on the buckling load. The load computed in this fashion may be regarded as a tangent-modulus load so that a slight increase to the final collapse load, in accordance with the ideas introduced by Shanley ⁽⁸⁾, will occur.

* See the design method presented in Chapter 4.

The first three tests reported below were designed to provide experimental support for these ideas.

2.7.3 Column 1.1 (Figures A.1 and A.2)

(i) Object of Test

This short, heavy, wide-flanged member represented a column that would remain laterally stable until failure by excessive major axis deflection occurred. The squash load (= total area x yield stress = 8804 pounds) is the maximum possible under any consideration and the elastic critical load of one flange, in this case 68600 pounds, was far in excess of this value. Heavy initial major axis moment was applied; equal to 89 per cent of the fully plastic moment. The holding load plus beam shear prevented yield in tension at this stage although the entire compression flange had yielded. Beam dimensions in this case meant that the column was effectively fixed-ended about both axes.

(ii) Results

Failure occurred at 8300 pounds or 95.6 per cent of the squash load. Major axis deflections increased linearly during the application of beam moment, part OA of the curve in Figure A.2, then increased slowly with axial load until failure was approached. At failure they accelerated and physical collapse occurred with insignificant minor axis deflections and twist.

(iii) Comment on performance

Beam moments decreased throughout and became negative at about 7500 pounds. At this stage much of the compression flange

must have unloaded, i. e. the strain decreased after yield. However in this, the first test, strain gauges were present at the central cross-section only and this was not detected. The central strain gauges did show, however, that at this critical cross-section no yield in tension occurred until the final collapse process was well in progress.

2.7.4 Column 2.1 (Figures A.3 and A.4)

(i) Object of Test

In order to examine the question of lateral stability further a second test was conducted with the elastic critical load of one flange reduced to 40 per cent of the squash load. This was achieved by using a narrow flanged section in conjunction with the omission of the minor axis beams. Heavy initial major axis beam moment was applied again, 79 per cent of the fully plastic moment, and this in combination with the holding load and beam shear just produced yield in compression.

(ii) Results

Failure occurred at 1430 pounds by bending about the minor axis accompanied by only insignificant amounts of twist. The curves of Figure A.4 show that during the application of the major axis beam moment there was a tendency for minor axis deflections to develop, 0.006 inches in all. A central twisting displacement of 0.2 degrees also developed. With the application of axial load minor axis deflections magnified and then accelerated rapidly approaching and during collapse. Twist also increased but during the deformation caused by the final load increment, i. e. during the actual physical collapse, whilst the minor axis

deflections doubled (0.12 inches to 0.25 inches), the central twist increased from only 1.72 degrees to 1.95 degrees.

(iii) Comment on performance

An analysis of the strain gauge results indicated that just prior to collapse the compression flange was plastic along the entire column length, so that the internal strain distribution was causing the column stiffness to conform to the minimum requirements set out in paragraph 2.7.2. According to the reasoning given the elastic critical load of one flange should lie slightly below 1430 pounds. Evaluation of $\pi^2 EI_Y / 2L^2$ (= 1370 pounds) showed that its value conformed to this requirement; it is only 4.2 per cent below. Further analysis of the strain gauge results revealed that unloading had occurred approaching collapse as required in paragraph 2.7.2 and this explains why the experimental collapse load exceeds 1370 pounds. The fact that twisting displacements did not increase significantly during failure indicated that their effect was slight and that further calculation with their influence included would be unlikely to alter the theoretical collapse load very much.

2.7.5 Column 2.2 (Figures A.5 and A.6)

(i) Object of Test

This was the column of test 2.1 straightened but with minor axis support. It was included to study the influence of minor axis restraint on lateral stability and so provide further confirmation of the above interpretation of the behaviour of this class of column. An initial major axis moment approximately

equal to the same as that of column 2.1 was applied so that a direct comparison of the results was possible.

(ii) Results

The member performed in a similar fashion to the stiff column of test 1.1, relaxing its beam moments as necessary to sustain axial load, but due to imperfections lateral displacements developed under the high initial bending moments and these were subsequently magnified and produced failure about the minor axis as the squash load was approached. As in test 2.1 the increments of displacement during collapse were minor axis only, see Figure A.6.

(iii) Comment on performance

Little can be said about the performance of this column as the imperfections introduced by the straightening masked most other effects. This became evident when the column deflected about the minor axis in a direction opposite to that which would be expected from the influence of axial shortening. However, the provision of minor axis restraint obviously had important beneficial effects as can be seen by comparing the collapse loads of columns 2.1 and 2.2.

2.7.6 Further details of the work have been given by Gent ⁽⁵⁾ in his paper, together with further explanation of how the stiffness of a column deteriorates with the onset of plasticity. These details ~~shall~~ ^{will} not be given in this thesis since this would involve too much unnecessary repetition.

2.7.7 While the three tests described above fall somewhat short of the number desirable for a fully convincing demonstration no further work was done since the major aim was to study biaxial behaviour. The biaxial tests, however, provided further evidence of the small significance of torsional action, the only debatable assumption in the simplified theory above. In this study attention was centred on wide-flanged Universal column sections as it was felt that the narrow-flanged types such as 2.1 and 2.2 would be used in cases of major axis ^{bending} only. In these tests no simple stability criterion was anticipated, the chief purpose being to examine experimentally the effects of various parameters in conjunction with the theoretical calculations. The discussion below traces the history of the tests and describes certain other aspects but a discussion of the correlation between the results and the theory is deferred until the end of Chapter 3.

2.7.8 Column 1.2 (Figures A.7 and A.8)

(i) Object of Test

This, the first test with biaxial bending, was a repetition of test 1.1 so far as column and beam dimensions were concerned. Initial moments were applied so as to produce equal curvatures in the two principal planes their combined magnitudes being sufficient to cause stresses equal to the lower yield value in the column.

(ii) Results

Failure occurred at approximately the same load as column 1.1 by a mode in which minor axis deflections predominated. Major axis deflections increased also during the final physical collapse but the twist remained constant. Reversal of beam moment about both axes took place at approximately the same axial load, the value of which was quite close to the final failure load, see Figure A.8.

(iii) Comment on performance

The main point of interest was the fact that considerable minor axis moment had not reduced the collapse load as compared with column 1.1. However, in view of the fact that the mode of failure had switched to a predominant minor axis collapse condition, i. e. the minor axis moments had caused an effective reduction in stiffness, it was thought the effect might be more severe on slender columns and cause large reductions in the load carrying capacity. The next four tests, all on the same reduced column section, were made to examine this question.

2.7.9 Column 3.1 (Figures A.9 and A.10)

(i) Object of Test

Apart from the increase in slenderness ratio, from 46.3 to 98.4, this test was a repetition of the previous one. Beam stiffness was reduced but on a proportional basis was not significantly lower. Initial moments again provided column stresses equal to the yield value with equal principal curvatures

in the two principal planes.

(ii) Results

Axial load application resulted in the column failing by minor axis bending at 76 per cent of the squash load. Major axis deflections actually decreased slightly during the last two load increments and twist values remained constant, see Figure A.10.

(iii) Comment on performance

To support the axial load above 2500 pounds, the minor axis beam moments had to reverse their direction rather rapidly. The increase to the final collapse load of 3210 pounds indicated the reserve of strength that was available above the pin-ended condition. It also indicated the method by which the column counteracted its high slenderness ratio and enabled it to sustain its high axial load.

2.7.10 Column 3.2 (Figures A.11 and A.12)

(i) Object

In the two previous biaxial tests the application of moderate minor axis moment, in combination with the major axis moment, had caused considerable reduction of minor axis stiffness to below the elastic critical load of one flange. This had resulted in the increasing deflections, in this direction, at failure so that a column in which reduced minor axis moment was applied was studied next. The initial curvature vector was inclined at $22\frac{1}{2}$ degrees to the major axis, i. e. with more major axis curvature, and the initial column moments caused stresses

equal to the lower yield point value. During the application of the major axis moment, minor axis deflections increased by 0.007 inches because the major axis beams had not been accurately welded to the column. This resulted in joint rotations of 1.7×10^{-2} radians being present, about the major axis, at this stage.

(ii) Results

Collapse occurred at 3430 pounds by predominantly major axis deflection, although there was a slight and sudden increase in minor axis deflection but a decrease in twist during actual physical collapse.

(iii) Comment on performance

The interesting point about this particular experiment is that the presence of high major axis curvatures had no influence on the column's load-carrying capacity. In many respects this test can be likened to test 1.1 in that one flange at least was elastic for most of the test, due to the small minor axis curvatures, enabling the column to remain laterally stable. Also, in accordance with the column of test 1.1, this column was able to sustain quite high major axis deflections before it finally failed by major axis bending.

2.7.11 Column 3.3 (Figures A.13 and A.14)

(i) Object of test

As part of the general series to investigate the effect of variations of the initial curvature vector a reduction was made in the major axis moment used for column 3.1 whilst retaining all other features of that test. It was thought that with only part of the total possible major axis moment applied, minor axis effects might predominate, induce plasticity in both flanges, and cause collapse at a reduced level.

(ii) Results

The test results, see Figures 2.6, A.14, A.15, show clearly that this was not the case. Collapse was by minor axis bending at 3350 pounds at which stage a positive moment was still being applied from the major axis beams.

(iii) Comment on performance

The test obviously indicates that the particular variation of beam loading that has been used has had no adverse effects on the load-carrying capacity of the column. Although this may be true for all conceivable variations of beam loads below their full maximum values, it is not possible to draw this conclusion on the basis of one test. The point has not been investigated further, however.

2.7.12 Column 3.4 (Figures A.15 and A.16)

(i) Object of test

All the previous tests were performed with relatively stiff beams. To investigate the effect of a reduced minor axis beam restraint the considerable reduction indicated in Figure 2.6 was made. The column was tentatively designed to fail at a load of 2500 pounds on the basis of the one flange elastic assumption of the major axis tests. The elastic critical load of one flange was 1930 pounds in a pin-ended condition and this was raised to the above figure by a suitable selection of minor axis beams. As with column 3.2 major axis beam moment was fixed at 670 inch pounds, i. e. producing an initial joint rotation of 1.7×10^{-2} radians. Minor axis moment was limited

to 25 inch pounds because considerable joint rotation was necessary to relax the beam moment and it was thought desirable to limit this to some extent. ~~arguments of paragraph 2.7.12.~~

(ii) Results

Collapse occurred at 2240 pounds in a predominantly minor axis mode accompanied by slight major axis displacements but decreasing twists.

(iii) Comment on performance

The load versus deflection graphs indicate approximately linear behaviour up to 1400 pounds followed by non-linearity to failure. Subsequent calculations and analysis of the strain results showed that yielding first occurred at 1300 pounds so that the change in behaviour was attributed to this. The fact that the experimental collapse load was below the design figure was attributed to the plasticity induced in the tension flange by minor axis curvatures.

2.7.13 The completion of the experimental programme involved the testing of two columns with an intermediate slenderness ratio. Cross-sectional dimensions were the same as 1.1 and 1.2 above but the length was increased. Two tests were performed, one with the usual equal initial principal curvatures and first yield condition, and a second in which the major axis beam stiffness was reduced. It is doubtful whether this second test is representative of any practical conditions but it does investigate a further aspect of the fundamental behaviour and

complements test 3.4.

2.7.14 Column 1.3 (Figures A.17 and A.18)

(i) Object of test

As explained above, this column was tested under the equal initial curvatures condition with initial bending stress equal to first yield in the extreme fibres. Both major and minor axis beams were the same as those used in tests 3.1 to 3.3 above.

(ii) Results

The application of axial load brought about failure at 7800 pounds in a mode in which there were approximately equal amounts of major and minor axis deflection, see Figure A.18. Positive major and minor axis beam moments were sustained until close to collapse, see Figure A.17.

(iii) Comment on performance

After failure this column was straightened, reloaded with precisely the same initial moments, and failed again. The displacement and moment curves have not been plotted as they lay quite close to those obtained in the original version of the test. There were only slightly higher twists and deflections generally, for the same load. The really interesting point, however, was that the failure load was unaffected, suggesting that residual stresses, in general, will not be serious in restrained columns.

2.7.15 Column 1.4 (Figures A.19 and A.20)

(i) Object of Test

For the column major axis beam stiffness was considerably reduced, as compared with column 1.3, although the minor axis beams were not altered. Initial major axis moment of 500 inch pounds only was applied, due to limitations on beam stresses. Minor axis moment was fixed at the same value to retain some degree of realism in the test as it was thought this could hardly be the larger of the two.

(ii) Results

Failure occurred at 7400 pounds in a major axis mode. A little minor axis bending also occurred but very little twist. Major axis deflections, which were small to begin with, and major axis beam moment, changed very little in the early part of the test with the column elastic. As loading proceeded the section became plastic and the major axis deflections accelerated rapidly causing failure.

(iii) Comment on performance

Of interest in this test was the fact that the lighter major axis beams had not dramatically reduced the collapse load as was the case with slender minor axis beams in column 3.4.

2.8 CONCLUSIONS ON COLUMN PERFORMANCE

2.8.1 The following general conclusions can be drawn from the work above.

1. Variations in the initial moments applied to a column, provided the yield stress is not exceeded under their influence

alone, have but a small effect on the load-carrying capacity.

2. The collapse load is much more sensitive to changes in beam stiffness than to the amount of initial moment applied; in particular it is sensitive to changes in minor axis beam stiffness.

3. Twisting occurs during the application of axial load but it must be considered a secondary effect since in no case did it increase to any marked extent during collapse. In three cases it actually decreased.

4. Initial imperfections due to straightening the specimen do not affect its load-carrying capacity provided the beams are relatively stiff.

2.8.2 In view of conclusion (3) above, the following further conclusions may be drawn, concerning the major axis tests.

1. Provided the tension flange remains elastic the critical load of it alone provides a lower limit for the load at which lateral instability will occur.

2. The actual collapse load may be higher than that calculated in (1) above due to the effect of unloading.

CHAPTER 3

THEORETICAL STUDY

Theory of Elastically Restrained Elastic-Plastic H-Columns

3.1 NOTATION

3.1.1 The following symbols are adopted in the text below:

A	total column cross-sectional area
B	breadth of flange
b_1, b_1', b_2'	parameter defining the strain distribution at a cross-section
c	parameter defining the strain distribution at a cross-section
D	depth of section
E	modulus of elasticity
G	modulus of rigidity
I_{BX} and I_{BY}	moments of inertia of the beams restraining the columns about the major and minor axes
I_{ξ}	moment of inertia of the total cross-section about ξ axis
I_{η}	moment of inertia of the total cross-section about η axis
L	length of column between beam centre lines
h	$L/10$
h'	parameter defining the strain distribution at a cross-section
L_{BX} and L_{BY}	lengths of the beams restraining the columns about the major and minor axes

M_X	bending moment about an axis parallel to the X axis
M_Y	bending moment about an axis parallel to the Y axis
M_Z	bending moment about an axis parallel to the Z axis
M_ξ	bending moment about the ξ axis
M_η	bending moment about the η axis
M_ζ	bending moment about an axis through the effective shear centre parallel to the ζ axis
M'_U M'_L	flange bending moments
P	axial load
r	perpendicular distance from the effective centre of twist to a fibre
s	arc length along a cross-sectional element defining the warping displacement
T	torque
t_f	thickness of flange
t_w	thickness of web
u	deflection in X direction due to pure translation
\bar{u}	total deflection in X direction
v	deflection in Y direction due to pure translation
\bar{v}	total deflection in Y direction
V_{Uf} V_{Lf}	shear force in a flange
w	warping displacement
x	coordinate in the direction of the X axis
x_0	coordinate of the shear centre in direction of the X axis
y	coordinate in the direction of the Y axis
y_0	coordinate of the shear centre in the direction of the Y axis
z	coordinate in the direction of the Z axis
Δ	axial shortening of the column

Δ_u & Δ_v	deflections at ends of minor and major axis beams after applying the initial moment
α	parameter defining the strain distribution at a cross-section
ϵ	strain
ϵ_y	yield strain
ξ	coordinate in the direction of the ξ axis
η	coordinate in the direction of the η axis
ζ	coordinate in the direction of the ζ axis
ρ	curvature
σ	unit stress normal to the cross-section
ϕ	angle of twist

3.1.2 The axes X, Y, Z are a reference set which coincide with the major, minor and longitudinal axes of the column section in the undeformed state. The ξ, η, ζ are a set in which the ξ and η axes correspond to the major and minor axes of the column section in the deformed state and ζ is an axis tangent to the curved column axis.

3.2 AIMS OF THE THEORETICAL STUDY

3.2.1 The aims of the theoretical study were twofold:

- (a) to develop computational procedures that would enable a theoretical study of restrained elastic-plastic columns to be undertaken,
- (b) to determine the significant parameters affecting the column behaviour and therefore obtain reasonable correlation between theoretical results and the experimental results discussed in Chapter 2.

3.2.2 The initial endeavours in these directions restricted attention to the stresses induced in the column by the action of bending moments and axial load. The stress-strain relation was taken as that shown in Figure 3.1 with plastic strain assumed recoverable. Subsequent work extended the analysis to include such phenomena as strain reversal, strain hardening and in an approximate fashion the action of torsion moments. The inclusion of strain reversal and strain hardening was necessary to interpret certain experimental results and the inclusion of torsional effects was undertaken to obtain some theoretical indication of their significance. Torsional effects were not considered to be of great importance however and studies were made on two columns only.

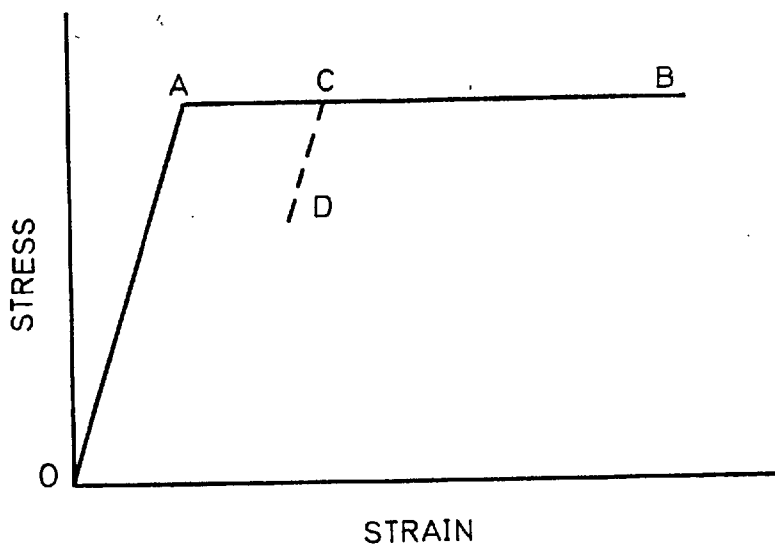


FIG. 3.1

3.2.3 From the outset numerical techniques were employed to obtain the results and the computation procedures, which are presented below, were developed with this in mind. During their development it was found that it was possible to solve the column problem in a fashion that is rigorously correct within the sense normally understood in engineering mechanics. Accordingly, these ideas are presented below for two reasons, firstly to clarify the degree of approximation introduced into the actual but approximate torsion calculation and secondly to provide a record of this exact procedure that would enable the approximations to be removed from future studies as desired.

3.3 INTRODUCTION

3.3.1 To allow a full comparison of theoretical and experimental results a calculation procedure which follows the loading path of the experiments is required. Consequently the method developed begins by establishing the equilibrium shape of the column after the application of beam loads. It then proceeds to compute displacements and axial load values for a series of equilibrium shapes defined by increments of curvature at the central cross-section. In doing this it is found that initially, with increasing curvature, the axial load also increases but that with the spread of plasticity this tendency is reversed and failure has occurred. Graphs of axial load versus central displacement, a translation or a twist, are drawn and the maximum load, which is taken as failure, is read off.

3.3.2 The inclusion of strain reversal, strain hardening and torsion in the analysis means that calculations were performed under varying assumptions. For convenience in referring to these varying calculations they have been numbered as follows:

- (a) calculation 1 ignores all the phenomena mentioned above, i. e. strain reversal, strain hardening and torsion.
- (b) calculation 2 includes torsional effects but excludes strain reversal and strain hardening.
- (c) calculation 3 includes strain reversal and also, where it is indicated, strain hardening but it ignores torsion.

3.3.3 The assumptions used in calculation 1, which is the simplest form possible and convenient for the derivation of design methods, are given below. They are:

1. Twisting and thus warping are negligible so that during loading plane sections remain plane.
2. The material stress-strain curve is as shown in Figure 3.1, i. e. there is no upper yield point.
3. Plastic strain is recoverable, i. e. the stress-strain relationship is defined uniquely by the line OAB. This means the solutions so obtained are unique.
4. Shear stresses are small and have no effect on deflections or in producing a combined stress yield condition.
5. Deflections are small so that curvature is given by d^2u/dz^2 and d^2v/dz^2 , etc.

3.3.4 In calculation 2 assumption 1 was removed and in calculation 3 assumption 3 was removed and strain hardening added.

3.4 GENERAL PRINCIPLES OF CALCULATION PROCEDURE

3.4.1 Before setting out the mathematical formulae used in the solution to the problem it is advantageous to consider some of the more general principles involved. In the discussion which follows the rigorous solution that was mentioned previously in paragraph 3.2.3 is outlined and this is followed by further discussion of certain underlying principles used in the computational methods.

3.4.2 Outline of an Accurate Calculation Procedure

1. To calculate the equilibrium configuration of a column subject to axial load P and moments M_X , M_Y and M_Z about axes X , Y and Z (see Figure 3.2(b)), taking the secondary forces arising from member displacements into account, it is necessary to compute and equate internal and external forces at a general displaced section as shown in Figure 3.2(a). For any such section the moments acting about the two principal axes of the section, ξ and η , and the ζ axis are called M_ξ , M_η and M_ζ respectively. The computation of the external values of these moments is straightforward and follows the well-known procedures used to compute the same quantities in the elastic case, e.g. reference (13) pp 244 and 245. However, for internal member resistance such information is not available and the procedure outlined below must be adopted.

(a) Apply displacements u and v , see Figure 3.2(a), together with axial compression simultaneously to the column using the conventional assumption of plane sections remaining plane. The

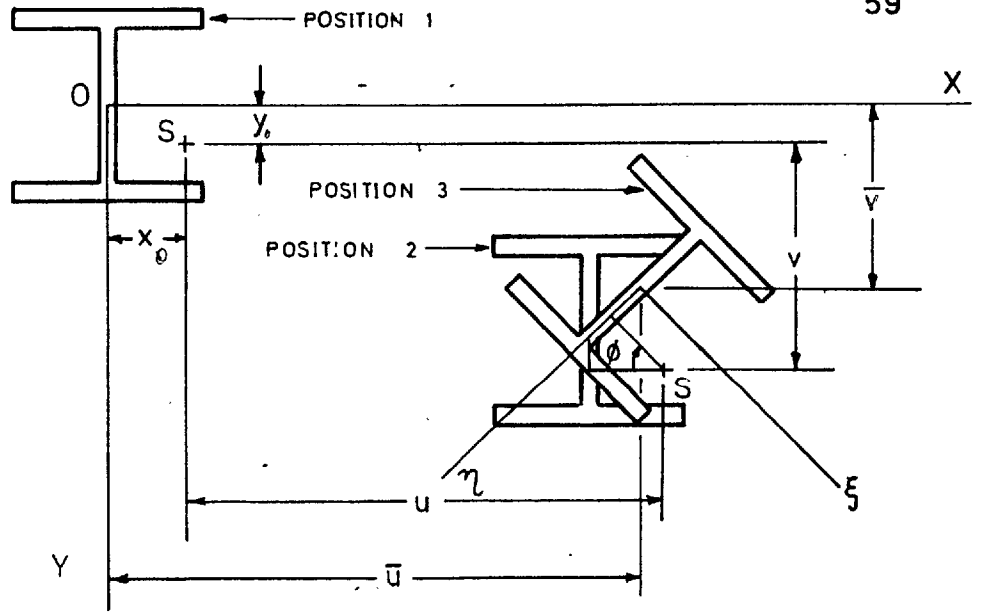


FIG. 3.2(a)

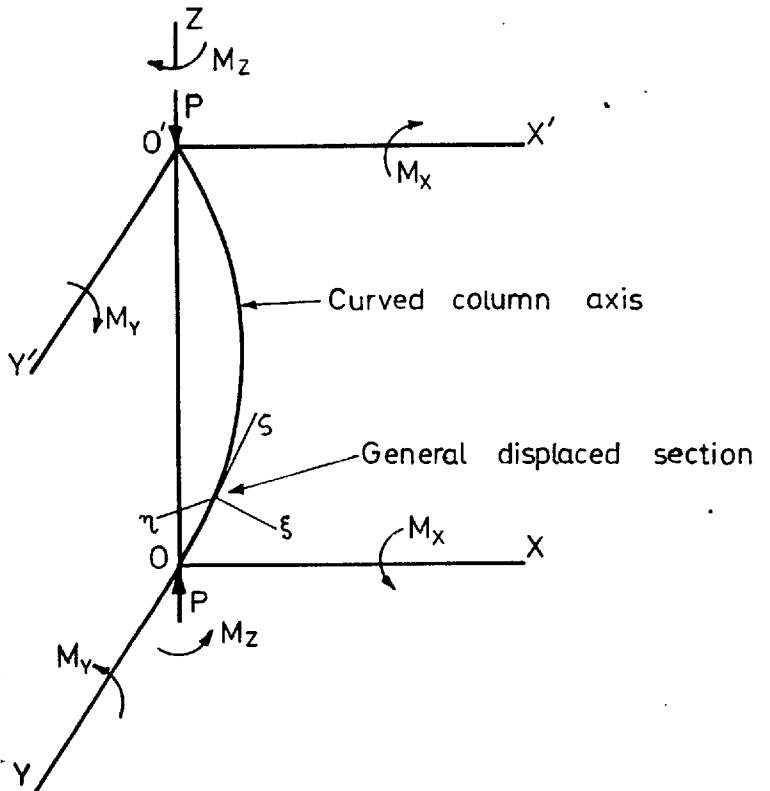


FIG. 3.2 (b)

amount of each displacement component is adjusted to satisfy equilibrium of the forces P , M_{ξ} , M_{η} taking due account of the amount of plasticity and strain reversal that occurs during the process. The flange and web shears which develop during this stage need not be considered.

(b) Twisting displacement about the point S , called the effective centre of twist, is now applied as indicated in Figure 3.2(a). This point is chosen so that after superimposing the warping strains due to twisting on top of the strains due to the displacements of step (a) above the internal values of the forces P , M_{ξ} , M_{η} remain unchanged. The magnitude of the twisting displacements must be adjusted to produce equilibrium of the torsion moment M_{ζ} , considering strain reversal and plasticity in the process. In computing the component of torsion resistance in an elastic-plastic member corresponding to warping resistance in an elastic member it must be remembered that S is not a shear centre in the classical, or any other sense. In an elastic member the shears due to u and v displacement components would have no resultant torsion moment about a true shear centre but this does not follow for the point S , as defined above, in an elastic-plastic member. Thus in considering flange and web shears it is their total magnitude, i. e. due to all displacement components, which must be used.

(c) During twisting the external values of the forces M_{ξ} , and M_{η} change slightly, see equations 3.3(a) and (b), so that an iterative cycle must be set up. The values of M_{ξ} and M_{η} are used to obtain new u and v displacements and these in turn alter the

external torque values. At each iteration the member must be considered to start again at 0 in Figure 3.2(a), the only purpose of the iteration being to adjust the external forces. In fact if all forces could be known at the outset no such iteration would be necessary. The process is continued until successive values of the external forces differ by less than a small specified amount.

3.4.3 The reason for placing on axial compression and u and v displacements simultaneously followed by twist in a separate operation is because torsional resistance depends on two derivatives of the same quantity of different order. Thus moment resistance can be obtained from axial compression and the curvatures d^2u/dz^2 and d^2v/dz^2 but torque depends on $d\phi/dz$ and $d^3\phi/dz^3$. Hence in the finite difference expressions by assuming values of $d\phi/dz$ at all station points the first part of the torque can be found. However, to obtain the second part numerical differentiation of these values must occur so that the full resistance at each station depends on $d\phi/dz$ at other stations. The procedure to satisfy torsion equilibrium is therefore different.

3.4.4 To take account of unloading of plastically deformed fibres the cross-section has been divided into a number of small elemental areas, thirty in each flange and ten in the web. The maximum strain occurring in each is allocated to a fixed memory location in the computer. The calculation is allowed to proceed

in small increments of curvature at the central cross-section and at each step the strain at each small element is compared with the previous maximum value. It overwrites the previous maximum value if it is larger or leaves it if it is smaller. In assessing the internal force account must be taken of unloading in both displacement stages mentioned in paragraph 3.4.2 above. Further details are given later.

3.4.5 The use of small increments of central curvature also settles the question of load path dependence, i. e. lack of uniqueness of the solution. This is because during an incremental increase in curvature the stress-strain relation is uniquely defined from the strains produced at previous stages in the computation. Since these represent fixed conditions so far as iteration for a new equilibrium position is concerned the only error involved is concerned with how small the increment is made and not with the basic philosophy. In the computer programme the increment is made small.

3.5 GENERAL EQUATIONS FOR INELASTIC BIAXIAL BENDING OF COLUMNS

3.5.1 Geometry

1. A column cross-section which undergoes the general displacements mentioned in the sections above is shown in Figure 3.2(a). It starts initially in position 1, then under the action of u and v displacements moves to position 2, and finally by twisting about an axis through S it moves to position 3.

Displacements u and v , the twist ϕ , and the coordinates of S , viz. x_0 and y_0 , are all positive as shown. The quantities u , v and ϕ are small so that the geometry for small displacements applies.

2. During the twisting process the axes ξ and η rotate relative to the X and Y axes through an angle ϕ and the displacement components of the centroid change from u and v to \bar{u} and \bar{v} where,

$$\bar{u} = u + y_0 \phi \quad 3.1(a)$$

$$\bar{v} = v - x_0 \phi \quad 3.1(b)$$

3. Another geometric change which occurs during the member displacement is the inclination of the ζ axis to the Z axis caused by the slopes $d\bar{u}/dz$ ($\doteq dv/dz$) and $d\bar{v}/dz$ ($\doteq dv/dz$). This and the column twisting means that forces computed in the XYZ coordinate system differ from those computed for the $\xi \eta \zeta$ system. Since force transformations between the two systems are required to compute the external loads acting at a cross-section it is convenient to have a table of the relevant direction cosines. The one below is reproduced from Timoshenko and Gere⁽¹³⁾ p.252.

	x	y	z
ξ	1	ρ	$-du/dz$
η	$-\rho$	1	$-dv/dz$
ζ	du/dz	dv/dz	1

3.5.2 External Forces

1. In establishing equilibrium between internal and external forces at any cross-section complete freedom is available concerning the choice of axes about which moments are taken provided the same ones are used for internal and external forces. Here moments M_{ξ} and M_{η} are taken about axes ξ and η through the centroid of the section and torsion moment M_{ζ} about an axis parallel to the ζ axis and passing through S. Moment sign is in accordance with the right-hand screw rule.
2. The external moments about a set of axes parallel to the XY axes but with their origin at the centroid of the displaced section are calculated first. They are then resolved about the ξ and η axes. Torsion moment M_{ζ} depends on the way the external loads distribute themselves over the cross-section and the relevant equation is developed separately.
3. Taking the axial load on the column as P, positive when compressive, and the beam moments about the X and Y axes as M_{BX} and M_{BY} , the total moments about the displaced set

of X and Y axes, at a section where displacements \bar{u} and \bar{v} occur, are

$$M_X = M_{BX} - P\bar{v} \quad 3.2(a)$$

$$M_Y = M_{BY} + P\bar{u} \quad 3.2(b)$$

Due to the symmetry of loading the value of torsion moment M_Z is zero. By resolving the moment M_X and M_Y about the ξ and η axes, using the table of direction cosines, the result,

$$M_\xi = M_X + \phi M_Y \quad 3.3(a)$$

$$\text{and } M_\eta = M_Y - \phi M_X \quad 3.3(b)$$

is obtained.

4. To evaluate M_ξ consider a point in the cross-section defined by coordinates x and y with respect to the displaced set of XY axes so that after bending and twisting the components of deflection of that point in the X and Y directions are $u' = u + (y_0 - y) \phi$ and $v' = v - (x_0 - x) \phi$ respectively. The slopes of a longitudinal fibre beneath this point in the XY and YZ planes are du'/dz and dv'/dz so that vertical components of force per unit area σ , parallel to the Z axis and acting on a small area dA , will exert components of force in the X and Y directions of $(-\sigma dA)du'/dz$ and $(-\sigma dA)dv'/dz$. The contribution these make to the total torque is given by,

$$dM_G = -(\sigma dA)(y_0 - y) du'/dz + (\sigma dA)(x_0 - x) dv'/dz \quad 3.4$$

Substituting for u' and v' , integrating over the area, noting that,

$$\int_{A_T} \sigma dA = P, \quad \int_{A_T} \sigma y dA = M_x, \quad \int_{A_T} \sigma x dA = M_y,$$

and writing $r^2 = (x_0 - x)^2 + (y_0 - y)^2$

the result,

$$M_G = P(y_0 du/dz - x_0 dv/dz) + M_x du/dz - M_y dv/dz - d\phi/dz \int_{A_T} \sigma r^2 dA \quad 3.5$$

is obtained.

3.5.3 General Discussion of Internal Forces

1. Internal resistance at a cross-section is calculated by integration of the stresses over the total area following the applications of strains as explained in the introduction. During the application of curvatures and axial load plane sections are assumed to remain plane so that the resulting strain distribution may be expressed in terms of the three parameters, b, c, α , defined from the diagram in Figure 3.3. From these strains, stresses are deduced and the values of P, M_x and M_y obtained. Flange and web shears occur also but need not be calculated. The warping strains which are the result of twisting about S are now superimposed on the strains above. Web and flange shears arising from all displacement components must now

be computed and the moment they cause about S calculated.

This in addition to the normal St. Venant's term gives the full value of the torsional resistance. The details follow.

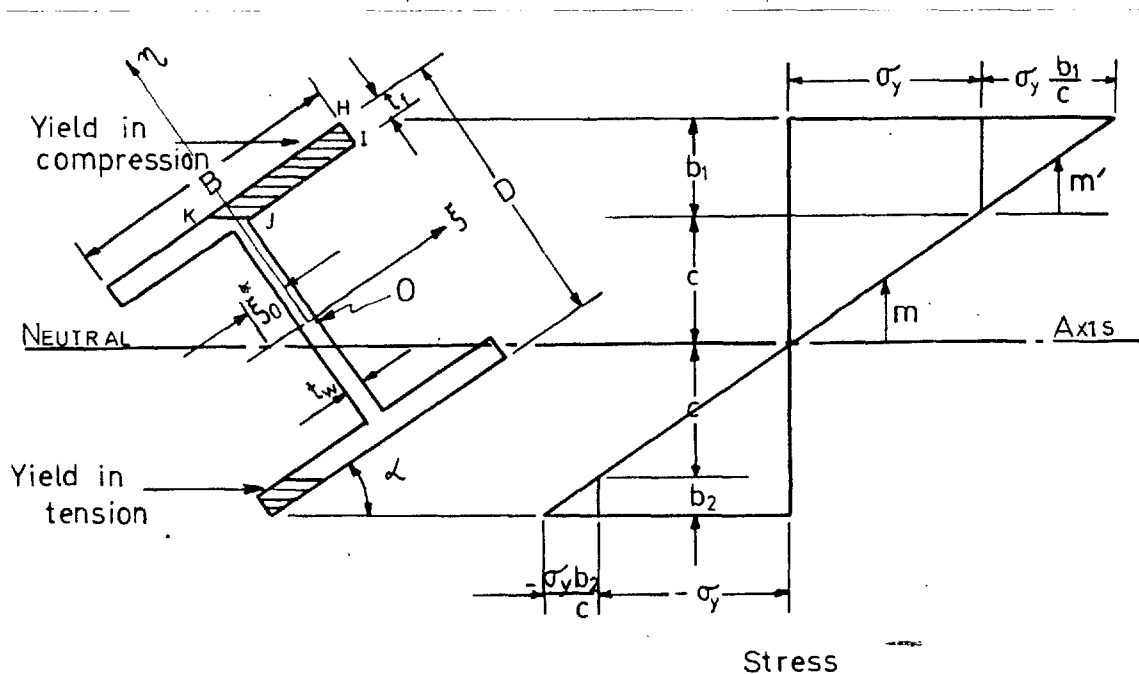


FIG. 3.3

3.5.4 Forces Due to Principal Curvatures and Axial Compression

1. A general stress distribution is shown in Figure 3.3 above where yield in both compression and tension has occurred according to the plane sections assumption. The evaluation of forces is made now ignoring unloading since the equations as such were used in calculation 1. The corrections for unloading will be made later.

2. A coordinate m , defined as shown in Figure 3.3, enables the stress at any point in the elastic zone to be expressed as,

$$\sigma = \sigma_y m / c \quad 3.6$$

where $m = \eta \cos \alpha + (\xi + \xi_0) \sin \alpha \quad 3.7$

and $\xi_0 = \operatorname{cosec} \alpha [(b_1 + c) - (D \cos \alpha / 2 + B \sin \alpha / 2)] \quad 3.8$

By substituting equation 3.7 into 3.6 the expression,

$$\sigma = \sigma_y [\eta \cos \alpha + (\xi + \xi_0) \sin \alpha] / c \quad 3.9$$

is obtained. In the plastic zone the stress is σ_y .

3. The internal forces are given by the equations,

$$P = \int_{A_e} \sigma dA + \sigma_y A_p \quad 3.10(a)$$

$$M_\xi = \int_{A_p} \sigma \eta dA + \sigma_y \bar{\eta} A_p \quad 3.10(b)$$

$$M_\eta = \int_{A_e} \sigma \xi dA + \sigma_y \bar{\xi} A_p \quad 3.10(c)$$

where A_e is the area elastic, A_p the area plastic and $\bar{\eta}$ and $\bar{\xi}$ the coordinates of the centroids of the plastic zones. Substituting equation 3.9 into equations 3.10 leads to the equations,

$$P = \sigma_y \int_{A_e} (\eta \cos \alpha + \xi \sin \alpha + \xi_0 \sin \alpha) dA / c + \sigma_y A_p \quad 3.11(a)$$

$$M_\xi = \sigma_y \int_{A_e} (\eta^2 \cos \alpha + \eta \xi \sin \alpha + \eta \xi_0 \sin \alpha) dA / c + \sigma_y \bar{\eta} A_p \quad 3.11(b)$$

$$M_\eta = \sigma_y \int_{A_e} (\xi^2 \sin \alpha + \eta \xi \cos \alpha + \xi \xi_0 \sin \alpha) dA / c + \sigma_y \bar{\xi} A_p \quad 3.11(c)$$

In this thesis these equations are re-written in the form of an elastic solution less a correction for plasticity, that is the integration is made over the whole area A_T assuming the member remains elastic and a correction is then applied for plasticity.

In this form they become,

$$P = \sigma_y \xi_0 \sin \alpha A_T / c - \sum_{A_p} F$$

or by substituting for the value of ξ_0 ,

$$P - P_y = \sigma_y [b_1 - (D \cos \alpha / 2 + B \sin \alpha / 2)] A_T / c - \sum_{A_p} F \quad 3.12(a)$$

$$M_\xi = \sigma_y I_\xi \cos \alpha / c - \sum_{A_p} F \bar{\eta}' \quad 3.12(b)$$

$$M_\eta = \sigma_y I_\eta \sin \alpha / c - \sum_{A_p} F \bar{\xi}' \quad 3.12(c)$$

where $P_y = A_T \sigma_y$, F is the force correction for a plastic zone and the \sum_{A_p} denotes their summed effect. The quantities $\bar{\eta}'$ and $\bar{\xi}'$ are the coordinates of the centroids of these zones. The detailed calculations involved in making these corrections are lengthy but not difficult and are therefore deferred to appendix A. The corrections themselves are entirely functions of b_1, c and α so that the full force equations 3.12 are functions of these variables also.

4. It is a straightforward matter to obtain curvatures and axial compression from these cross-sectional parameters. The relevant equations are,

$$\rho_\eta = d^2 u / dz^2 = \sigma_y \sin \alpha / Ec \quad 3.13(a)$$

$$\rho_\xi = d^2 v / dz^2 = \sigma_y \cos \alpha / Ec \quad 3.13(b)$$

for curvatures and,

$$\epsilon_{av} = \sigma_y [(b_1 + c) + (b_1 + c - D \cos \alpha - B \sin \alpha)] / 2Ec \quad 3.13(c)$$

for the average strain.

5. In the method of determining the deflected shape that is presented later the solution of the equations 3.12 for b_1, c, λ with fixed force values is required. These are three non-linear algebraic equations which in general have no analytical solution and must be solved iteratively. However, provided no yield in tension occurs one of the unknowns, c , can be eliminated by dividing the equations in pairs and the resulting two equations then solved iteratively for b_1 and λ . Tension yield generally does not occur before the maximum load is reached, provided the initial moments of themselves are not capable of causing it so that considerable savings in computer time result from this procedure. Additionally this fact is fundamental to the design approach presented in Chapter 4. In order to see that c may indeed be eliminated reference to Figure 3.3 is made again where a coordinate m' is defined. The correction stress at any point is ~~obviously~~ given by,

$$\sigma_c = \sigma_y m' / c \quad 3.14(a)$$

$$\text{where } m' = \eta \cos \lambda + \xi \sin \lambda + b_1 - (D \cos \lambda + B \sin \lambda) / 2 \quad 3.14(b)$$

Thus on an elemental area dA where the correction stress is σ_c the infinitesimal correction to axial load is given by,

$$dP^c = \sigma_y m' \cdot dA / c \quad 3.15(a)$$

The corresponding corrections to moment are,

$$dM_{\xi}^C = \sigma_y m' \eta \cdot dA/c \quad 3.15(b)$$

$$dM_{\eta}^C = \sigma_y m' \xi \cdot dA/c \quad 3.15(c)$$

By integration over the total area of plastic compression, the corresponding total corrections can be expressed in the form,

$$P^C = \sigma_y \int_{A_p} m' dA/c \quad 3.16(a)$$

$$M_{\xi}^C = \sigma_y \int_{A_p} m' \eta dA/c \quad 3.16(b)$$

$$M_{\eta}^C = \sigma_y \int_{A_p} m' \xi dA/c \quad 3.16(c)$$

where \int_{A_p} indicates integration over the areas plastic.

Substituting these expressions into equations 3.12 and removing the common factor σ_y/c the equations,

$$P - P_y = \sigma_y [(b_1 - (1/2D \cos \alpha + 1/2B \sin \alpha)) A_T - \int_{A_p} m' dA]/c \quad 3.17(a)$$

$$M_{\xi} = \sigma_y [I_{\xi} \cos \alpha - \int_{A_p} m' \eta dA]/c \quad 3.17(b)$$

$$M_{\eta} = \sigma_y [I_{\eta} \sin \alpha - \int_{A_p} m' \xi dA]/c \quad 3.17(c)$$

are obtained. Since m' is a function of b_1 , and α only division in pairs eliminates c and produces the equations,

$$M_{\xi} / (P - P_y) = F_1 (b_1, \alpha) \quad 3.18(a)$$

$$M_{\eta} / (P - P_y) = F_2 (b_1, \alpha) \quad 3.18(b)$$

which are solved iteratively. The value of e is obtained by back substitution into equation 3.17(a).

6. The allowances for fibres that unload and for strain hardening are made as corrections to the force expressions given above. Since the strain at each and every point in the cross-section may be expressed in terms, b , c , α the stresses and thus the internal forces P , M_{ξ} , M_{η} will still be functions of these three parameters. In the solution of the equations no division in pairs can now occur since the stresses are not linear functions of m . The full details of making the corrections are given in appendix B.

3.5.5 Forces Due to Twisting

1. The torsional resistance offered by a section about an axis of twist such as the one through S is due to the combined effect of a pure torsion or St. Venant's term and the effect discussed previously in paragraphs 3.4.2(i) and 3.5.3(i) of flange and web shears. The evaluation of the St. Venant's term follows along the lines of current research into this problem, e.g. reference (16). It is straightforward and in an engineering sense exact. Flange and web shear terms however are evaluated only approximately and it is here that the simplifications mentioned earlier in paragraphs 3.2.2 and 3.2.3 have been introduced.

Prior to the presentation of these approximations, however, the more general equations for the exact evaluation of flange and web shear effects are given in outline. The equations that have been used in the actual computations to date are then presented in detail.

2. The St. Venant's term may be expressed in the form,

$$T_1 = C d\phi/dz \quad 3.19(a)$$

where C is known, in the elastic case, as the torsion constant.

For an elastic section composed of thin walled elements,

$$C = \frac{1}{3}G \sum t^3 l \quad 3.19(b)$$

where t is the thickness and l the length of a typical element. The summation is for all elements. In the elastic-plastic case C varies with the spread of plasticity due to a decrease in the value of G. The value of G has never been clearly established, particularly for cases where non-uniform bending moment occurs along the length of the member, but it would appear to be conservative ⁽¹⁶⁾ to take G as zero for the plastic zones and to use the full elastic value elsewhere.

3. General Expressions for Flange and Web Shear Terms

(i) The resistance offered by flange and web shear terms is based on the thin-walled elements assumptions, and is therefore the product of the total shear force in each element multiplied by its perpendicular distance from S. (It must be remembered that external torsion moments were evaluated about S as the internal ones will be now). In addition to the shears caused by the u and v

bending displacements, which in general have a resultant twisting moment about S, warping displacements due to twisting also cause shears which have a moment about S. Both components can be obtained simultaneously by adding the warping strains to the strains due to u and v displacements, evaluating longitudinal stress and then calculating shear stress, using the well-known expression (see Timoshenko and Gere, p. 222),

$$\partial(\tau t)/\partial s = -t\partial\sigma_z/\partial z \quad 3.20$$

The torsional resistance, T_2 , offered by these shears, is given by,

$$\begin{aligned} T_2 &= \int_0^m \tau t r \cdot ds \\ &= -\int_0^m \int_0^s (t\partial\sigma_z/\partial z \cdot ds) r \cdot ds \end{aligned} \quad 3.21(a)$$

where m is the total length of walls in the section and t is their thickness. The expression can be re-written as,

$$T_2 = -\partial \left[\int_0^m \int_0^s (t\sigma_z ds) r ds \right] / \partial z \quad 3.21(b)$$

or, if $(t\sigma_z ds)$ is written as a force dF acting on an area $(t ds)$, then as,

$$T_2 = -\partial \left[\int_0^m F r ds \right] / \partial z \quad 3.21(c)$$

The term $[\int_0^m Fr ds]$ can be evaluated at each station point and differentiated numerically to obtain T_2 .

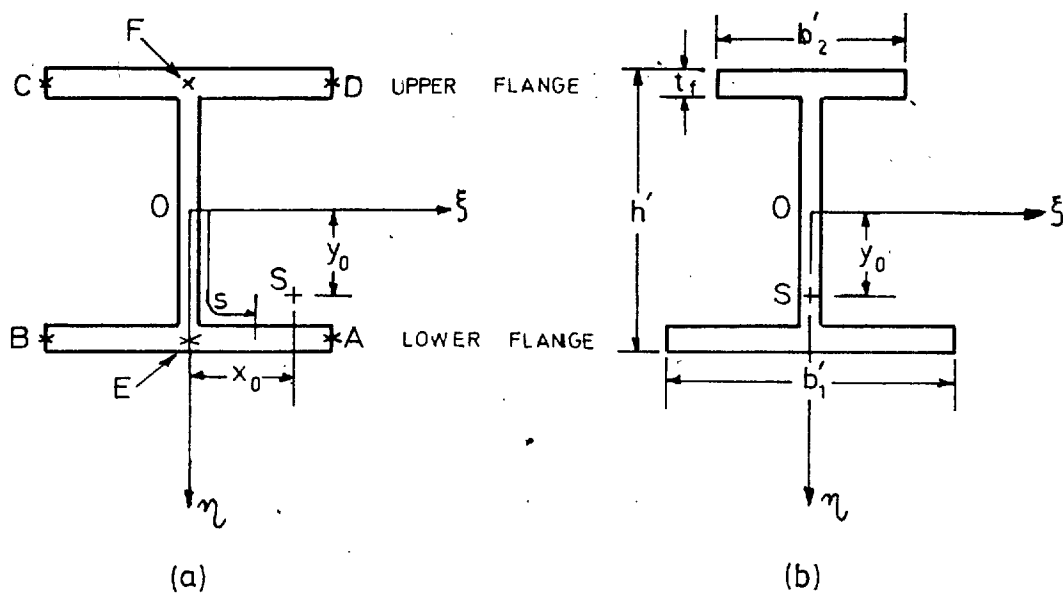


FIG. 3.4

(ii) Reference to Figure 3.4(a) shows the effective centre of twist S defined with reference to the axes ξ and η by the quantities x_0 and y_0 . When twisting occurs about S the resulting warping displacements are given by,

$$w = w_0 - (d\phi/dz) \int_0^s r ds \quad 3.22$$

where r is the perpendicular distance from S to the fibre under consideration and w_0 is the displacement at the origin of s , taken as 0. The following expressions for warping obtain,

(a) for the web,

$$w = w_0 - (d\phi/dz) x_0 s \quad 3.23(a)$$

(b) for the lower flange,

$$w = w_0 - (d\phi/dz) [x_0 \{(D-t_f)/2 - y_0\} \pm \{(D-t_f)/2 - y_0\} (s - (D-t_f)/2)] \quad 3.23(b)$$

(c) for the upper flange,

$$w = w_0 + (d\phi/dz) [x_0 \{(D-t_f)/2 + y_0\} \pm \{(D-t_f)/2 + y_0\} (s - (D-t_f)/2)] \quad 3.23(c)$$

These expressions are differentiated with respect to z to obtain strains which are added to those already present due to u and v displacements. The contribution to the torque is then calculated as explained in section 3(i) above.

(iii) Values of the quantities w_0 , x_0 , y_0 are obtained from the requirement that the stresses induced by twisting do not affect the internal values of P , M_ξ , M_η , see also paragraph 3.4.2. The three conditions give rise to three non-linear algebraic equations which must be solved iteratively at each section of the column to obtain w_0 , x_0 , y_0 . No further details of this shall be given.

2. Approximate Calculation for Web and Flange Shear Terms

(i) The main approximation introduced into the torsion calculation consists of evaluating the web and flange shear terms assuming the reduced elastic section shown in Figure 3.4(b). The quantities b_1' , b_2' , h' are the lengths of elastic upper flange, lower flange and web respectively, which remain after applying the u and v displacements. This simplification avoids the necessity of solving the non-linear algebraic equations for w_0 , x_0 , y_0 mentioned above. It is not altogether an unreasonable procedure as the actual movement of S , for the cases where the torsion calculation was used, i. e. with reasonably large major axis moments, is more or less described by this method. In accordance with these approximations the values of x_0 and w_0 are zero and y_0 is given by,

$$y_0 = \frac{1}{2}(D - t_f) - h' \left[1 - \frac{b_1'^3}{(b_1'^3 + b_2'^3)} \right] \quad 3.24$$

(ii) In conjunction with the assumption above it was considered that the significant contribution from the web and flange shear terms could be evaluated computing the shears arising out of twisting displacements alone. This follows because the point about which the shear forces due to u and v displacement have a zero resultant torsion moment should be reasonably close to the point S .

(iii) Following from these approximations the calculation of web and flange shear terms is straightforward. The equations are written in such a form that the extension to the more

accurate calculation merely involves replacement by a more accurate equation. The steps to be followed are as set out below. (a) Compute the strains due to u and v displacements alone at the points ABCDEF of the section shown in Figure 3.4(a). The values are,

$$\epsilon_A = \sigma_y(b_1 + c - (1/2)t_1 \cos \alpha) / E_c \quad 3.25(a)$$

$$\epsilon_B = \sigma_y(b_1 + c - B \sin \alpha - (1/2)t_1 \cos \alpha) / E_c \quad 3.25(b)$$

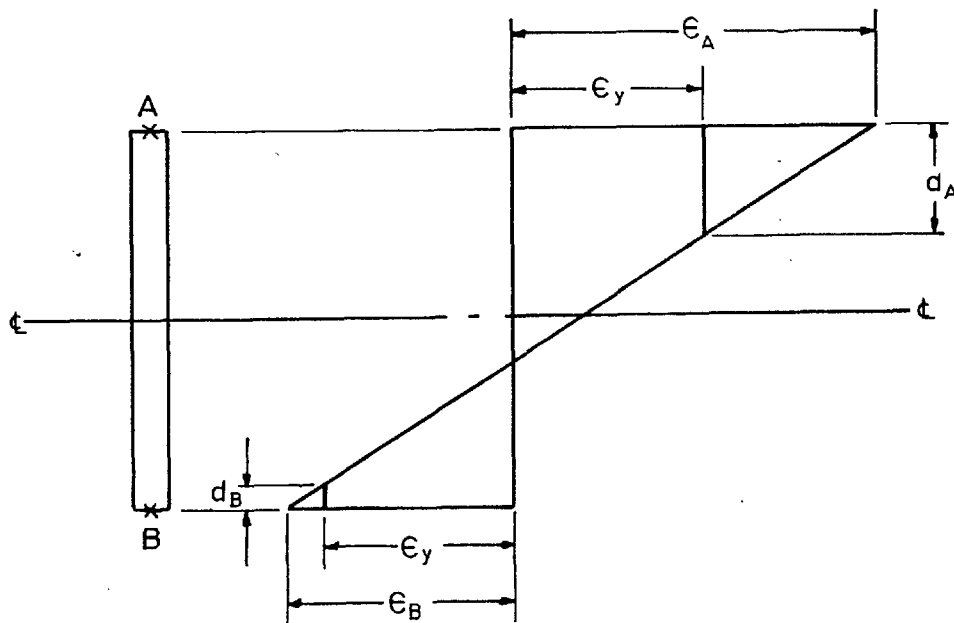
$$\epsilon_C = \sigma_y(b_1 + c - B \sin \alpha - D \cos \alpha + (1/2)t_1 \cos \alpha) / E_c \quad 3.25(c)$$

$$\epsilon_D = \sigma_y(b_1 + c - D \cos \alpha + (1/2)t_1 \cos \alpha) / E_c \quad 3.25(d)$$

$$\epsilon_E = \sigma_y(b_1 + c - (1/2)B \sin \alpha - (1/2)t_1 \cos \alpha) / E_c \quad 3.25(e)$$

$$\epsilon_F = \sigma_y(b_1 + c - (1/2)B \sin \alpha - D \cos \alpha + (1/2)t_1 \cos \alpha) / E_c \quad 3.25(f)$$

This step replaces computing the strains at the same points due to all displacement components in the more accurate procedure.



STRAIN

FIG. 3.5

(b) Compute the lengths of elastic top flange, lower flange and web, i. e. b_1' , b_2' , h' . A typical element, AB, is shown in Figure 3.5 with strains ϵ_A and ϵ_B at its ends and depths of plastic compression and tension zones given by d_A and d_B where,

$$d_A = B(\epsilon_A - \epsilon_y) / (\epsilon_A - \epsilon_B)$$

3.26(a)

$$d_B = B(\epsilon_B - \epsilon) / (\epsilon_A - \epsilon_B) \quad 3.26(b)$$

from which the elastic portion is readily obtained by,

$$b'_1 = B - d_A - d_B \quad 3.26(c)$$

A similar process is carried out to obtain b'_2 and h' .

(c) Calculate the curvatures of the upper flange and lower flange using,

$$1. \text{ upper flange} \quad \rho'_U = (d^2\phi/dz^2)[0.5(D-t_f) + y_0] \quad 3.27(a)$$

$$2. \text{ lower flange} \quad \rho'_L = (d^2\phi/dz^2)[0.5(D-t_f) - y_0] \quad 3.27(b)$$

and compute warping moments using,

$$1. \text{ upper flange} \quad M'_U = Eb'^3_U \rho'_U / 12 \quad 3.27(c)$$

$$2. \text{ lower flange} \quad M'_L = Eb'^3_L \rho'_L / 12 \quad 3.27(d)$$

(d) Numerically differentiate the flange moments to obtain shear V_{Uf} and V_{Lf} for the upper and lower flanges respectively and sum their effect to obtain the second part of the torque, T_2 , where

$$T_2 = V_{Uf}[0.5(D-t_f) - y_0] + V_{Lf}[0.5(D-t_f) + y_0] \quad 3.28$$

The steps (b), (c) and (d) above replace the calculation of the integral for T_2 from the strains ϵ_A to ϵ_F as in section 3(i) for the

more accurate procedure.

3.6 CALCULATION OF THE DEFLECTED SHAPE

3.6.1 In the preceding sections the relationships existing between the displacements and the internal and external forces have been established. In this section and the next it is shown how this geometry may be expressed in terms of finite difference equations and the relationships mentioned above used to establish equilibrium shapes. Two separate calculations are required to trace the load path of the experiments, one which determines the column shape for known values of the end moments and axial load, i. e. corresponding to the application of the initial moments, and a second which determines the shape after the distances between the beam ends have been fixed. The procedures are outlined below followed by further details.

3.6.2 Initial Shape

(i) A solution suitable for this type of problem was first proposed by Newmark⁽¹⁷⁾ and can be summarised in the following way.

1. Assume a deflected form for the column. Zero deflections have been used in the computer programme.
2. Calculate the external forces acting on the column, including the magnification of the moments M_X and M_Y due to deflections and axial load and the torsion moments.
3. Considering these moments as the external loads, calculate the deflected shape.

4. Compare this deflected shape with the one assumed. If it agrees to a specified accuracy proceed to step 5; if not, replace the assumed shape with this newly-calculated one and return to step 2. This new shape is regarded as a new assumed shape for the purposes of the comparison just mentioned.
5. Calculate the deflection of the ends of the beams.

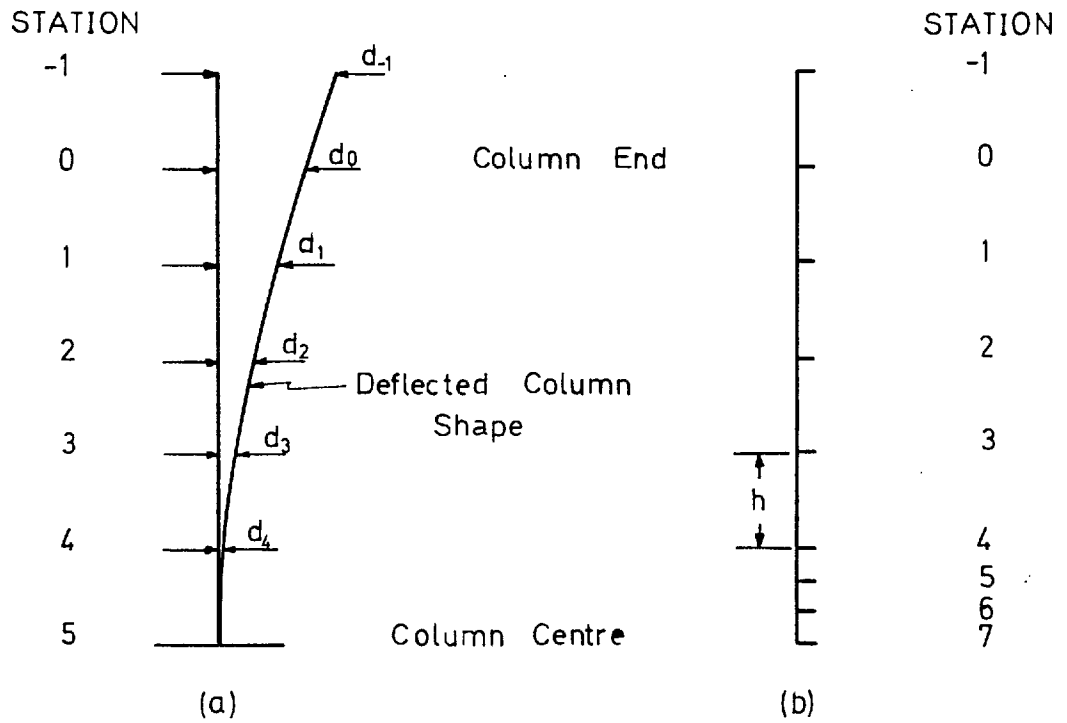


FIG. 3.6

3.6.3 Subsequent Shapes

(i) To enable the calculation of the subsequent deflected shapes to cover points on the falling branch of the load versus central

displacement curves, the procedure outlined below was adopted. This effectively continuously increases the central curvatures ρ_{ξ} and ρ_{η} in proceeding from one equilibrium configuration to the next. In order to reduce the computer time required the iteration between the u and v displacement application and the twisting application mentioned in paragraph 3.4.2 (1) does not occur. Instead in calculating a new deflected shape values of twist from the previous equilibrium position are assumed. Only when these have been established are new twist values found. Thus in a sense the twist values are always a step behind the u and v displacements but the error is not large with the small curvature increments used. In the procedure given below, it is assumed that the column length has been divided into ten sub-units, see Figure 3.6(a), for the purposes of finite difference computation.

(ii) The steps can be outlined as follows.

1. Increment the parameter b_1 at the centre, i. e. at the station 5 in Figure 3.6(a). Select trial values of ρ_{ξ_5} and ρ_{η_5} and take the values of angle of twist from the last calculated equilibrium configuration.
2. Using the values of $b_1, \rho_{\xi_5}, \rho_{\eta_5}$ calculate P, M_{ξ_5}, M_{η_5} at the central station.
3. From the central curvatures calculate the offset distances d_4 using finite difference expressions.
4. Calculate the reduced values of the moment M_{X_4} and M_{Y_4} ($= M_5 - Pd_4$), convert these to M_{ξ_4} and M_{η_4} using equations 3.3, and solve the equations for b_1, α, c at station 4. Since ρ_{ξ_4} and ρ_{η_4} are obtained immediately from α and c , see equations 3.13, the value d_3 can then be calculated from finite difference

expressions.

5. Step 4 is repeated for the stations up the column until the offset d_{-1} is obtained.

6. Numerically differentiate the offset values to obtain the column slopes and compute the deflections at the beam ends.

If this agrees with the deflections calculated in paragraph

3.6.2(i) step 5 above, then proceed to step 7; if not adjust ρ_{ξ_5} and ρ_{η_5} and return to step 2.

7. Calculate the external torque at all stations using equation 3.5, and estimate values of twist to carry this torque as described above.

8. Continue to increment the parameter b_1 until either the axial load values decrease or yield in tension occurs. Either of these occurrences is taken as indicating failure.

3.7 DETAILS OF CALCULATION PROCEDURE

3.7.1 In the procedures above the solution of the equations 3.12 for b_1 , α , c is required. For this the generalised Newton-Raphson iterative algorithm has been employed. Basically this consists of selecting trial values of the unknowns and basing corrections to those on a Taylor series expansion of the functions ignoring derivatives of order higher than the first. If the functions are F_1 , F_2 , F_3 the expansion is,

$$\begin{aligned}
 &F_1(b_1^n + \delta b_1^n, \mathcal{L}^n + \delta \mathcal{L}^n, c^n + \delta c^n) \\
 &= F_1(b_1^n, \mathcal{L}^n, c^n) + (\partial F_1 / \partial b_1)^n \cdot \delta b_1^n + (\partial F_1 / \partial \mathcal{L})^n \cdot \delta \mathcal{L}^n + (\partial F_1 / \partial c)^n \cdot \delta c^n
 \end{aligned} \tag{3.29(a)}$$

$$\begin{aligned}
 &F_2(b_1^n + \delta b_1^n, \mathcal{L}^n + \delta \mathcal{L}^n, c^n + \delta c^n) \\
 &= F_2(b_1^n, \mathcal{L}^n, c^n) + (\partial F_2 / \partial b_1)^n \cdot \delta b_1^n + (\partial F_2 / \partial \mathcal{L})^n \cdot \delta \mathcal{L}^n + (\partial F_2 / \partial c)^n \cdot \delta c^n
 \end{aligned} \tag{3.29(b)}$$

$$\begin{aligned}
 &F_3(b_1^n + \delta b_1^n, \mathcal{L}^n + \delta \mathcal{L}^n, c^n + \delta c^n) \\
 &= F_3(b_1^n, \mathcal{L}^n, c^n) + (\partial F_3 / \partial b_1)^n \cdot \delta b_1^n + (\partial F_3 / \partial \mathcal{L})^n \cdot \delta \mathcal{L}^n + (\partial F_3 / \partial c)^n \cdot \delta c^n
 \end{aligned} \tag{3.29(c)}$$

where the superscripts denote the n^{th} approximation to the correct answers. If $(b_1^n + \delta b_1^n)$, $(\mathcal{L}^n + \delta \mathcal{L}^n)$, $(c^n + \delta c^n)$ are to be the correct solution, then,

$$0 = F_1(b_1^n, \mathcal{L}^n, c^n) + (\partial F_1 / \partial b_1)^n \delta b_1^n + (\partial F_1 / \partial \mathcal{L})^n \delta \mathcal{L}^n + (\partial F_1 / \partial c)^n \delta c^n \tag{3.30(a)}$$

$$0 = F_2(b_1^n, \mathcal{L}^n, c^n) + (\partial F_2 / \partial b_1)^n \delta b_1^n + (\partial F_2 / \partial \mathcal{L})^n \delta \mathcal{L}^n + (\partial F_2 / \partial c)^n \delta c^n \tag{3.30(b)}$$

$$0 = F_3(b_1^n, \mathcal{L}^n, c^n) + (\partial F_3 / \partial b_1)^n \delta b_1^n + (\partial F_3 / \partial \mathcal{L})^n \delta \mathcal{L}^n + (\partial F_3 / \partial c)^n \delta c^n \tag{3.30(c)}$$

These are three simultaneous linear equations which can be solved by standard matrix inversion techniques to obtain δb_1^n , $\delta \mathcal{L}^n$, δc^n . The $(n + 1)$ th approximation to the answers is given by,

$$b_1^{n+1} = b_1^n + \delta b_1^n \quad 3.31(a)$$

$$\mathcal{L}^{n+1} = \mathcal{L}^n + \delta \mathcal{L}^n \quad 3.31(b)$$

$$c^{n+1} = c^n + \delta c^n \quad 3.31(c)$$

The process is continued until successive approximations agree to a specified accuracy. The derivatives are obtained numerically using backward difference formulae since no great numerical accuracy is required of these values, i. e. formulae of the type,

$$\partial F_1 / \partial b_1 = [F_1(b_1, \mathcal{L}, c) - F_1(b_1 - \Delta b_1, \mathcal{L}, c)] / \Delta b_1 \quad \text{etc.}$$

are used. The process of adjusting ρ_ξ and ρ_η to close the end beam deflections is done using the same process with only two variables.

3.7.2 Finite Difference Expressions

(i) Initial Shape, u and v displacements

The finite difference expressions for u and v displacements at the r^{th} station are of the form,

$$u_{r+1} - 2u_r + u_{r-1} = h^2 (d^2 u / dz^2)_r - C u_r^* \quad 3.32$$

*

$$C u_r = \left(-\frac{1}{12} \delta^4 + \frac{1}{90} \delta^6 - \dots \dots \dots \right) u_r$$

where the d_i 's are offset distances. This enables the step-by-step integration explained above to proceed up the column. The higher order correction terms were generally found to be small except in some cases when approaching failure. This is because certain columns require the formation of a plastic or near plastic hinge before failure is possible. Instead of attempting to allow for this in the finite difference expressions, e.g. by calling a reasonably large curvature a plastic hinge, yield in tension is taken as failure. Some reduction in the size of the finite difference mesh was attempted however, as indicated by Figure 3.6 (b) and the effect of this is discussed in section 3.3. To change the size of the mesh the expressions,

$$d_7 = 0 \quad 3.35(a)$$

$$d_6 = \frac{1}{9} h^2 (-\partial^2 u / \partial z^2)_7 \quad 3.35(b)$$

$$d_5 = \frac{1}{9} h^2 (-\partial^2 u / \partial z^2)_6 + 2d_6 \quad 3.35(c)$$

$$d_4 = \frac{1}{9} h^2 (-\partial^2 u / \partial z^2)_5 + 2d_5 - d_6 \quad 3.35(d)$$

$$d_3 = \frac{2}{3} h^2 (-\partial^2 u / \partial z^2)_4 - 3d_4 + 4d_5 \quad 3.35(e)$$

$$d_2 = h^2 (-\partial^2 u / \partial z^2)_3 + 2d_3 - d_4 \quad 3.35(f)$$

etc.

must be used in order for each of the u and v displacements,

3.7.2 The values of the slope of the column at each station are found using the expression,

$$(du/dz)_r = \frac{1}{2} (u_{r+1} - u_{r-1})/h \quad 3.36$$

and the beam deflection Δ_u is calculated using,

$$\Delta_{u_v} = \text{Axial shortening of Column} + (du/dz)_o L_{BY} + M_{BY} L_{BY}^2 / (3EI_{BY}) \quad 3.37$$

3.7.4 Axial shortening is due to a combination of axial compression of the column and the effect of column curvature. The total, Δ , is given by,

$$\Delta = \left[\epsilon_{av} + \frac{1}{2} (dw/dz)^2 \right] dz \quad 3.38$$

where ϵ_{av} is obtained using equation 3.13(c) and w equals $\sqrt{u^2 + v^2}$. The integration is performed numerically using the trapezoidal rule. Thus putting

$$B = \left[\epsilon_{av} + \frac{1}{2} (dw/dz)^2 \right] \quad 3.39$$

the expression for the coarse grid with ten column sub-divisions is,

$$\Delta = h \left[\frac{1}{2} B_0 + B_1 + B_2 + B_3 + B_4 + \frac{1}{2} B_5 \right] \quad 3.40(a)$$

where the subscripts refer to station points shown in Figure 3.6(a). For the finer mesh shown in Figure 3.6(b),

$$\Delta = h \left[\frac{1}{2} B_0 + B_1 + B_2 + B_3 + B_4 + \frac{1}{2} B_7 \right] \quad 3.40(b)$$

3.7.5 For the twisting displacements the procedure generally consists of assuming values of $d\phi/dz$ for the stations 1 to 4 (it was only done with the coarse sub-division) and regarding the equilibrium at each station as non-linear functions of these variables. The generalised Newton-Raphson algorithm has again been employed to adjust the $d\phi/dz$ values. The boundary conditions are,

$$(i) \text{ at } z = 0 \quad \phi = 0 \text{ and } d\phi/dz = 0$$

and(ii) at $z = L/2$, $d\phi/dz = 0$ due to symmetry.

From the trial $d\phi/dz$ values $d^2\phi/dz^2$ is computed at stations 1 to 5 using the finite difference expressions,

$$(d^2\phi/dz^2)_r = \frac{1}{2} \left[(d\phi/dz)_{r+1} - (d\phi/dz)_{r-1} \right] / h \quad 3.41$$

Flange warping moments are next computed using the equations given in paragraph 3.5.3. Next flange shears are obtained by numerically differentiating these moments, but recourse must be made to forward difference formulae as insufficient moment values are available to do otherwise. Therefore,

$$V = (M_{r+1} - M_r) / h \quad 3.42$$

The total internal torque is calculated and compared with the external torque. The $d\phi/dz$ values at each station are adjusted until these values agree to a specified accuracy. Following this the $d\phi/dz$ values are integrated by Simpson's rule to obtain the

angles of twist ϕ , except at station 1. Here an approximation is made and ϕ_1 is found by,

$$\phi_1 = \frac{1}{2}h(d\phi/dz)_1 \quad 3.43(a)$$

followed by,

$$\phi_r = \phi_{r-1} + \frac{1}{3}h \left((d\phi/dz)_{r+1} + 4(d\phi/dz)_r + (d\phi/dz)_{r-1} \right) \quad 3.43(b)$$

for the other station points.

3.7.6 The accuracy of the torsion calculation, as given above, can be improved in some respects, e.g. a fictitious value of $d\phi/dz$ outside the column should be computed and the differential equation for torsion written at station 0. Also, this would enable ϕ_1 to be computed more accurately by expanding the Taylor series for ϕ at station 0. Additionally, a larger number of station points would improve the numerical accuracy. However, in view of the secondary significance of torsion, this has not been undertaken.

3.8 DISCUSSION OF THE COMPUTATION METHOD

3.8.1 Before presenting and discussing the results that were obtained during the theoretical study it is advantageous to consider the numerical accuracy of the solutions of the differential equations that were involved and other salient features of the computation method. In particular specific numerical difficulties are mentioned, such as these which arose due to the use of a given mesh length in the finite difference computations along with the numerical problems which occurred when considering unloading and strain hardening. Mesh length is discussed with respect to u and v displacements only. No further discussion of the twisting displacements computations is given as this was only an exploratory investigation.

3.8.2 The principal difficulties with the numerical accuracy of the solutions for u and v displacements occurred when columns were so short and heavy that the formation of what could amount to a plastic hinge was required at the centre before collapse was possible (see "The Steel Skeleton" ⁽⁶⁾ pp 273). By assuming that yield in tension constituted failure the necessity for allowing for such behaviour in the theory was avoided but the tension yield criterion still required the existence of considerable curvature gradients and led to some numerical difficulty. Columns 1.1 and 1.2 were the most troublesome in this respect and it is instructive to consider typical difference tables for deflections for one of these members.

3.8.3 The first table shown below is for column 1.2 during a

calculation where a mesh length of $L/10$ was used throughout. The axial load is 7.80 kips and the column is almost to the stage of exhibiting tension yield at the central section.

Station Fig. 3.6(a)	v ins $\times 10^5$	δ	$\frac{\delta^2}{h^2 \rho}$	δ^3	δ^4	Cvr Eqn. 3.32
-1	4305	-818				
0	3487	-305	13	13		
1	2682	-779	26	21	8	-1
2	1903	-732	47	32	11	-1
3	1171	-653	79	56	24	-2
4	518	-518	135	901	845	-70
5	0		1036		-1802	+150

Examination of the table reveals that the curvature at station 4 is only $1/8$ the value at station 5. This results in the fourth order corrections shown in the final column and it is found that no matter how far the table is extended the differences never become small and oscillatory as they should in a "well-behaved" table ⁽¹²⁾. This means that tabulation at a smaller interval is required. However, since away from the influence of the rapid curvature variation, near the column centre, the corrections are small, the use of the smaller interval can be restricted to the central zone.

3.8.4 The second table shown is for the same column carrying an axial load of 7.83 kips but with the mesh length reduced to $L/30$ over the central portion as explained in paragraph 3.7.2. The

table is restricted to the central zone of the column where the mesh is constant. Curvatures in this table may be compared with the curvatures in the first table when multiplied by 9.

Station Fig. 3. 6(b)	v ins. x10 ⁵	δ	$\frac{\delta^2}{\frac{1}{8}h^2\rho}$	δ^3	δ^4	Cvr Eqn. 3. 32
4	437	-180	15	3		
5	257	-162	18	49	46	-4
6	95	-95	67	133	84	-7
7	0		190		-266	+22

From the table it can be seen that the fourth order terms are considerably smaller than the previous values although further reduction in mesh length would obviously improve the result further. Another feature exhibited by the table that is relevant to this discussion is the fact that the curvature at the central station is 60 per cent higher than the value given by using the coarser mesh. This indicates that there are considerable differences in the internal strain distributions particularly at and near the centre of the column. In spite of this the second computation, using the finer mesh, may be taken as sufficiently accurate. This is because at 7.2 kips values of central curvature for the two mesh sizes agree to within $1\frac{1}{2}$ per cent and at 7.0 kips the difference is negligible. Hence the use of the finer mesh should restrict significant error to the load range above about 7.6 kips at which stage the final theoretical collapse load has been so closely approached that the failure load could not

possibly be significantly affected by reducing mesh length further. For this reason additional investigation of mesh size effects was not considered to warrant further attention.

3.8.5 In addition to the problems described above the possibility, with the long and more flexible columns, of a large negative moment producing a significant fourth order correction arose due to the switch from positive to negative curvatures. To check this condition the difference table for deflections for column 3.1 at 3.00 kips was formed. (This case is discussed since the largest negative curvatures occurred here). It was found that despite the retention of the L/10 mesh size in the region of the point of contraflexure the correction terms were reasonably small, e.g. $1/12 \delta^4 v_1 = 2 \times 10^{-5}$ when $v_1 = 7670 \times 10^{-5}$ inches. The corrections rose somewhat above this load but no significant variation in the collapse load was considered likely as the theoretical collapse load of 3.14 kips was only slightly above 3.00 kips.

3.8.6 A further problem arose during the computations which investigated the effects of unloading and strain hardening. This occurred due to a loss in numerical accuracy in solving the equations B.5(a), (b), (c) for b, c, α particularly when α was small. This was because when integrating for the force corrections from the stresses in each of the 70 small rectangles (see Appendix B), it was possible with α extremely close to zero for a whole row of rectangles to change from an unloading

or strain hardening type behaviour to a non-unloading or non-strain hardening type behaviour, due to small changes in b_1 , c , α . Because of this the solution failed to converge unless a certain loss of numerical accuracy was accepted or else if the accuracy requirements were maintained a solution was obtained only by chance and the computation time began to rise. The alternative of using more small rectangles, was not attempted, because this would have also caused the computation time to rise. Therefore some of the computations involving unloading and strain hardening have been terminated prematurely owing to this condition although in all cases sufficient computation has been done to show that the presence of one or both these parameters adequately explains certain discrepancies between experiment and theory. At present an investigation is under way where unloading is neglected and the integration at a section for strain hardening effects is performed analytically. Results will be reported when available.

3.8.7 A further aspect which is of interest is that although the computation procedures were developed to solve the biaxial problem in particular an extension to single axis bending is possible. The method works best when the member fails in the plane of bending but it can also be made to calculate the lateral collapse mode as occurred in column 2.1. By proceeding in sufficiently small increments of spreading plasticity at the central section it is possible to obtain the lateral collapse load as accurately as desired. The problem of

locating directly the exact load where bifurcation of the equilibrium position is first possible has been tackled elsewhere⁽¹⁹⁾ although a method of the type described in sections 3.1 to 3.8 above must be used to obtain the post-buckling behaviour.

3.9 DISCUSSION OF THE THEORETICAL RESULTS AND THEIR COMPARISON WITH THE EXPERIMENTAL RESULTS

3.9.1 As explained previously in paragraphs 2.1.1 and 3.2.1 the chief purpose of the theoretical study was to determine the significant parameters affecting column behaviour. No exhaustive investigation of all the various parameters involved was undertaken, the main effort having been directed towards modifying the computer programme to obtain correlation between experiment and theory, i. e. including the effects of unloading, strain hardening and torsion.

3.9.2 Early in the work it was found that large discrepancies (up to 23 per cent) occurred between experiment and theory when using calculation 1, i. e. the simplest form. Generally however, the theoretical collapse loads were between 0 per cent and 8 per cent below the experimental results but on three columns, viz. 1.1, 1.3 and 3.2, larger discrepancies between 11 per cent and 23 per cent below were obtained. It was an attempt to explain these results which became the major theoretical undertaking of this project. After eliminating a possible influence due to mesh size effects, as explained previously, it was considered that the explanation lay with one of the following:-

- (i) small variations in yield stress,
- (ii) unloading,
- (iii) strain hardening
- (iv) the existence of an upper yield point,
- (v) a combination of all four effects.

The influence of the first three of these parameters was then investigated, where possible, on columns 1.1, 1.3 and 3.2. In addition to these effects calculations were carried out to study the action of torsion moments (these always lower the collapse load) on two columns.

3.9.3 All of the theoretical results have been expressed graphically and they are given, along with the experimental curves, in Figures A.1 to A.20. The calculation method, i. e. whether calculation 1, 2 or 3, is clearly shown in the legend on each graph and the yield stress value in kips per square inch is also indicated.

3.9.4 Column 1.1. (Figures A.1 and A.2)

(i) The results for this column are given in Figures A.1 and A.2. Only major axis deflections and moments are plotted as the minor axis values were negligible throughout. Three theoretical curves are shown. The lowest, curve (A), was calculated with the effect of axial shortening neglected and forms the only instance in the entire series where this occurs. Curve (B) ignores unloading but includes axial shortening, and curve (C) shows the effect of unloading.

(ii) Curve (A) indicates a theoretical collapse load equal to 5.03 kips, a value which is 39 per cent below the experimental result. The curve demonstrates the behaviour expected of elastic-plastic columns in that axial load increases to a maximum and then decreases. It is this maximum value which is taken as the theoretical failure load and it is important to realise that this can occur without requiring the beam moments to become negative. This is due to the dependence of part of the column loading, i.e. the Pv stability moments and beam moments, on the column deformations. At failure and beyond these forces develop rapidly enough to maintain the spread of plasticity in the column without increase in the externally applied axial load. This computation exhibits this type of behaviour. The influence of neglecting axial shortening can best be noticed in the moment-axial load curve. It can be seen that moment values are slightly high compared with the experiment due to neglecting a portion of the moment reducing influence.

(iii) Curve (B) demonstrates the considerable improvement in correlation brought about by considering the effect of moment relaxation due to axial shortening. The last point plotted for this curve occurs at the onset of tension yield so that the corresponding axial load of 7.4 kips is taken as failure. At this stage with a 1 inch deep section subject to major axis moment only the computation indicated $b_1 = 0.96^{in}$, i.e. only 0.04" of the original tension flange remained elastic. Despite this curvatures were still high enough to produce tension yield and

also to cause the maximum compressive strains to exceed 50 times the yield value. It can be seen that allowing for the existence of a plastic hinge in the theory would not improve the correlation of the collapse loads to any extent as the large disagreement of deflections has resulted due to the excessively high central curvature. The existence of some further phenomenon is required to prevent this happening.

(iv) Curve (C) demonstrates the influence of unloading. It was obtained after running the programme for 10 minutes on Atlas. The computation was not continued further as the convergence of the iterative cycles was slow at this stage, see paragraph 3.8.6, and the theoretical and experimental results were beginning to disagree anyhow. Although no tension yield had occurred the maximum compressive strains were 9.5 times the yield values due to the development of an excessive central curvature. It therefore appears that on the basis of the results indicated by both curves (2) and (3) that only the existence of strain hardening can possibly improve the correlation by the desired amount. Unfortunately no proper verification of this will be possible as the requisite basic material properties were not recorded although, as will be seen from the results for later columns, this would be perfectly capable of improving the correlation by the desired amount.

3.9.5 Column 2.1 (Figures A.3 and A.4)

(i) The results for this narrow flanged member are given in Figures A.3 and A.4. The relationship of the observed failure load to the elastic critical load of one flange has already been discussed in Chapter 2, and it is the presentation and discussion of the computer result which will be the chief consideration now. In obtaining the result calculation 1, i. e. ignoring torsion, was used.

(ii) The actual numerical computation was interesting in that the computer programme calculated equilibrium positions above the theoretical collapse load. This was because in order to avoid division by zero at certain places in the programme, a small positive minor axis moment was applied (0.0001 inch kips), which was maintained throughout the computation.

The last equilibrium configuration that was obtained below the elastic critical load of one flange ($P = 1.37$ kips) was at $P = 1.32$ kips. At this point b_1 varied between 0.133, at the column end, and 0.267 at the centre, meaning that the entire compression flange was plastic. When the central b_1 value was incremented the programme was unable to obtain equilibrium shapes and continued to be unable to do so until b_1 equalled 0.367. Subsequent increments then produced a series of equilibrium configurations with the compression flange still remaining entirely plastic initially. Minor axis stability was maintained by the column developing negative deflections so that the original positive moment was effectively acting as a restraint and causing a point of contraflexure to move towards

the centre. A slide rule computation revealed that the distance between the points of contraflexure was such that the Euler load of one flange based on this distance equalled the total axial load on the column. Although the result was of no practical significance it at least provided a check on the functioning of the computer programme.

(iii) The correlation with the experimental results, especially the pattern of major axis moment relaxation and the development of major axis deflections, is considered to be extremely good. The fact that minor axis deflections developed in the experiment below 1.37 kips is attributed to the presence of initial imperfections. **Effects of this type have not been** considered theoretically so that the question cannot be discussed further. The programme is capable of extension to include **such** influences.

3.9.6 Column 2.2 (Figures A.5 and A.6)

(i) This was the column of test 2.1 straightened and with minor axis supporting beams attached. These should theoretically have caused the development of negative minor axis deflections due to axial shortening effects but in fact, due to imperfections, it collapsed with increasing positive ones. For this reason no theoretical result was computed.

3.9.7 Column 1.2 (Figures A.7 and A.8)

(i) The results for this column are shown in Figures A.7 and A.8. Only one set of theoretical curves is given and this was obtained using calculation 1. Theoretical failure in this case was characterised by the existence of tension yield at 8 kips, i. e. at a load 4.8 per cent below the observed failure load. The agreement was considered satisfactory and no further investigation was undertaken. From the result it can be concluded only that the effects of strain hardening and unloading played little part in providing column stiffness. As mentioned in Chapter 2, the values of the angle of twist were so small in this case that their effect can be regarded as negligible.

(ii) Very little further useful discussion of this result is possible except to point out that whilst the theoretical result indicated a predominating build up of major axis deflections nearing failure, the experimental results showed the minor axis ones were predominant. No direct investigation was made of this point but it is assumed that this occurs due to unloading and/or strain hardening, which because of a shape factor effect, will be more significant in the major axis direction. However, since in both experiment and theory both deflection components were increasing it is really only a question of a minor directional change.

3.9.8 Column 3.1 (Figures A.9 and A.10)

- (i) The results for this column are given in Figures A.9 and A.10. There are two sets of theoretical curves plotted, both obtained by calculation 2. Set (A) is for a yield stress of 33 kips per square inch and set (B) for 35 kips per square inch. Corresponding curves were obtained ignoring torsion but these have not been plotted as the two results lie close to one another. Agreement between experimental and theoretical values of all parameters that are plotted is reasonable and no theoretical collapse load is more than 5 per cent different from the observed collapse load.
- (ii) The first set of curves, (A), which was computed using the 33 kips per square inch yield stress, gave excellent agreement between moments although the deflection curves disagreed slightly. The result was obtained using a mesh length of $L/10$ throughout because this corresponded to that used in the torsion sub-routine. This led to the development of high curvatures at the centre before the maximum load was reached and resulted in a tension yield type failure. However, at the stage where theoretical failure occurred ($P = 3.08$ kips) the deflections were increasing quite rapidly with axial load (0.01 inches for a 10 pound change). Twisting displacements did not agree particularly well with the experimental results although the characteristic of decreasing values approaching failure was obtained. For the corresponding result, ignoring torsion, the finer mesh size, $L/30$, was used in the central region and a true maximum of 3.14 kips was obtained.

(iii) The second set of curves, (B), obtained using the higher yield stress, showed better agreement of some variables, notably the twisting displacements, at the expense of others, particularly major axis moments. The latter effect was presumably directly due to the use of the higher yield stress and this in turn produced larger twists because the term $Mx \frac{du}{dz}$ formed a major contribution to the external torque. As occurred when using the lower yield stress value axial load did not produce a maximum although the same flattening of the curves was obtained. The failure load of 3.25 kips, compared with a corresponding figure of 3.35 kips obtained by ignoring torsion.

(iv) The results obtained above show that torsional action has played only a minor role in the failure process. However, it must be acknowledged that due to the use of a coarse mesh size in the finite difference expressions that the influence of this rather small effect has not been obtained accurately. A more accurate assessment will form part of future investigations where a higher order of accuracy is used.

3.9.9 Column 3.2 (Figures A.11 and A.12)

(i) The results for column 3.2 are given in Figures A.11 and A.12. The column is one for which the simplified computation, i.e. calculation 1, did not produce satisfactory agreement. Two further sets were obtained to investigate the effects of unloading and strain hardening. In all the theoretical results the value of initial minor axis moment, as measured in the experiment,

has been increased, 110 inch pounds as against 100 inch pounds in the experiment. This is because the major axis beams were inaccurately welded and were applying a component of minor axis moment, see paragraph 2.7.10. The experimental results plotted show the actual values of minor axis beam moment as recorded during the experiment.

(ii) The curves produced by calculation 1, with a mesh length of $L/10$, indicate failure at a load of 2.7 kips due to yield in tension, a value which is 20 per cent. below the observed figure of 3.4 kips. Agreement between experiment and theory is satisfactory until a load 2.5 kips is reached when major axis deflections begin to develop rapidly.

(iii) Calculation (3) was used in an attempt to improve the correlation and the yield stress was raised to 35 kips per square inch. The result shown was obtained after allowing the computer programme to run for 4 minutes during a development run. It was found that unloading did not explain the discrepancy and no further calculation on this basis was attempted.

(iv) Strain hardening was included in calculation 3 and the programme was run until the cross-section equations failed to produce solutions as explained in paragraph 3.3.6. The stress-strain curve used was that shown in fig. 2.8 except that the yield stress was reduced to 33 kips per square inch. The use of this curve was not strictly valid, however, as the column material was from a different heat treated batch to that tested. The theoretical effect produced by strain hardening is seen in Figures A.11 and A.12 where the major axes stiffness

is adequately explained, but the same detrimental effect on minor axis deflections and moments that was caused by unloading is seen to occur. It is difficult to explain the minor axis behaviour but the explanation is assumed to lie with one or a combination of the following.

1. The material properties given in Figure 2.8 may differ slightly from those of the material used in the column. This could involve variations of yield stress, length of plastic plateau and strain hardening modulus.
2. The existence of accidental end eccentricities. It is known, see column 2.2, that minor axis behaviour is sensitive to small variations of moment when that moment is small. (Note: at 3 kips a 0.007 inch eccentricity would cause the central bending moment to increase from 0.1 inch kips to 0.12 inch kips, i. e. by 20 per cent). This could combine with the material properties effect described above.

3.9.10 Column 3.3 (Figures A.13 and A.14)

(i) Results for this column are given in Figures A.13 and A.14. The curves shown were computed for a yield stress of 35 kips per square inch using calculation 1. A second result using 33 kips per square inch was obtained but is not plotted. It showed the same tendencies throughout but reduced the theoretical collapse load from 3.20 kips to 3.10 kips. This meant that the effect of a 5.5 per cent reduction in the yield stress was to cause a 4.8 per cent reduction in the collapse load, i. e. a roughly proportional change. Both results however, were regarded as

being in satisfactory agreement with the experiment.

(ii) The major axis beam moments were slightly high throughout the calculation, but the difference was quite small. Some improvement occurred when using the lower yield stress value so that this was presumably due to minor variations in material properties. An interesting feature of the computations also occurred here in that major axis deflections tended to decrease after the maximum load had been reached and the beam moments increased, but only slightly. This is evidently a property of the theoretical solution.

3.9.11 Column 3.4 (Figures A.15 and A.16)

(i) The results for this column are given in Figures A.15(a), (b), and A.16(a), (b). Two sets of curves are shown, one using the simplified method, calculation 1, and a second, calculation 2, which includes the effects of torsion. Twisting displacements are plotted in addition to u and v displacements.

(ii) Calculation 1 produced a result for which the collapse load was very slightly above the observed failure load; 2.26 kips as against 2.24 kips for the experiment. Generally throughout the agreement between observed and theoretical values was excellent. This is probably brought about by the slender minor axis beams permitting collapse without requiring the development of large amounts of plasticity. Thus the effects of unloading and strain hardening are largely ruled out.

(iii) Calculation 2 provides a second example where the influence of torsional displacement components is illustrated. Their inclusion caused the failure load to drop from 2.26 kips to 2.11 kips, i. e. by 6.6 per cent. Figure A.16(b) shows that despite the large number of assumptions used in the torsion calculation there is reasonably good agreement of experimental and theoretical twist values. The main discrepancy is that theoretical twist values do not decrease when approaching the collapse load as the experimental quantities do. This results in an exaggerated reduction of the collapse load and causes a slight worsening of the agreement of the minor axis moment and deflection curves. The difference is not large. The importance of these results, however, is that the 6.6 per cent reduction calculated is an accurate and reliable figure for the twist values used and it is not clouded by the existence, in this case, of large curvature gradients near the centre. Furthermore, it indicates that even by over-estimating the magnitude of the twist values that the collapse load reduction is not exceptionally large.

3.9.12 Column 1.3 (Figures A.17 and A.18)

(i) The results for this column are given in Figures A.17 and A.18. In this case, as with columns 1.1 and 3.2, the curves obtained by calculation 1 did not produce satisfactory agreement with the experiment. Inclusion of unloading caused no significant improvement but the inclusion of strain hardening effects was found to be capable of explaining the column strength.

(ii) Calculation 1 indicated failure at 6.0 kips, i. e. 23 per cent below the experimental value of 7.8 kips, due to yield in tension. A mesh length of $L/10$ was used to obtain this result. Agreement of all curves was satisfactory until near the theoretical failure load where the experimental column apparently gains some extra reserve of stiffness.

(iii) Calculation 3 was next used to investigate the effect of unloading and the curve shown indicates the result obtained after allowing the computer programme to run for 4 minutes during a trial run. No significant improvement in the correlation was apparent and no further computation was attempted.

(iv) Strain hardening effects were next included in the analysis and the computer programme was allowed to run until the numerical accuracy problems, described in paragraph 3.8.6, occurred. The stress-strain curve, which was obtained experimentally (see Figure 2.8 and paragraph 2.6.5) was used as the basis of the calculation. Immediate improvement of the correlation occurred and it was concluded that strain hardening was the chief source of column stiffness above 6 kips. Results are now awaited from the analytical integration method discussed previously, paragraph 3.8.6.

3.9.13 Column 1.4 (Figures A.19 and A.20)

- (i) The results for this column are shown in Figures A.19 and A.20. Only one set of theoretical curves is given and this was obtained using calculation 1. A yield stress of 33 kips per square inch was adopted. The theoretical collapse load of 6.9 kips compares favourably with the observed value of 7.4 kips, a difference of 6.8 per cent.
- (ii) Reference to Figure A.19 shows that above a load of 4.5 kips the theoretical minor axis beam moments tend to be too small. Figure A.20 shows that this is accompanied by slightly excessive major and minor axis deflections. On the basis of previous calculations it was presumed that exact correlation could be produced by modifications to the yield stress value or by the inclusion of strain hardening. The errors were not considered large enough to make this worthwhile.
- (iii) The solution itself exhibited the same characteristics as that for column 3.3 except that the positions of major and minor axis deflections were reversed. Thus, following the maximum load, minor axis deflections decrease and major axis ones increase. The beam moments exhibit corresponding characteristics.

3.10 CONCLUSIONS ON THEORETICAL RESULTS

3.10.1 Generally speaking, the aims of the theoretical study as described in section 3.2 have been achieved. A computation procedure has been developed and the important factors, residual stress apart, required in the analysis of a column bent in symmetrical single curvature have been determined. The results of these findings are summarised below.

1. The collapse load computed on the basis of ignoring unloading and strain hardening produces a conservative estimate of the collapse load.
2. The influence of unloading is to increase the collapse load. No general proof of this statement has been given but the theoretical results obtained tend to confirm the belief.
3. The influence of strain hardening is to increase the collapse load. In cases where heavy major axis moment has been applied and the plastic plateau of the stress-strain curve is short, it has been shown to provide a major contribution to column stiffness. The effect does not appear to depend on the length of the column to any large extent.
4. Small changes in the yield stress produce more or less proportional changes in the collapse load.
5. The collapse load is sensitive to changes in beam stiffness. This conclusion corresponds to conclusion 2 of paragraph 2.8.1 at the end of the experimental chapter.
6. The theoretical results obtained by ignoring strain hardening indicate a significant decrease in the load-carrying

capacity due to high initial moments in certain cases, viz. 3.2 and 1.3. This means that conclusion 1 of paragraph 2.8.1 may have to be viewed with some reservations as it appears that for a material with a large plastic plateau that the collapse load could be lowered. It would be interesting to repeat tests 3.2 and 1.3 with such a material.

7. The reduction in the load-carrying capacity due to torsional displacements is not large. No thorough investigation has been made of this aspect but the two results calculated, along with the experiments, tend to confirm it. However, since the influence of unloading raises the collapse load and torsion decreases it there are two phenomena working in opposite directions which may not always cancel. The best hope of eliminating the awkward twisting displacements from consideration lies with proving their influence is small and this matter should receive further attention.

CHAPTER 4

A DESIGN APPROACH

4.1 INTRODUCTION

4.1.1 In Chapter 1 it was mentioned that a possible approach to structural design could be based on assuming suitable deflection configurations and force distributions for the structure. In so far as the design of columns in the elastic-plastic range is concerned, this requires the calculation of internal forces, caused by the assumed deflections, and their comparison with the corresponding external forces. For satisfactory performance of any chosen member the internal forces must equal or exceed the external ones at all sections of the column. The purpose of this chapter is to show how, at a particular section, given values of axial load, major and minor axis moments to be resisted, and principal curvatures ρ_ξ, ρ_η , the internal forces may be obtained and the requisite comparisons made. The selection of which particular cross section or cross sections should be checked is not discussed, however. It is assumed the critical section(s) are known.

4.1.2 For this purpose the equations for internal resistance, developed in Chapter 3, have been non-dimensionalised and presented graphically in Figure 4.1 so that a single entry to the chart provides immediate values of the internal forces. In particular equations 3.17 have been used, i. e. strain reversal, strain hardening, torsion and tension yield are all ignored, to

obtain values of $M_{\xi}/D(P_y - P)$ and $M_{\eta}/D(P_y - P)$ corresponding to constant values of $D^3 \rho_{\xi}/(P_y - P)$ and $D^3 \rho_{\eta}/(P_y - P)$ obtained from equations 3.13 and 3.17(a). Hence by assuming the axial load condition is satisfied, i. e. internal and external P values are equal, it is a simple matter to use the given curvatures and the chart to obtain internal moments and check the section.

4.1.3 The assumptions upon which the calculations for the curves have been made are as follows:

1. Torsional effects are insignificant and can be neglected for restrained columns.
 2. The effect of unloading is to increase the collapse load so that neglecting its effect, as is done, is to be conservative.
 3. No yield in tension occurs.
 4. Imperfections can be considered by increasing the external loads.
- These assumptions are discussed below and justified, as far as possible, for columns bent in symmetrical single curvature. Although they may possibly apply to a wider range of loading conditions the basic investigation has not been undertaken so that for the present their application must be limited to columns bent in symmetrical or near symmetrical single curvature.

4.1.4 The first of these assumptions is considered justified on the basis of the experimental and theoretical results reported in the previous chapters. Experiments with model Universal H-columns of slenderness ratio up to 100 have been conducted without any evidence of twist increasing significantly during the actual physical

collapse. This was confirmed to some extent by the theoretical calculations where the limited number of results obtained showed its effect on the collapse load was small, see paragraph 3.10.1. Slenderness ratios above 100 generally only arise with narrow flanged I type members which are usually subjected to primary major axis bending moments only. Here again the only result available, column 2.1, shows that lateral stability can be checked by ignoring torsion and calculating the elastic critical load of one flange. However, although the mathematical equations below apply to any shape of section the approach is intended to apply particularly to Universal H-column sections.

4.1.5 Regarding the second assumption it has been shown that for the particular cases in which unloading was considered it has been shown to increase the collapse load. Although this cannot be proved generally, see paragraph 3.10.1, these tendencies shall be considered to apply unprovisionally to all columns bent in symmetrical or near symmetrical curvature.

4.1.6 Yield in tension is eliminated by a suitable check in the method. No investigation has been made of imperfections, i. e. residual stress and initial deflections. However, it is essential to the approach that residual stress, in particular, be eliminated from the graphical procedure since otherwise division of equations 3.17 in pairs cannot be performed and the simple chart shown cannot be drawn.

4.2 PRINCIPLE OF THE METHOD

4.2.1 From the assumptions and discussion above, it is seen that the basic mathematical equations upon which the procedure has been based are equations 3.17. Since torsional effects have been ignored the subscript symbols ξ and η may be replaced by X and Y to conform to the more usual notation used in the bi-axial bending expressions. Similarly coordinates ξ and η are changed to x and y. In this form the equations become,

$$P - P_y = \sigma_y \left[\left\{ b_1 - \left(\frac{1}{2} D \cos \alpha + \frac{1}{2} B \sin \alpha \right) \right\} A_T - \int_{A_p} m' dA \right] / c \quad 4.1(a)$$

$$M_X = \sigma_y \left[I_X \cos \alpha - \int_{A_p} m' y dA \right] / c \quad 4.1(b)$$

$$M_Y = \sigma_y \left[I_Y \sin \alpha - \int_{A_p} m' x dA \right] / c \quad 4.1(c)$$

4.2.2 To non-dimensionalise these expressions equation 4.1(a) is divided by D^3 and equations 4.1(b) and 4.1(c) by D^4 . Therefore,

$$\frac{(P - P_y)/D^3}{(cD^3)} = \sigma_y \left[\left\{ b_1 - \left(\frac{1}{2} D \cos \alpha + \frac{1}{2} B \sin \alpha \right) \right\} A_T - \int_{A_p} m' dA \right] \quad 4.2(a)$$

$$\frac{M_X/D^4}{(cD^4)} = \sigma_y \left[I_X \cos \alpha - \int_{A_p} m' y dA \right] \quad 4.2(b)$$

$$M_Y/D^4 = \sigma_y \left[I_Y \sin \alpha - \int_{A_p} m' x \, dA \right] / (cD^4) \quad 4.2(c)$$

Considering the terms on the right hand side in square brackets it is seen that if b_1/D , B/D , m'/D , A_T/D^2 , etc., are all replaced by b_1 , B , m' , A_T , etc., these new symbols will represent quantities on a scaled down section. This section will have D equal to 1 inch and all other sizes reduced proportionately. Quantities on the left hand side and c will still apply to the full-sized column, however. The equations thus become,

$$(P - P_y)/D^3 = \sigma_y \left[\left\{ b_1 - \left(\frac{1}{2} \cos \alpha + \frac{1}{2} B \sin \alpha \right) \right\} A_T - \int_{A_p} m' dA \right] / c \quad 4.3(a)$$

$$M_X/D^4 = \sigma_y \left[I_X \cos \alpha - \int_{A_p} m' y \, dA \right] / c \quad 4.3(b)$$

$$M_Y/D^4 = \sigma_y \left[I_Y \sin \alpha - \int_{A_p} m' x \, dA \right] / c \quad 4.3(c)$$

Division in pairs and multiplication of both sides by -1 produces the results,

$$M_X / \left[D(P_y - P) \right] = F_1(\alpha, b_1) \quad 4.4(a)$$

$$\text{and } M_Y / \left[D(P_y - P) \right] = F_2(\alpha, b_1) \quad 4.4(b)$$

where the functions F_1 and F_2 are computed in non-dimensionalized form, i.e. for the scaled-down or reduced sized section.

4.2.3 Non-dimensionalised curvature functions can be found beginning with equations 3.13(a) and (b). In the present notation these become,

$$\rho_X = \sigma_y \cos \alpha / (EC) \quad 4.5(a)$$

$$\text{and } \rho_Y = \sigma_y \sin \alpha / (EC) \quad 4.5(b)$$

Introducing equation 4.3(a) into these relationships leads to the final results,

$$D^3 \rho_X / (P_y - P) = - \cos \alpha / \left[E \left(\left\{ b_1 - \left(\frac{1}{2} \cos \alpha + \frac{1}{2} B \sin \alpha \right) \right\} A_T - \int_A m' dA \right) \right] \quad 4.6(a)^*$$

and

$$D^3 \rho_Y / (P_y - P) = - \sin \alpha / \left[E \left(\left\{ b_1 - \left(\frac{1}{2} \cos \alpha + \frac{1}{2} B \sin \alpha \right) \right\} A_T - \int_A m' dA \right) \right] \quad 4.6(b)^*$$

where again the quantity in square brackets must be computed in non-dimensional form.

4.2.4 Since equations 4.1 contain no allowance for yield in tension this must be prevented. Referring back to Figure 3.3 of Chapter 3 it can be seen that the requisite condition is,

* These functions are not fully non-dimensionalised. To do this both sides should be multiplied by E. However, the expression is left in this form since it simplifies the design calculation.

$$\sigma_y (b_1 + c - D \cos \alpha - B \sin \alpha) / c + \sigma_y > 0 \quad 4.7$$

which becomes on rearrangement,

$$2c > D \cos \alpha + B \sin \alpha - b_1 \quad 4.8$$

Using equation 4.1(a) to eliminate c , the condition becomes,

$$\begin{aligned} -2\sigma_y \left[\left\{ b_1 - \left(\frac{1}{2} D \cos \alpha + \frac{1}{2} B \sin \alpha \right) \right\} A_T - \int_{A_p} m' dA \right] / (P_y - P) \\ > D \cos \alpha + B \sin \alpha - b_1 \end{aligned} \quad 4.9$$

or

$$\begin{aligned} -2\sigma_y \left[\left\{ b_1 - \left(\frac{1}{2} D \cos \alpha + \frac{1}{2} B \sin \alpha \right) \right\} A_T - \int_{A_p} m' dA \right] / \left[\Delta \sigma A_T \right] \\ > D \cos \alpha + B \sin \alpha - b_1 \end{aligned} \quad 4.10$$

where $\Delta \sigma = (P_y - P) / A_T$ is the difference between the yield stress and the average stress over the section. If both sides of the equation are divided by D then the condition is,

$$\begin{aligned} -2\sigma_y \left[\left\{ b_1 - \left(\frac{1}{2} D \cos \alpha + \frac{1}{2} B \sin \alpha \right) \right\} A_T - \int_{A_p} m' dA \right] / D^3 / \left[\Delta \sigma A_T / D^2 \right] \\ > \cos \alpha + B \sin \alpha / D - b_1 / D \end{aligned} \quad 4.11$$

so that introducing the non-dimensionalised parameters the result,

$$-2 \sigma_y \left[\left\{ b_1 - \left(\frac{1}{2} \cos \alpha + \frac{1}{2} B \sin \alpha \right) \right\} A_T - \int A_p m' dA \right] / (\Delta \sigma A_T) > \cos \alpha + B \sin \alpha - b_1 \quad 4.12$$

is obtained. Since the expression $\left[\left\{ b_1 - \left(\frac{1}{2} \cos \alpha + \frac{1}{2} B \sin \alpha \right) \right\} A_T - \int A_p m' dA \right]$ is always negative for a compressive load 4.12 can be rewritten as,

$$\Delta \sigma < -2 \sigma_y \left[\left\{ b_1 - \left(\frac{1}{2} \cos \alpha + \frac{1}{2} B \sin \alpha \right) \right\} A_T - \int A_p m' dA \right] / \left[A_T (\cos \alpha + B \sin \alpha - b_1) \right] \quad 4.13$$

4.2.5. The solution of the mathematical equations above relating geometry and forces, as well as the checking of the tension yield condition, is undertaken graphically in the design method. The relevant curves are shown in Figure 4.1 where the two sets of heavy lines represent curves of constant value of $D^3 \rho_X / (P_y - P)^*$ and $D^3 \rho_Y / (P_y - P)^*$ and the lighter set constant values of $\Delta \sigma$. Numerical values for the heavy lines were obtained by computing the non-dimensionalised functions in square brackets of the equations 4.3 for various values of b_1 and α . These were then divided in pairs to obtain $M_X / D(P_y - P)$ and $M_Y / D(P_y - P)$ and the expressions 4.6 used to obtain corresponding values of $D^3 \rho_X / (P_y - P)$ and $D^3 \rho_Y / (P_y - P)$. Interpolation of the results enabled the particular

* $E = 30000 \text{ kips inches}^{-2}$

constant curvature lines shown to be plotted. The ΔO curves were obtained in the same fashion using condition 4.13 as an equation and taking $\sigma_y = 36$ kips per inch².

4.2.6 Whilst the equations above have been non-dimensionalised the various Universal column sections are shaped differently and cannot therefore be represented by one set of curves. The set shown is for a 14 x 16 x 426 lbs. U.B. and should strictly only be used for checking this particular member. Although it has not been investigated it is possible that other sections can be checked on these curves and it is likely that all sections can be checked, with reasonable accuracy, by three or four sets.

4.2.7 Before considering how the diagram, Figure 4.1, can be used for column checking one further feature of it will be explained. It can be seen that the curves which represent constant curvature functions all pass through either A or B. These points correspond to extremely high curvatures and their coordinates cannot be obtained numerically since they represent a limiting condition requiring the division of (\dot{a}/a) . Reference to Figure 4.2 shows a single curve of constant $D^3 \rho_X / (P_y - P)$, the line CA, in a skeleton graph. When α is zero, as at C, the value of $M_Y / D(P_y - P)$ is also zero but in moving towards A an increase in α occurs accompanied by an increase in $M_Y / D(P_y - P)$ and a decrease in $M_X / D(P_y - P)$.

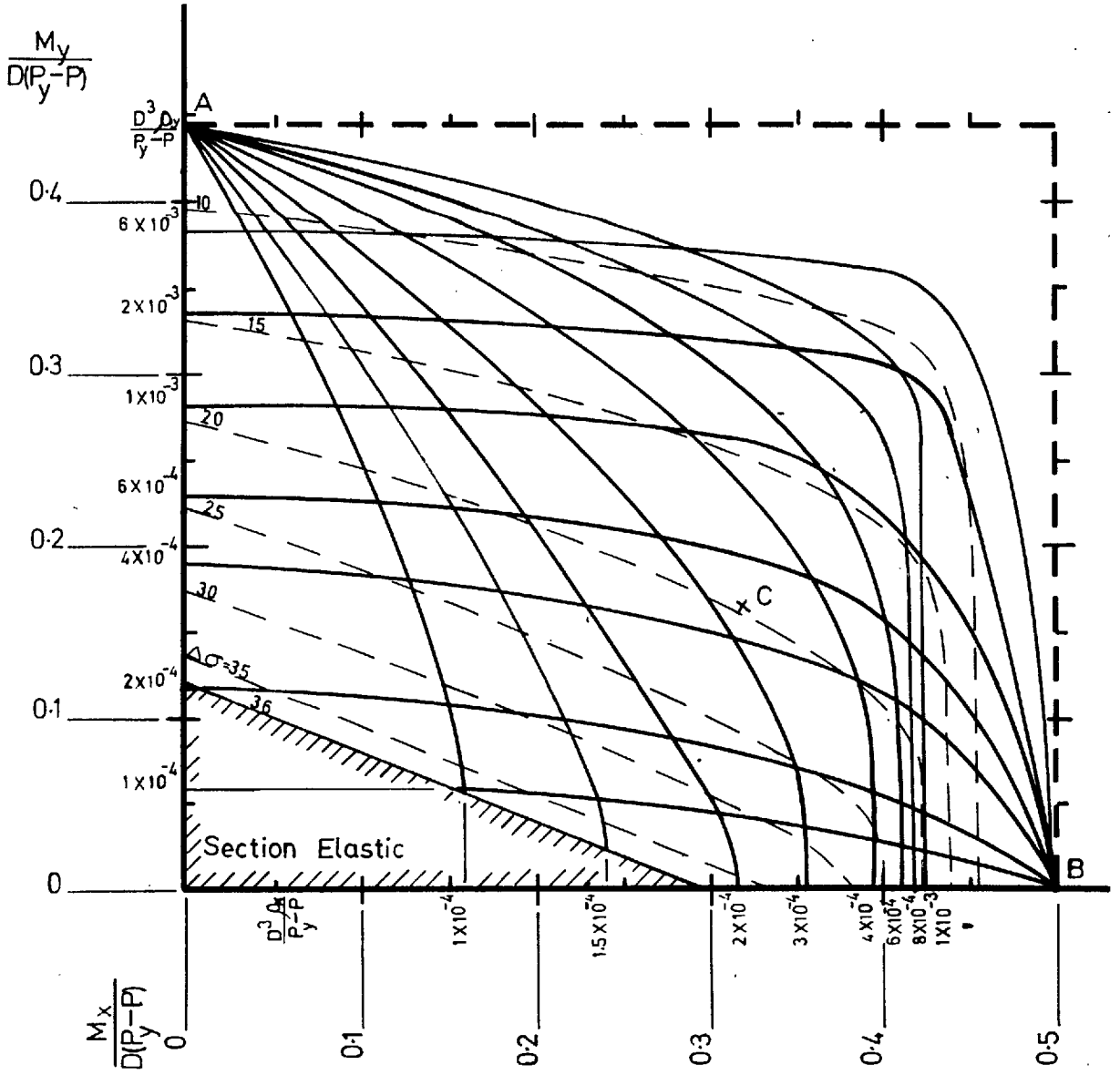


FIG. 4.1

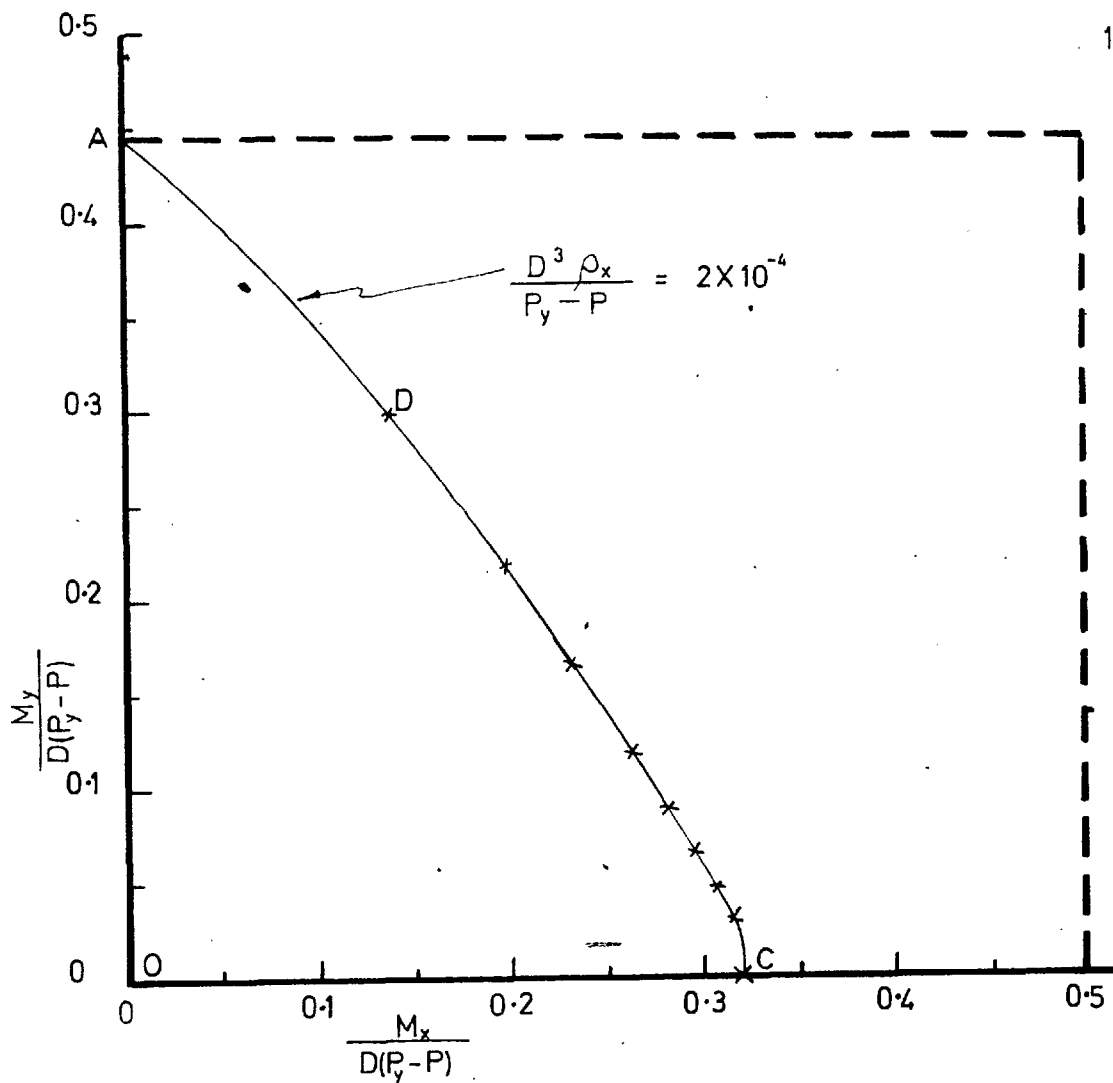


FIG. 4.2

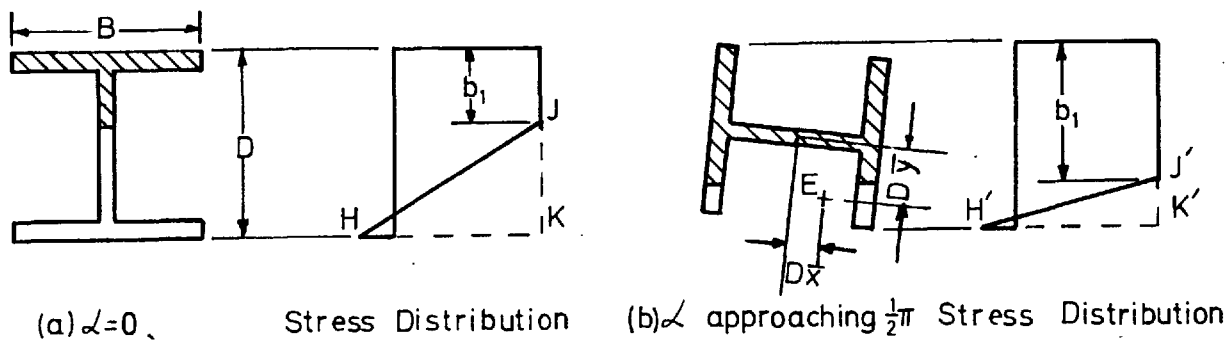


FIG. 4.3

In order that $D^3 \rho_X / (P_y - P)$ remains constant the value of b_1 must also increase as can be seen by referring to Figures 4.3(a) and (b). In Figure 4.3(a) the angle α is zero. The value of $(P_y - P)$ is the integral of the stresses HJK over the unshaded elastic area and the curvature is given by the slope of the line HJ. In Figure 4.3(b) α is shown approaching $\pi/2$ and b_1 is shown at an increased value. Obviously $(P_y - P)$ is smaller as consequently the resolved slope of H'J' must be to hold the curvature function constant. Other possibilities, not requiring an increase in b_1 , come to mind but they can be rejected on the basis of various arguments, e.g. ρ_X and $(P_y - P)$ both increasing with b_1 decreasing is eliminated because with α approaching $\frac{1}{2}\pi$ and yield in tension ignored $(P_y - P)$ would eventually change sign. Other cases can be argued similarly so that by a process of elimination the only remaining possibility is that as α approaches $\frac{1}{2}\pi$ then b_1 approaches B.

4.2.8 To deduce the actual value of the limits a simple geometric interpretation of equations 4.4 is used. If these are written in the form,

$$M_X / D(P_y - P) = \bar{y} \quad 4.14(a)$$

$$M_Y / D(P_y - P) = \bar{x} \quad 4.14(b)$$

or, alternatively as,

$$M_X = (P_y - P)(D\bar{y}) \quad 4.15(a)$$

$$M_Y = (P_x - P)(D\bar{x}) \quad 4.15(b)$$

then evidently the values $D\bar{y}$ and $D\bar{x}$ are the coordinates of the centroid of the force $(P_y - P)$, drawn at E in Figure 4.3(b). (This is a full-sized member, whereas \bar{x} and \bar{y} are values appropriate to a non-dimensionalised or scaled-down section). Obviously as α approaches $\frac{1}{2}\pi$ the elastic portions of the flanges become equal and $D\bar{x}$ approaches zero whilst with b_1 approaching B, $D\bar{y}$ approaches $B/2$, or in the non-dimensionalised form \bar{y} approaches $B/2$. A similar type of situation arises as α approaches zero with the positions of the moment functions reversed. Mathematically these conditions can be stated as,

$$\lim_{\alpha \rightarrow \pi/2} M_X / D(P_y - P) = 0 \quad 4.16(a)$$

$$\lim_{\alpha \rightarrow \pi/2} M_Y / D(P_x - P) = B/2 \quad 4.16(b)$$

$$\lim_{\alpha \rightarrow 0} M_X / D(P_y - P) = 1/2 \quad 4.16(c)$$

$$\lim_{\Delta \rightarrow 0} M_Y / D(P_Y - P) = 0$$

4.16(d)

4.3 USE OF THE CURVES

4.3.1 Given external values of the forces P , M_X , M_Y and curvatures ρ_X and ρ_Y at a section the adequacy of a column can be checked by the following procedure.

1. Calculate $(P_y - P)$ on the basis of $\sigma_y = 36$ kips per inch².
2. Calculate $M_X / D(P_y - P)$, $M_Y / D(P_y - P)$, $D^3 \rho_X / (P_y - P)$, $D^3 \rho_Y / (P_y - P)$ and $\Delta \sigma (= (P_y - P) / A_T)$.
3. Using the computed values of $D^3 \rho_X / (P_y - P)$ and $D^3 \rho_Y / (P_y - P)$ locate a point on the design curves, Figure 4.1, by interpolation between the appropriate curvature function lines. Read off values of $M_X / D(P_y - P)$ and $M_Y / D(P_y - P)$ from the axes.
4. If the section is adequate then these values of $M_X / D(P_y - P)$ and $M_Y / D(P_y - P)$ must be larger than the externally computed ones. Additionally the value of $\Delta \sigma$ read off the chart should be greater than the value of $\Delta \sigma$ calculated in step (2) above.

4.3.2 Example

(i) Consider that a 14 x 16 x 420 lbs. U.B. is to be checked under the following conditions.

$$P = 3500 \text{ kips. } M_X = 4800 \text{ inch kips. } M_Y = 2500 \text{ inch kips.}$$

$$\rho_X = 5 \times 10^{-5} \text{ inches}^{-1}. \quad \rho_Y = 7 \times 10^{-5} \text{ inches}^{-1}.$$

(ii) The following quantities may be calculated from this data,

$$P_y - P = 1009 \text{ kips}$$

$$M_X / D(P_y - P) = 0.254, \quad M_Y / D(P_y - P) = 0.133,$$

$$D^3 \rho_X / (P_y - P) = 3.27 \times 10^{-4} \text{ kips}^{-1} \text{ inches}^2,$$

$$D^3 \rho_Y / (P_y - P) = 4.58 \times 10^{-4} \text{ kips}^{-1} \text{ inches}^2,$$

$$\Delta \sigma = 8.06 \text{ kips inches}^{-2}.$$

3. Reference to Figure 4.1 shows the point C located by the curvature functions where obviously internal forces are higher than the corresponding external ones so the loads can be stably supported. In addition for the point C located, $\Delta \sigma \doteq 19 \text{ kips per inch}^{-2}$, which is greater than the figure above so that no yield in tension occurs.

CHAPTER 5

CONCLUSIONS AND NOTES RELEVANT TO FUTURE WORK

The work has investigated both experimentally and theoretically the behaviour of elastic-plastic, elastically restrained, H-section columns bent in symmetrical single curvature about two axes. Ten columns in all have been studied for which correlation between experimental and theoretical collapse loads has been obtained to within 8 per cent, except for one case, where the difference was 11 per cent. The following points summarise the findings and give information that should be helpful in future investigations.

5.1 Significant Features of the Column Analysis

The work has indicated most of the important factors which should be included in the analysis of a column bent in symmetrical single curvature. The influence of unloading has been considered as well as strain hardening and torsion although further investigation of some of these aspects would be desirable. It has been shown that unloading is not extremely important except, perhaps, when columns are subjected to very heavy initial moments from stiff restraining beams, e.g. column 1.1. Its effect is to raise the collapse load but as, in general, this does not appear to be by extremely large

amounts it would seem justifiable and convenient to omit this awkward feature from future investigations. Strain hardening, however, should be included as it has been shown for a column bent by heavy major axis moment and made of material with a short plastic plateau, e. g. columns 3.2 and 1.3, that the collapse load is raised considerably. Torsion is discussed separately in section 5.3.

5.2 Beam Stiffness and Beam Loads

Variations of minor axis beam stiffness appear to affect the collapse load considerably, e. g. the collapse load of column 3.4 is 55 per cent of the squash load which compares with the other columns of the same dimensions whose collapse loads are all above 75 per cent of the squash load. Major axis beam stiffness appears to matter less as shown by the collapse load of column 1.4 being 7400 pounds as against a column, viz. 1.3, of similar dimensions whose collapse load was 7800 pounds. Likewise variations in beam loads, equivalent to variations of initial moments in this thesis, appear to have little effect on the collapse load provided minor axis beam loads are not large*. However, in two instances, i. e. with columns 3.2 and 1.3, the existence of strain hardening at a fairly early stage was required to make this so; see also sections 3.10 and 5.1. Beam load

* The case of minor axis bending only is discussed elsewhere, e. g. reference 6, where significant reductions in load carrying capacity occur with heavy beam loads.

effects might therefore usefully receive further investigation with a different column material.

5.3 Torsional Action

Torsional action, for the load path adopted in this project, i. e. beam loads followed by axial load, does not appear to be an important consideration. However, work by Campus and Massonnet ⁽¹⁹⁾, and more recently in the U. S. A. ⁽²⁰⁾, on the lateral-torsional behaviour of pin-ended members, bent by eccentric loading in the plane of the web, indicates a much larger effect under these circumstances. Torsional action should therefore be more carefully investigated for biaxial bending cases under alternative loading paths.

5.4 Residual Stresses

Residual stresses are known to be the major column imperfections in pin-ended axially loaded members ⁽⁶⁾⁽²¹⁾. Their effect is less when the loading is eccentric and decreases as the eccentricity increases. It is possible for restrained columns that their effect is extremely small as was suggested by the reloading of column 1.3 after straightening it. This requires further verification however. Theoretically, this problem can be tackled by making a minor modification to the computation of this thesis which evaluates unloading effects. This will require the use of a finer sub-division into infinitesimal rectangles than that used so far and the computation required will be quite time consuming, even for a

computer.

5.5. Computation Procedure

It is felt that the computation procedure developed in this thesis with its full computerization will be of advantage particularly when the extension to unsymmetrical bending is being considered and adjustment of parameters at a large number of station points is required. Methods such as the one employed, in reference 15, where displacements ϵ_{av} , $\frac{d^2u}{dz^2}$, $\frac{d^2v}{dz^2}$, $\frac{d^2\phi}{dz^2}$ are adjusted manually, do have the advantage of knowing more of what is happening during the calculation. However, this could get tedious (it certainly must waste computer time) in dealing with unsymmetrical problems.

A further interesting comparison of the method of reference 15 and that of this thesis is the actual method of computing equilibrium configurations. As explained above the quantities ϵ_{av} , $\frac{d^2u}{dz^2}$, $\frac{d^2v}{dz^2}$, $\frac{d^2\phi}{dz^2}$ are adjusted at each station which means that if six station points are used, $6 \times 4 (= 24)$ simultaneous non-linear algebraic equations must be solved less the fixed boundary conditions which reduce it to 19. By the approach of this thesis the maximum number which must be solved at any one time is 5, when adjusting the twisting displacements, although a smaller number of equations must be solved several times. If both methods were fully computerized (the method of

reference 15 is capable of being computerised), it would be interesting to compare their computing efficiencies. Such a comparison at this stage is not possible.

5.6 Experimental Rig

The experimental rig that was used, whilst satisfactory in the present tests, is subject to one very important limitation; it cannot easily be extended to investigating unsymmetrical loading conditions. This is largely due to the unstable nature of the Buckton dead load machine that was used and the fact that the column shortens axially. The first difficulty means that random rigid body motions of the column can occur and, with the beam ends fixed in space, induce extraneous column bending moments. This may be overcome by building a more rigid loading frame to which the beam ends are connected. However, if due to axial shortening, equal changes of beam moments at the two column ends are required, each beam, at its turnbuckle end, must also be allowed to move in an appropriate manner. The present turnbuckle support screws should be capable of performing this function. In addition the end bearings will have to be modified to be capable of supplying horizontal reactions without jamming, probably by inserting bearings in the space that occurs in the present design.

5.7 Design Approach

The design curves developed show how three dimensional moment (M_X and M_Y)-curvature-axial load relationships may be represented, in a limited sense, on a two dimensional diagram. They are intended for use in checking members by a design approach in which the deflected shape of the column is assumed. From a knowledge of the external moments and axial load, and the column curvatures at any section, it is possible to check whether a particular member is adequate. It is realised that design methods such as this are in the embryo stage so far as elastic-plastic members are concerned, e.g. it is not yet known how to select the critical section(s) in the member for checking, but it is hoped that as these are developed the curves presented will be of some value.

5.8 Plastic Hinges

In future investigations it may be desirable to allow for plastic hinge action in the columns to compute, in particular, the falling branch of the axial load - deflection curves to determine whether the load capacity drops off rapidly, leading to a catastrophic type of failure. In this connection it should be noted that the calculation procedure described above always computes firstly the loads at the most heavily loaded section, the central section, and so avoids attempting to solve equations 3.12 for unreal values. Thus the solution with plastic hinges creates no special difficulties provided strain reversal is

ignored. After a certain stage a plastic hinge is inserted and the calculation proceeds in increments of slope at the central section instead of central curvature. A minor modification of the finite difference expression is required at the central section, but this difficulty is not insurmountable.

APPENDIX A

A.1 PLASTICITY CORRECTIONS

A.1.1 The corrections to the force equations for plastic yield begin by calculating the stress excess values at the twelve positions shown in Figure A.A1. For the three separate cross-sectional elements shown, these quantities are sufficient to allow stress excess at any point in the cross-section to be determined. All of these values can, and have been expressed in terms of the parameters b , c , α where c and α are defined as they were in Chapter 3, but b is taken to mean b_1 , or b_2 , depending on whether the correction is for compression or tension yield.

A.1.2 Lending consideration to the type of yield zones that can arise under the plane sections remaining plane assumption, it will be observed that if general formulae for the types shown in Figure A.A.2 are calculated, then the complete range will be covered. In Figure A.A.2 the m values are the stress excess quantities which, when substituted into the formulae below, allow the magnitude of the axial load correction to be calculated and its line of action to be located. In both cases this latter function is performed by taking moments about the lines AB or A'B' and AC or A'C'. The double or volumetric integrals which are required are as follows:

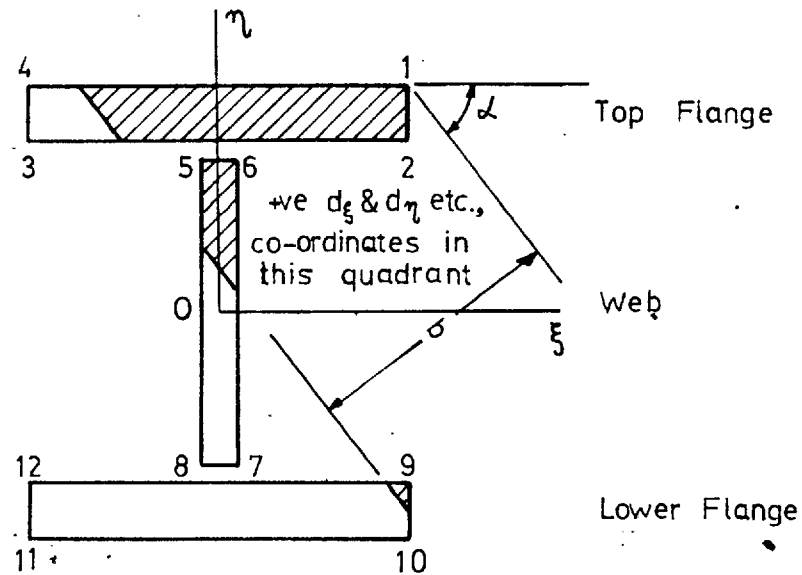
(a) Type 1 Zone

(i) axial load correction F

$$= dt(m_1 + m_2 + m_3 + m_4)/4 - t^2 \cot\beta (m_1 + 2m_2 + 2m_3 + m_4)/12$$

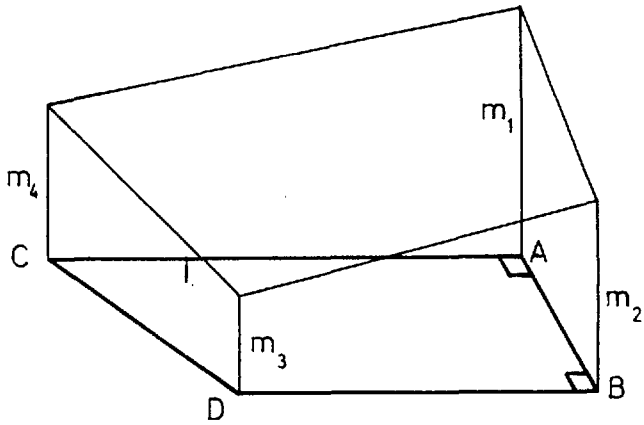
A.1(a)

(ii) moment about AB, M_{AB}

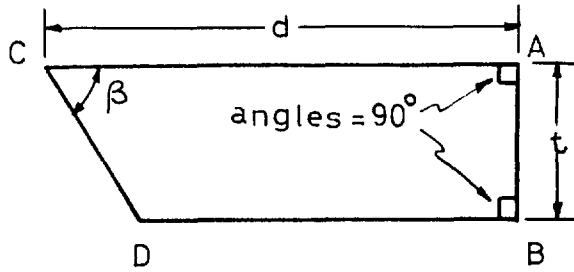


Point	Stress Excess (f)
1	$\sigma_y(b)/c$
2	$\sigma_y(b - t_f \cos \alpha)/c$
3	$\sigma_y(b - t_f \cos \alpha - B \sin \alpha)/c$
4	$\sigma_y(b - B \sin \alpha)/c$
5	$\sigma_y(b - 0.5B \sin \alpha - 0.5t_w \sin \alpha - t_f \cos \alpha)/c$
6	$\sigma_y(b - 0.5B \sin \alpha + 0.5t_w \sin \alpha - t_f \cos \alpha)/c$
7	$\sigma_y(b - 0.5B \sin \alpha + 0.5t_w \sin \alpha - D \cos \alpha + t_f \cos \alpha)/c$
8	$\sigma_y(b - 0.5B \sin \alpha - 0.5t_w \sin \alpha - D \cos \alpha + t_f \cos \alpha)/c$
9	$\sigma_y(b - D \cos \alpha + t_f \cos \alpha)/c$
10	$\sigma_y(b - D \cos \alpha)/c$
11	$\sigma_y(b - D \cos \alpha - B \sin \alpha)/c$
12	$\sigma_y(b - D \cos \alpha - B \sin \alpha + t_f \cos \alpha)/c$

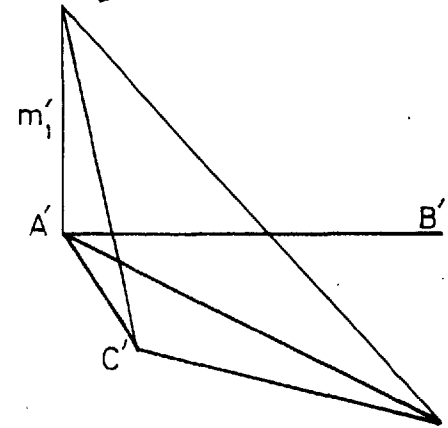
FIG. A-A1



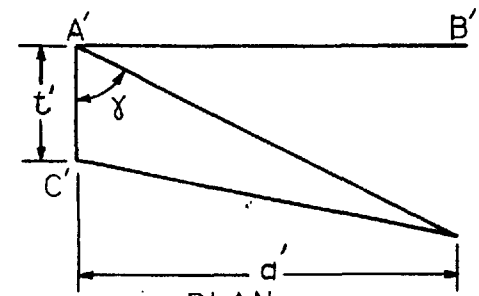
3-D Perspective View of Stress Distribution



PLAN
(a) Zone 1



3-D Perspective View of Stress Distribution



PLAN
(b) Zone 2

FIG. A.A2

$$= d^2 t(m_1 + m_2 + 2m_3 + 2m_4)/12 - dt^2 \cot \beta (m_1 + 2m_2 + 4m_3 + 2m_4) / 18 + t^3 \cot^2 \beta (m_1 + 3m_2 + 6m_3 + 2m_4)/72$$

A. 1(b)

(iii) moment about AC, M_{AC}

$$= dt^2(m_1 + 2m_2 + 2m_3 + m_4)/12 - t^3 \cot \beta (m_1 + 3m_2 + 3m_3 + m_4)/24$$

A. 1(c)

(b) Type 2 Zone

$$(i) F' = (1/6) t' m_1' d' \quad A. 2(a)$$

$$(ii) M'_{AB} = (1/24) t' m_1' d' (d' \cot \delta + t') \quad A. 2(b)$$

$$(iii) M'_{AC} = (1/24) t' m_1' d'^2 \quad A. 2(c)$$

If values d_{AB} , d_{AC} and d'_{AB} , d'_{AC} are now defined as distances measured parallel to the lines AB, AC and A'B', A'C' respectively which specify the location of F and F' then they may be obtained from the following expressions,

$$d_{AB} = \frac{M_{AC}}{F} \quad A. 3(a)$$

$$d_{AC} = \frac{M_{AB}}{F} \quad A. 3(b)$$

$$d'_{AB} = \frac{M'_{AC}}{F'} \quad A. 3(c)$$

$$d'_{AC} = \frac{M'_{AB}}{F'} \quad A. 3(d)$$

From these quantities the distances of F and F' from the geometric

centroid, 0, of the whole section, d_{ξ} , d_{η} , d'_{ξ} , d'_{η} can be found and the force corrections made. The positive sense of these new d coordinates is defined in Figure A.A.1. In making these corrections compression stress excess is considered positive so that F and F' must be subtracted from the axial load. Moment correction is performed however by always subtracting the absolute value of F or F' multiplied by a distance, i. e. one of d_{ξ} , d_{η} , d'_{ξ} , d'_{η} , as given in paragraphs A.4 to A.6 below.

A.1.3 In the equations A.1 and A.2 above the quantities t, d, t', d', β , δ appear without any explanation of their method of calculation. Their magnitude depends on the cross-sectional element for which the correction is being made as well as the amount of plasticity present. The full details for calculating these values as well as F and F' and the distances d_{ξ} , d_{η} , d'_{ξ} , d'_{η} now follow.

A.1.4 Top Flange

(i) All possible variations of the spread of plasticity in the top flange, requiring different correction expressions, are shown in Figure A.A.3 where the points 1, 2, 3, 4 correspond to those numbered in Figure A.A.2. Additionally, the lines AB, AC, A'B', A'C', show how the yield zones discussed above fit each particular case.

(ii) The setting of all quantities in the general formulae and the conditions under which each case occurs are as follows:

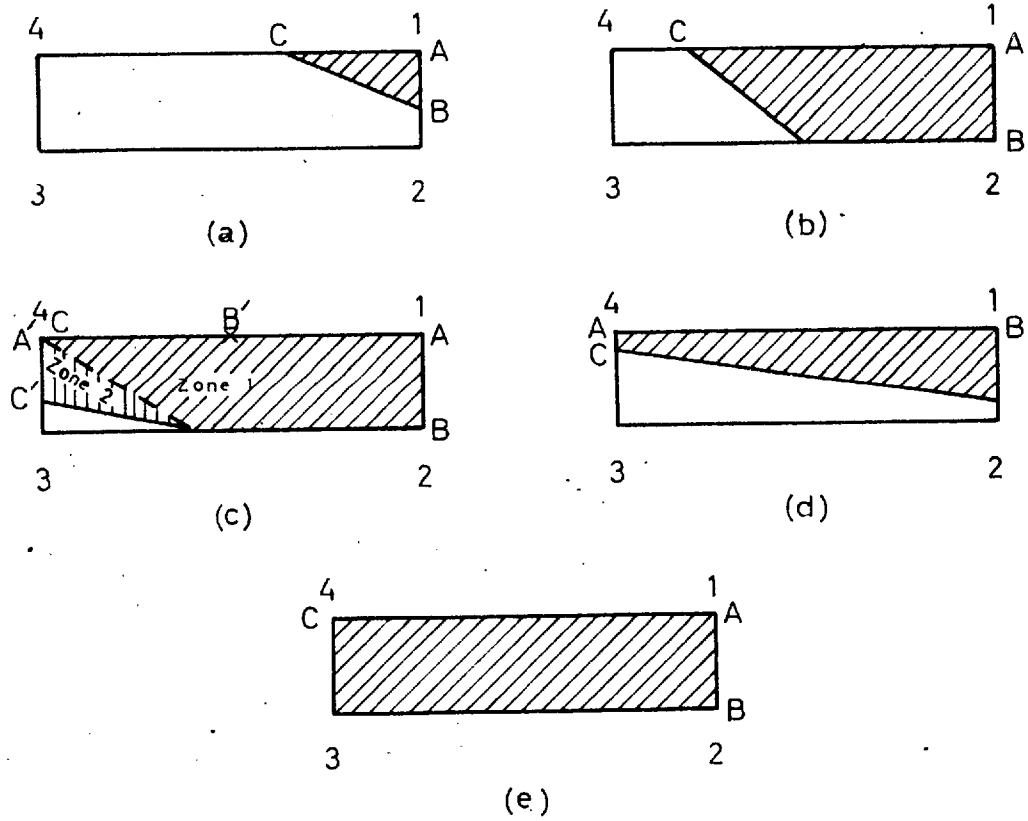


FIG. A.A3

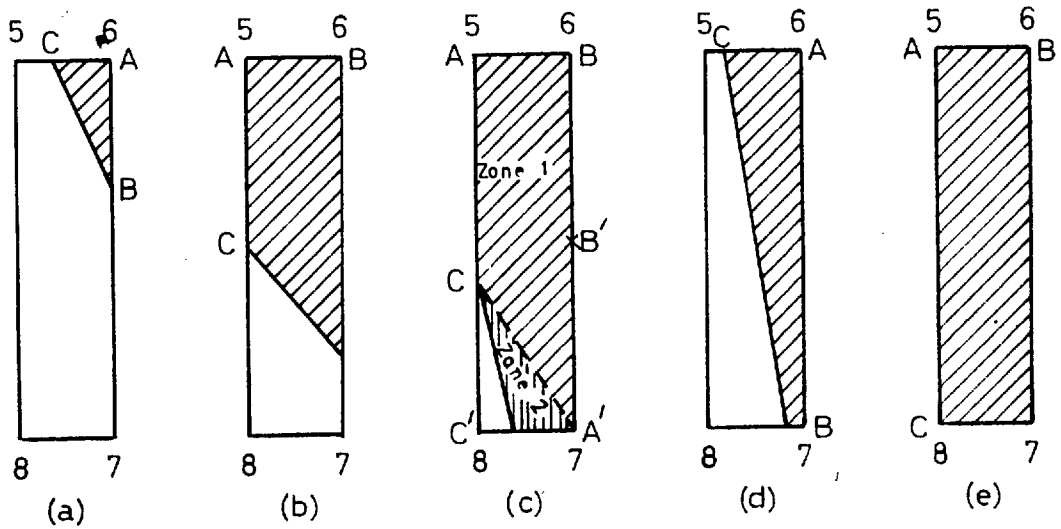


FIG. A.A4

Case (a) Only type 1 zone present (special case)

$$m_1 = f_1^* \text{ and } m_2 = m_3 = m_4 = 0$$

$$d = b \operatorname{cosec} \alpha$$

$$t = b \sec \alpha$$

$$\beta = \alpha$$

$$d_\xi = \frac{1}{2}B - d_{AC}$$

$$d_\eta = \frac{1}{2}D - d_{AB}$$

Conditions (i) $f_1 > 0$

$$(ii) f_2 = f_3 = f_4 = 0$$

Case (b) Only type 1 zone present

$$m_1 = f_1, m_2 = f_2 \text{ and } m_3 = m_4 = 0$$

$$d = b \operatorname{cosec} \alpha$$

$$t = t_f$$

$$\beta = \alpha$$

$$d_\xi = \frac{1}{2}B - d_{AC}$$

$$d_\eta = \frac{1}{2}D - d_{AB}$$

Conditions (i) $f_1 > f_2 > 0$

$$(ii) f_3 = f_4 = 0$$

*

The values f_1 to f_{12} are the stress excess values which can be taken from Figure A.2.2.

Case (c) Both type 1 and type 2 zones present

Zone 1

$$m_1 = f_1, m_2 = f_2, m_3 = m_4 = 0$$

$$d = B$$

$$t = t_f$$

$$\beta = \tan^{-1} \left[\frac{t_f}{(B - (b - t_f \cos \alpha)) \operatorname{cosec} \alpha} \right]$$

$$d'_\xi = \frac{1}{2}B - d_{AC}$$

$$d'_\eta = \frac{1}{2}D - d_{AB}$$

Zone 2

$$m'_1 = f_4$$

$$d' = B - (b - t_f \cos \alpha) \operatorname{cosec} \alpha$$

$$t' = (b - B \sin \alpha) \sec \alpha$$

$$\gamma = \frac{1}{2} \pi - \beta$$

$$d'_\xi = -\frac{1}{2}B + d'_{AB}$$

$$d'_\eta = \frac{1}{2}D - d'_{AC}$$

Conditions (i) $f_1 > f_2 > f_4 > 0$

(ii) $f_3 = 0$

Case (d) Only type 1 zone present

$$m_1 = f_4, m_2 = f_1, m_3 = m_4 = 0$$

$$d = (b - t_f \cos \alpha) \operatorname{cosec} \alpha$$

$$t = B$$

$$\beta = \frac{1}{2} \pi + \alpha$$

$$d'_\xi = -\frac{1}{2}B + d_{AB}$$

$$d'_\eta = \frac{1}{2}D - d_{AC}$$

Conditions (i) $f_1 > f_4 > 0$

(ii) $f_2 = f_3 = 0$

Case (e) Only type 1 zone present

$$m_1 = f_1, m_2 = f_2, m_3 = f_3, m_4 = f_4$$

$$d = B$$

$$t = t_f$$

$$\beta = \frac{1}{2} \pi$$

Condition is $f_1 > f_2 > f_3 > f_4 > 0$

A.1.5 Web

(i) The details given for the top flange in paragraph A.4 above are now repeated for the web. The various possible zones of plasticity are shown in Figure A.A.4 and the quantities and conditions corresponding to those given in paragraph A.4 are as follows:

Case (a) Only type 1 zone present (special case)

$$m_1 = f_6, m_2 = m_3 = m_4 = 0$$

$$d = (b - \frac{1}{2}B \sin \alpha + \frac{1}{2}t_w \sin \alpha - t_f \cos \alpha) \operatorname{cosec} \alpha$$

$$t = d \tan \alpha$$

$$\beta = \alpha$$

$$d\xi = \frac{1}{2}t_w - d_{AC}$$

$$d\eta = \frac{1}{2}D - t_f - d_{AB}$$

Conditions (i) $f_6 > 0$

$$(ii) f_5 = f_7 = f_8 = 0$$

Case (b) Only type 1 zone present

$$m_1 = f_5, m_2 = f_6, m_3 = m_4 = 0$$

$$d = (b - \frac{1}{2}B \sin \alpha - \frac{1}{2}t_w \sin \alpha - t_f \cos \alpha) \sec \alpha$$

$$t = t_w$$

$$\beta = \frac{1}{2}\pi + \alpha$$

$$d_\xi = -\frac{1}{2}t_w + d_{AB}$$

$$d_\eta = \frac{1}{2}D - t_f - d_{AC}$$

Conditions (i) $f_6 > f_5 > 0$

$$(ii) f_7 = f_8 = 0$$

Case (c) Both type 1 and type 2 zones present

Zone 1

$$m_1 = f_5, m_2 = f_6, m_3 = f_7, m_4 = 0$$

$$d = (b - \frac{1}{2}B \sin \alpha - \frac{1}{2}t_w \sin \alpha - t_f \cos \alpha) \sec \alpha$$

$$t = t_w$$

$$\beta = \frac{1}{2}\pi + \tan^{-1} \left[\frac{(B - d)/t_w}{1} \right]$$

$$d_\xi = -\frac{1}{2}t_w + d_{AB}$$

$$d_\eta = \frac{1}{2}D - t_f - d_{AC}$$

Zone 2

$$m'_1 = f_7$$

$$d' = B - d$$

$$t' = (b - \frac{1}{2}B \sin \alpha + \frac{1}{2}t_w \sin \alpha - D \cos \alpha + t_f \cos \alpha) \operatorname{cosec} \alpha$$

$$\gamma = \tan^{-1} \left[\frac{(B - d)/t_w}{1} \right]$$

$$d'_\xi = \frac{1}{2}t_w - d'_{AC}$$

$$d'_\eta = -\frac{1}{2}D + t_f + d'_{AB}$$

Conditions (i) $f_6 > f_5 > f_7 > 0$

$$(ii) f_8 = 0$$

Case (d) Only type 1 zone present

$$m_1 = f_6, m_2 = f_7, m_3 = m_4 = 0$$

$$d = (b - \frac{1}{2} B \sin \alpha + \frac{1}{2} t_w \sin \alpha - t_f \cos \alpha) \operatorname{cosec} \alpha$$

$$t = D - 2 t_f$$

$$\beta = \alpha$$

$$d_{\xi} = \frac{1}{2} t_w - d_{AC}$$

$$d_{\eta} = \frac{1}{2} D - t_f - d_{AB}$$

Conditions (i) $f_6 > f_7 > 0$

$$(ii) f_5 = f_8 = 0$$

Case (e) Only type 1 zone present

$$m_1 = f_5, m_2 = f_6, m_3 = f_7, m_4 = f_8$$

$$d = D - 2t_f$$

$$t = t_w$$

$$\beta = \frac{1}{2} \pi$$

$$d_{\xi} = -\frac{1}{2} t_w + d_{AB}$$

$$d_{\eta} = \frac{1}{2} D - t_f - d_{AC}$$

Condition is $f_6 > f_5 > f_7 > f_8 > 0$

A.1.6 Lower Flange

(i) For the lower flange reference to Figure A.A.3 again shows the possible plastic zones. However, case (e) need not be considered since the entire section would be plastic and therefore unstable. Case (c) was also considered to represent a condition where a section would be unstable and is therefore excluded. The conditions and parameters corresponding to those given above are as follows:

Case (a) Only type 1 zone present (special case)

$$m_1 = f_9, m_2 = m_3 = m_4 = 0$$

$$d = (b - D \cos \alpha + t_f \cos \alpha) \operatorname{cosec} \alpha$$

$$t = d \tan \alpha$$

$$\beta = \alpha$$

$$d_\xi = \frac{1}{2} B - d_{AC}$$

$$d_\eta = -\frac{1}{2} D + t_f - d_{AB}$$

Conditions (i) $f_9 > 0$

$$(ii) f_{10} = f_{11} = f_{12} = 0$$

Case (b) Only type 1 zone present

$$m_1 = f_9, m_2 = f_{10}, m_3 = m_4 = 0$$

$$d = (b - D \cos \alpha + t_f \cos \alpha) \operatorname{cosec} \alpha$$

$$t = t_f$$

$$\beta = \alpha$$

$$d_\xi = \frac{1}{2} B - d_{AC}$$

$$d_\eta = -\frac{1}{2} D + t_f - d_{AB}$$

Conditions (i) $f_9 > f_{10} > 0$

$$(ii) f_{11} = f_{12} = 0$$

Case (d) Only type 1 zone present

$$m_1 = f_{12}, m_2 = f_9, m_3 = m_4 = 0$$

$$d = (b - D \cos \alpha + t_f \cos \alpha) \sec \alpha$$

$$t = B$$

$$\beta = \frac{1}{2} \pi + \alpha$$

$$d_\xi = -\frac{1}{2} B + d_{AB}$$

$$d_\eta = -\frac{1}{2} D + t_f - d_{AC}$$

Conditions (i) $f_9 > f_{12} > 0$

$$(ii) f_{10} = f_{11} = 0$$

A.1.7 The total correction is found by summing the corrections for all plastic zones. Thus using the notation of Chapter 3 the corrections are as follows:

$$P^c = \sum_{A_P} F + \sum_{A_P} F' \quad \text{A.4(a)}$$

$$M_{\xi}^c = \sum_{A_P} (F d_{\eta}) + \sum_{A_P} (F' d'_{\eta}) \quad \text{A.4.(b)}$$

$$M_{\eta}^c = \sum_{A_P} (F d_{\xi}) + \sum_{A_P} (F' d'_{\xi}) \quad \text{A.4(c)}$$

where \sum_{A_P} denotes the summation for the plastic zones. It should be noted that all conditions and formulae above are for the angle α in the first quadrant, i. e. with M_{ξ} and M_{η} positive. If either of M_{ξ} or M_{η} is negative it must have its sign changed and then the curvature it causes negated at the completion of the solution of the cross-sectional equations.

APPENDIX B

B.1 UNLOADING CORRECTION

B.1.1 To obtain corrections to the equations 3.12 for unloading it has been found convenient, for the purposes of integrating correction stresses, to construct on the cross-section the imaginary grid shown in Figure A.B.1. Each enclosed rectangular area is considered to contain a single fibre, the behaviour of which coincides with that of the most centrally placed material. Thus by recording the maximum strain at all such central points and storing the result in a fixed location in the memory store of the computer, a sufficiently complete strain history may be kept.

B.1.2 Unloading of compression fibres only has been considered so that all strains are directly expressible in terms of b_1 , c and α . To obtain the strains at the centre of all grid rectangles shown and numbered in Figure A.B.1 the following procedure is adopted:

1. Strains are calculated at the points A, B, C, H, I, J and E in Figure A.B.1. The relevant equations are:

$$\epsilon_A = \sigma_y(b_1 + c - t_f \cos \alpha / 6) / E_c \quad \text{B.1(a)}$$

$$\epsilon_B = \epsilon_A - \sigma_y t_f \cos \alpha / 3E_c \quad \text{B.1(b)}$$

$$\epsilon_C = \epsilon_B - \sigma_y t_f \cos \alpha / 3E_c \quad \text{B.1(c)}$$

$$\epsilon_J = \epsilon_C - \sigma_y (D - t_f / 3) \cos \alpha / E_c \quad \text{B.1(d)}$$

$$\epsilon_I = \epsilon_J + \sigma_y t_f \cos \alpha / 3E_c \quad \text{B.1(e)}$$

$$\epsilon_H = \epsilon_I + \sigma_y t_f \cos \alpha / 3E_c \quad \text{B.1(f)}$$

$$\epsilon_E = \sigma_y (b_1 + c - 0.5B \sin \alpha - t_f \cos \alpha) / E_c \quad \text{B.1(g)}$$

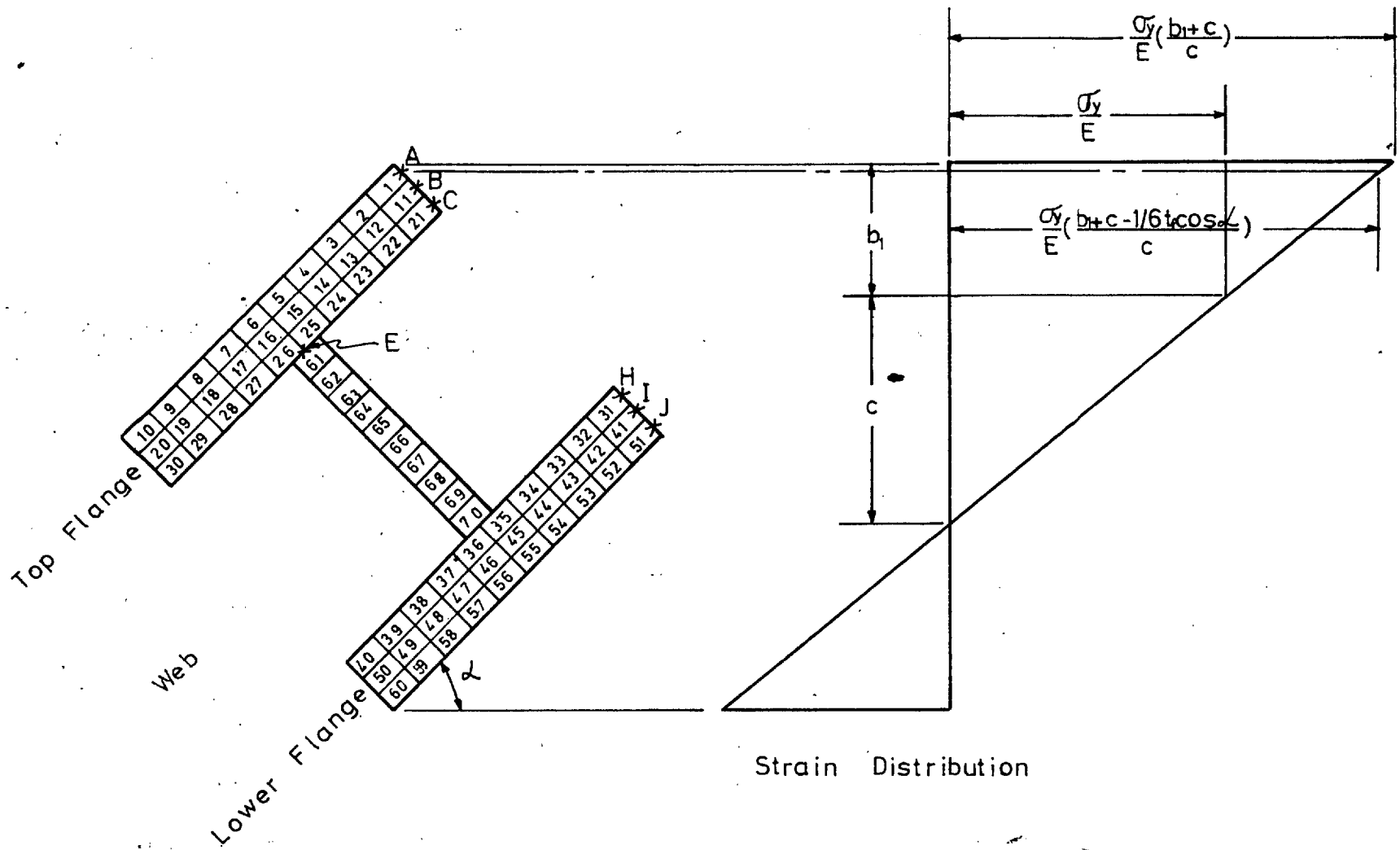


FIG. A.B1

2. Using the strains above, and noting that the strain gradients in the flanges and web are $(\sigma_y/Ec) \sin \alpha$ and $(\sigma_y/Ec) \cos \alpha$ respectively, the strains at the centres of the various numbered rectangles are found as follows:

$$\epsilon_1 = \epsilon_A - B\sigma_y \sin \alpha / 20 Ec \quad \text{B. 2(a)}$$

$$\epsilon_2 = \epsilon_1 - B\sigma_y \sin \alpha / 10 Ec \quad \text{B. 2(b)}$$

$$\epsilon_3 = \epsilon_2 - B\sigma_y \sin \alpha / 10 Ec \quad \text{B. 2(c)}$$

etc. etc.

$$\epsilon_{11} = \epsilon_B - B\sigma_y \sin \alpha / 20 Ec \quad \text{B. 3(a)}$$

$$\epsilon_{12} = \epsilon_{11} - B\sigma_y \sin \alpha / 10 Ec \quad \text{B. 3(b)}$$

$$\epsilon_{13} = \epsilon_{12} - B\sigma_y \sin \alpha / 10 Ec \quad \text{B. 3(c)}$$

etc. etc.

where this process must be continued for the six rows in each of the two flanges. For the web,

$$\epsilon_{61} = \epsilon_E - (D - 2t_f)\sigma_y \cos \alpha / 20 Ec \quad \text{B. 4(a)}$$

$$\epsilon_{62} = \epsilon_{61} - (D - 2t_f)\sigma_y \cos \alpha / 10 Ec \quad \text{B. 4(b)}$$

$$\epsilon_{63} = \epsilon_{62} - (D - 2t_f)\sigma_y \cos \alpha / 10 Ec \quad \text{B. 4(c)}$$

etc. etc.

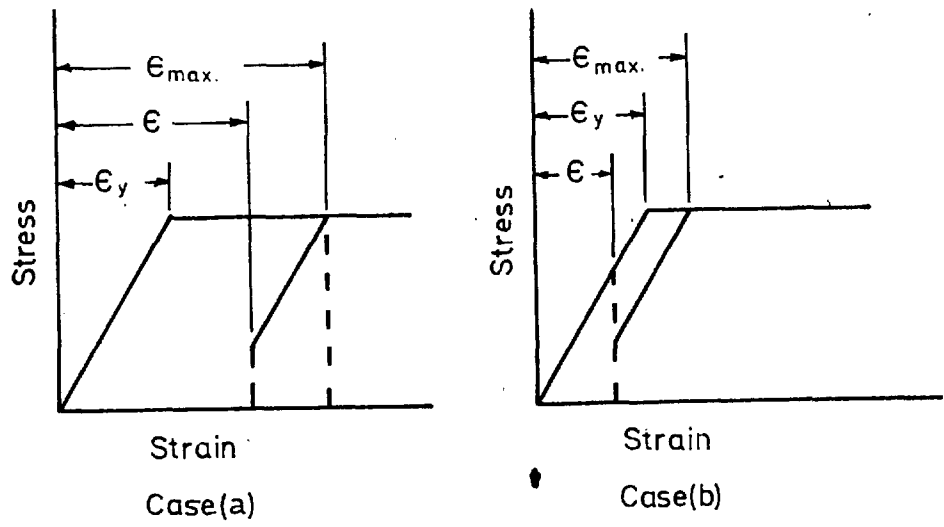


FIG. A-B2

B. 1. 3 Now bearing in mind that unloading effects are being considered as a correction to the original force equations, 3.12, it is seen that the two distinct unloading possibilities indicated in the stress-strain diagram, Figure A. B. 2, will need to be considered. Defining the quantities,

ϵ_{\max}	=	maximum strain on a fibre,
ϵ_y	=	yield strain,
ϵ	=	current strain,
a	=	area of a general elemental rectangle,

the force correction, F, on each element, and the associated conditions which arise in each case, are as follows:

Case (a)

$$F = E(\epsilon_{\max} - \epsilon)a \quad \text{B. 5(a)}$$

Conditions (i) $\epsilon > \epsilon_y$, otherwise it is case (b)

(ii) $E(\epsilon_{\max} - \epsilon) > 0$, otherwise $F = 0$

(iii) $E(\epsilon_{\max} - \epsilon) < 2\sigma_y$, otherwise $F = 2\sigma_y a$

Case (b)

$$F = E(\epsilon_{\max} - \epsilon_y)a \quad \text{B. 5(b)}$$

Conditions (i) $\epsilon < \epsilon_y$, otherwise it is case (a)

(ii) $E(\epsilon_{\max} - \epsilon) > 0$, otherwise $F = 0$

(iii) $E(\epsilon_{\max} - \epsilon) < 2\sigma_y$, otherwise $F = 2\sigma_y a$

In programming this for the computer it should be noted that the application of condition (i) distinguishes case (a) from case (b). The conditions (ii) and (iii) are the same for case (a) and case (b) and need only be programmed once. Also the force corrections F, (F_1 to F_{70}), corresponding to the strains ϵ_1 to ϵ_{70} may be allowed

to overwrite the strains since these are no longer required.

B.1.4 To obtain the modifications to the forces ($P - P_y$), M_ξ , M_η , viz. P^U , M_ξ^U , M_η^U , the following expressions are used.

$$P^U = \sum_{n=1}^{70} F_n \quad \text{B.6(a)}$$

$$M_\xi^U = \sum_{m=1}^3 [(D/2 + t_f/6) - mt_f/3] \sum_{n=1}^{10} (F_{10m+n-10} - F_{-10m+n+50}) \\ + \sum_{n=1}^{10} [(0.55D - 1.1t_f) - 0.1n(D - 2t_f)] F_{n+60} \quad \text{B.6(b)}$$

$$M_\eta^U = \sum_{m=1}^{10} (0.55B - 0.1mB) \sum_{n=1}^6 (F_{m+10n-10} - F_{-m+10n-1}) \quad \text{B.6(c)}$$

These corrections are all to be subtracted, in order, from the equations 3.12.

B.1.5 In the computer programme all elemental force corrections are placed in fixed locations in the memory store. Associated with each location are coordinates which define the location of the force with respect to the geometric centroid of the whole section. These are located correctly irrespective of the values of b_1 , c , α and enable the unloading corrections to be made without difficulty. However, the evaluation of the plasticity expressions as given in appendix A is valid only if $0 < \alpha < \frac{1}{2}\pi$. Outside this range b_1 and α must be modified

to b_{1c} and α_c , where α_c is an angle in the first quadrant, and the internal moments sign corrected. The last function is performed by multiplying M_x by d17 and M_y by d18. The evaluation of b_{1c} , α_c , d17, d18 is summarised below for $-2\pi < \alpha < 2\pi$.

Condition	α_c	b_{1c}	d17	d18
$-2\pi < \alpha < -3\pi/2$	$2\pi - \alpha $	b_1	1	1
$-3\pi/2 < \alpha < -\pi$	$ \alpha - \pi$	$b_1 + D \cos \alpha_c$	-1	1
$-\pi < \alpha < -\pi/2$	$\pi - \alpha $	$b_1 + D \cos \alpha_c + B \sin \alpha_c$	-1	-1
$-\pi/2 < \alpha < 0$	$ \alpha $	$b_1 + B \sin \alpha_c$	1	-1
$0 < \alpha < \pi/2$	$ \alpha $	b_1	1	1
$\pi/2 < \alpha < \pi$	$\pi - \alpha $	$b_1 + D \cos \alpha_c$	-1	1
$\pi < \alpha < 3\pi/2$	$ \alpha - \pi$	$b_1 + D \cos \alpha_c + B \sin \alpha_c$	-1	-1
$3\pi/2 < \alpha < 2\pi$	$2\pi - \alpha $	$b_1 + B \sin \alpha_c$	1	-1

B.2 STRAIN HARDENING

B.2.1 The correction for strain hardening is made utilising the same sub-division of the cross-section that was used for the unloading computation. The stress-strain relationship upon which the correction is based is shown in Figure A.B.3 where strain hardening first begins at A and results in a linear increase in stress

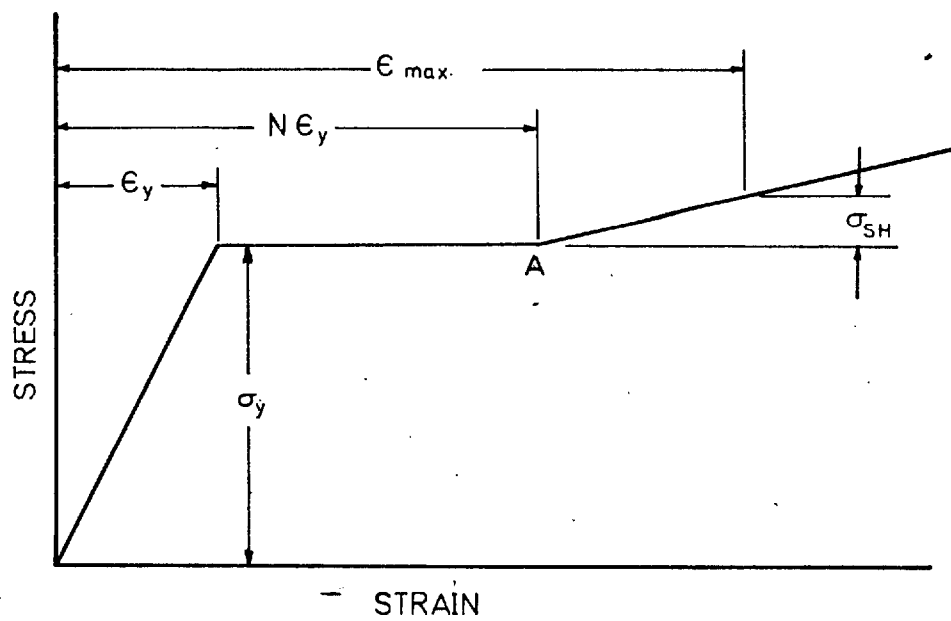


FIG. A.B3

above σ_y at a rate defined by the modulus E_{SH} .

B.2.2 The strain hardening correction must be applied to a fibre whenever the maximum strain that has occurred at any time during the loading process exceeds $N\epsilon_y$. It can be applied in conjunction with the unloading correction since, as can be seen in section B.1, the values of the maximum strains have already been obtained. (Note: for some of the small rectangles the current strains will be the maximum ones whilst for others, i. e. with fibres that have unloaded, it will have occurred at an earlier stage.)

B.2.3 To allow for strain hardening the force on a small elemental area, a , is evaluated using the expression,

$$F_s = E_{SH} (\epsilon_{max} - N\epsilon_y) a \quad B.7$$

which corresponds to equation B.5(a) of the unloading correction. Expressions B.6(a), (b), (c) may then be used, with F_s replacing F throughout, to obtain corrections P^{SH} , M_ξ^{SH} , M_η^{SH} . These corrections are then added, in order, to the values of P , M_ξ , M_η of equations 3.12.

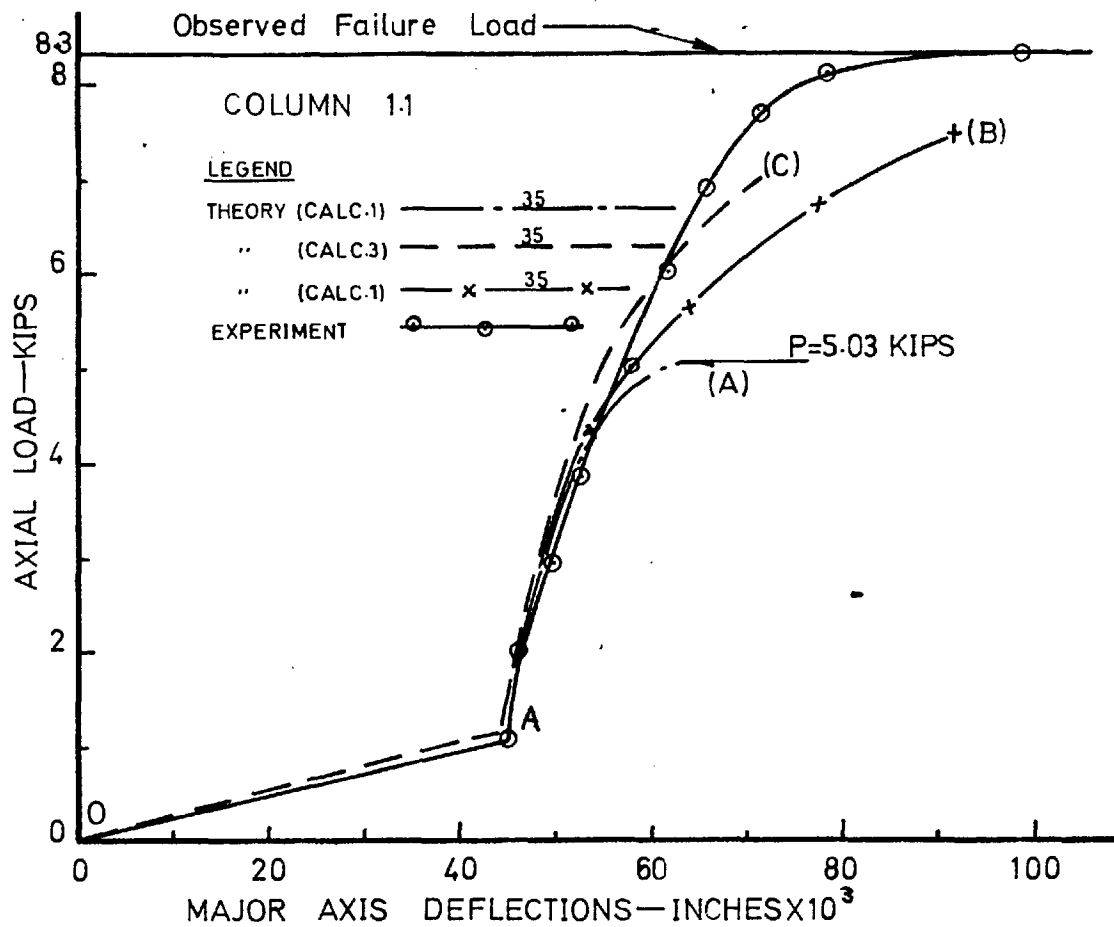
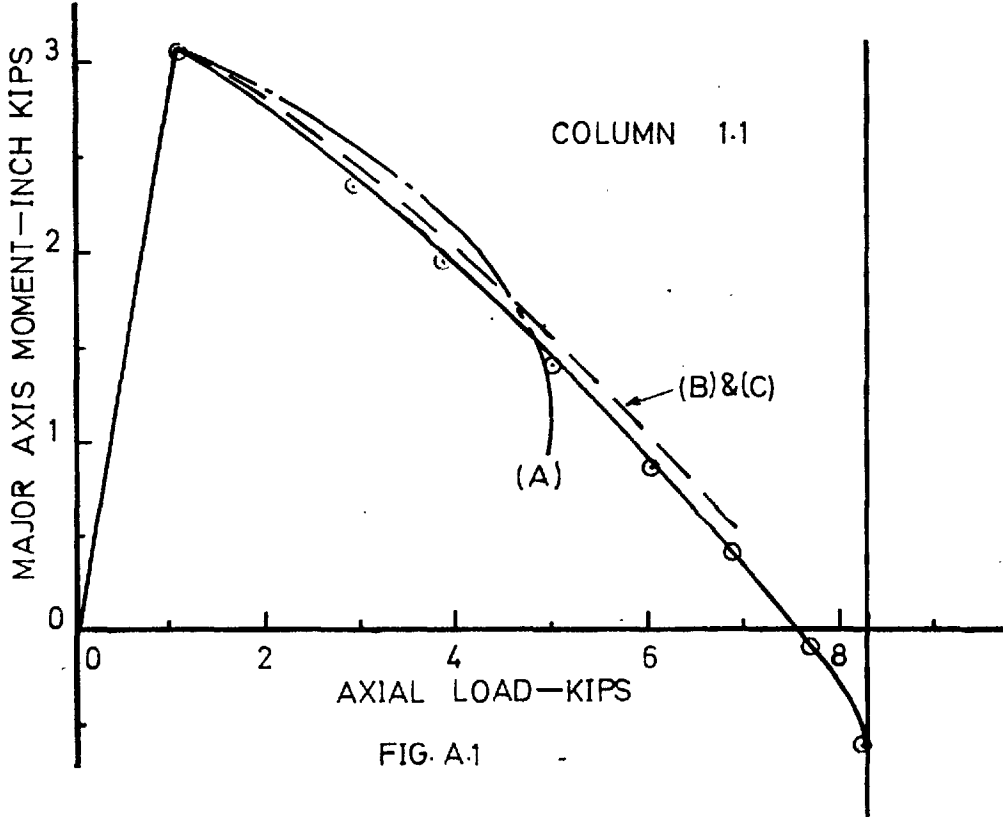
REFERENCES

1. J. Heyman: "Inverse design of beams and grillages", Proc. Instn. civ. Engrs., vol. 13, July 1959.
2. L.K. Stevens: "Direct design by limiting deformations", Proc. Instn. civ. Engrs., vol. 16, July 1960.
3. L.K. Stevens: "Control of stability by limitation of deformations", Proc. Instn. civ. Engrs., vol. 28, July 1964.
4. A.R. Gent: "The design of frame structures considering strength, stability, and deflexions", Proc. Instn. civ. Engrs., vol. 23, November 1962.
5. A.R. Gent: "Elastic plastic column stability and the design of no sway frames", Proc. Instn. civ. Engrs., awaiting publication.
6. J.F. Baker: M.R. Horne: J. Heyman: "The steel skeleton, Vol. II", Cambridge University Press, 1956.
7. B. Thurlimann: "New aspects concerning inelastic instability of steel structures", Proc. Amer. Soc. civ. Engrs., vol. 86, No. ST1, January 1960.
8. F. Bleich: H. H. Bleich: "Buckling strength of metal structures", McGraw-Hill Company, Inc., 1952.
9. G.F. Hauck: S. L. Lee: "Stability of elasto-plastic wide-flange columns", Proc. Amer. Soc. civ. Engrs., vol. 89, No. ST6, December 1963.

10. P.P. Bijlaard; G.P. Fisher; G. Winter: "Eccentrically loaded end-restrained columns", Trans. Amer. Soc. civ. Engrs., vol. 120, 1955.
11. P.P. Bijlaard: "Buckling of columns with equal and unequal end eccentricities and equal and unequal end restraints", Proc. of the Second U.S. Natl. Congress of Applied Mechanics, 1954.
12. M. Ojalvo: "Restrained columns", Proc. Amer. Soc. civ. Engrs., vol. 86, No. EM5, October 1960.
13. S.P. Timoshenko and J.M. Gere: "Theory of elastic stability", McGraw-Hill Book Company, Inc., 1961.
14. K. Klöppel; E. Winkelmann: "Experimentelle und theoretische untersuchungen über die traglast von zweiachsig aussermittig gedruckten stahlstaben", Der Stahlbau, vol. 31, no. 2, February 1962.
15. C. Birnstiel; J. Michalos: "Ultimate load of H-columns under biaxial bending", Proc. Amer. Soc. civ. Engrs., vol. 89, No. ST2, April 1963.
16. P. Campbell-Massey: "The torsional rigidity of steel I beams", Civil Engineering and Public Works Review, vol. 58, nos. 680 and 681, March and April 1963.
17. N.M. Newmark: "Numerical procedure for computing deflections, moments, and buckling loads", Trans. Amer. Soc. civ. Engrs., vol. 108, 1943.
18. National Physical Laboratory: "Modern Computing Methods", HMSO, London, 1957.

19. F. M. Campus; C. Massonnet: "Recherches sur le flambement de colonnes en acier A37, a profil en double te, sollicitees obliquement", IRSIA, Comptes Rendus de Recherches, 17, April 1956.
20. Lehigh University, Fritz Engineering Laboratory: "Plastic design of multi-storey frames", Report Nos. 273.20 and 273.24.
21. R. L. Ketter; E. L. Kaminsky; L. S. Beedle: "Plastic deformations of wide-flange beam-columns", Trans. Amer. Soc. civ. Engrs., vol. 120, 1955.

FIGURES A1 to A20



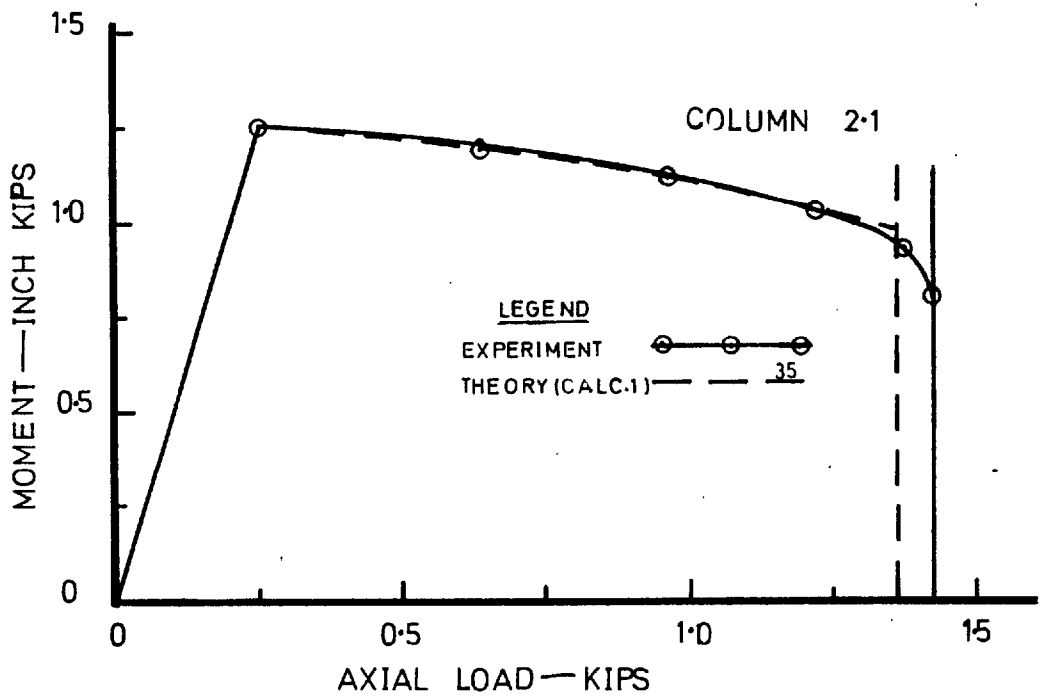


FIG. A-3

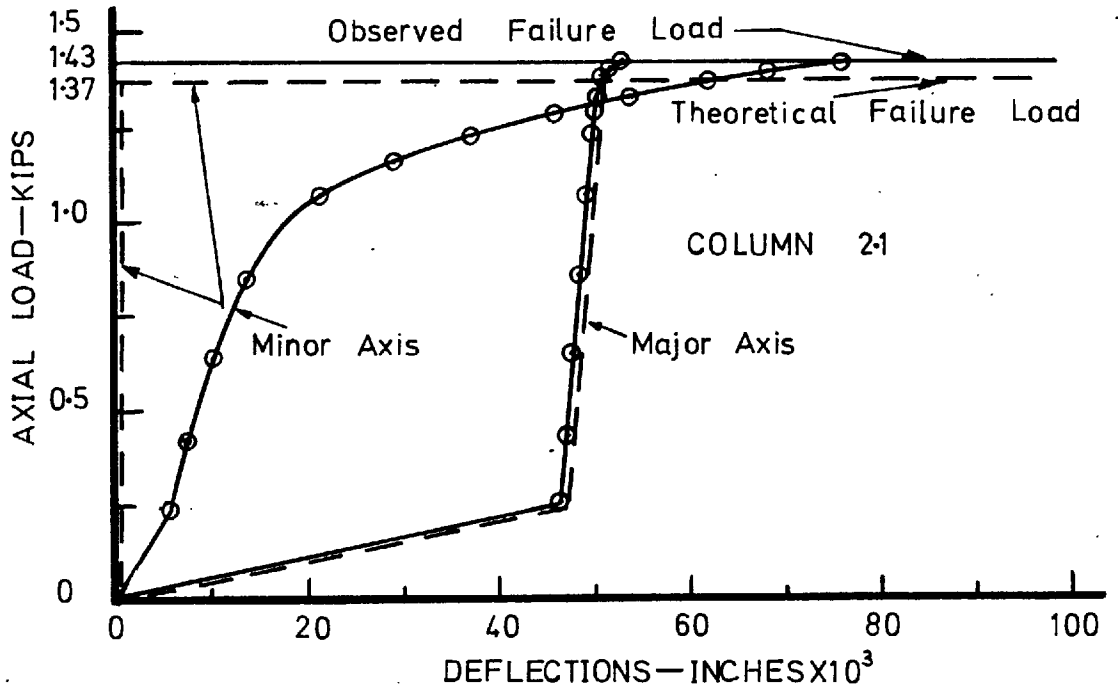


FIG. A-4

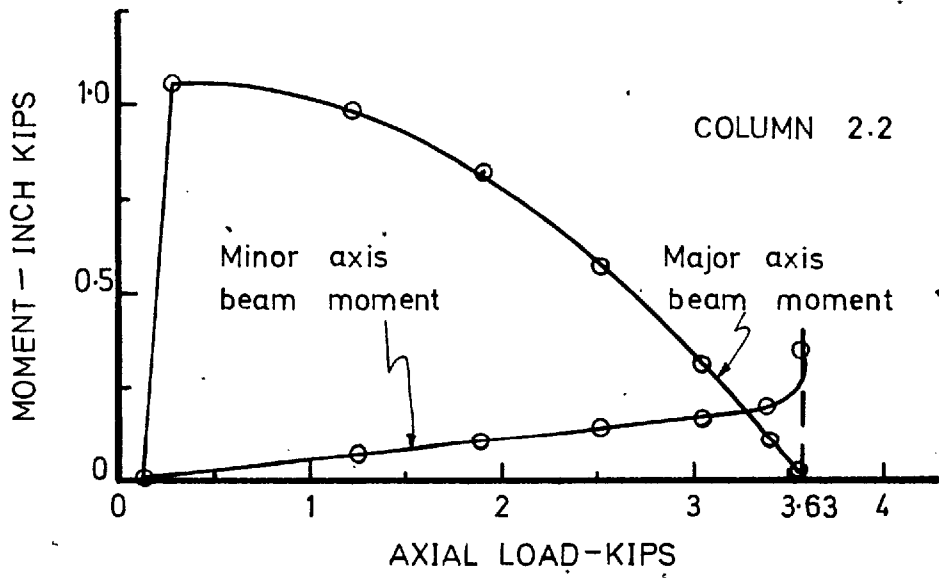


FIG. A.5

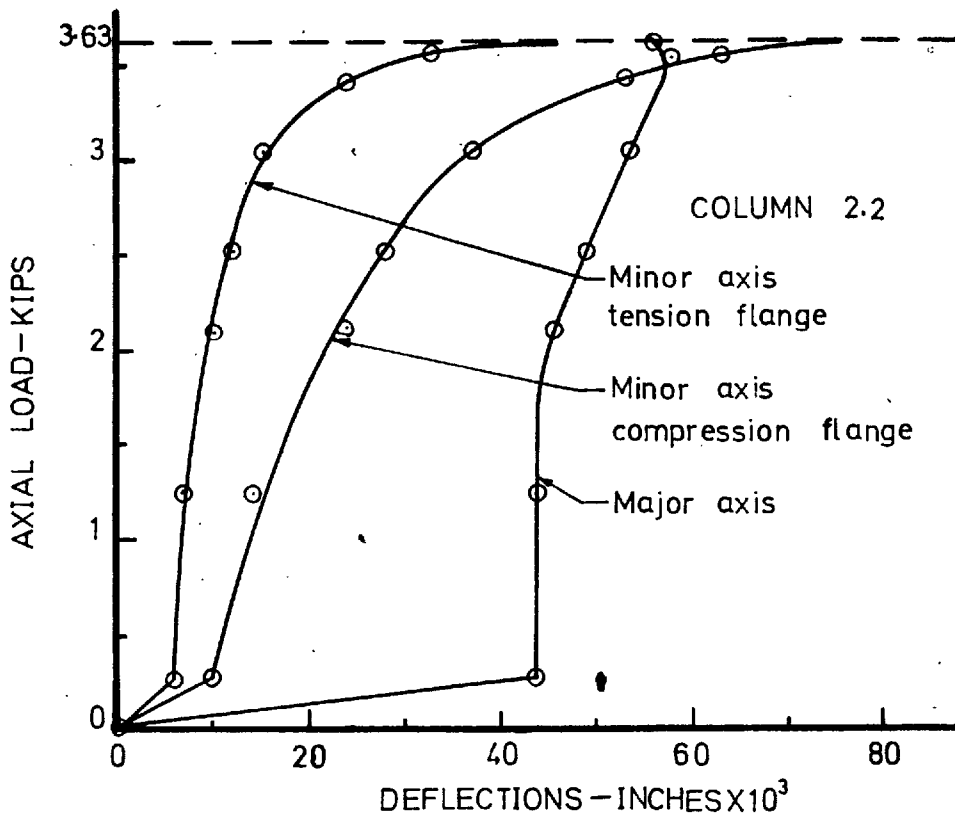


FIG. A.6

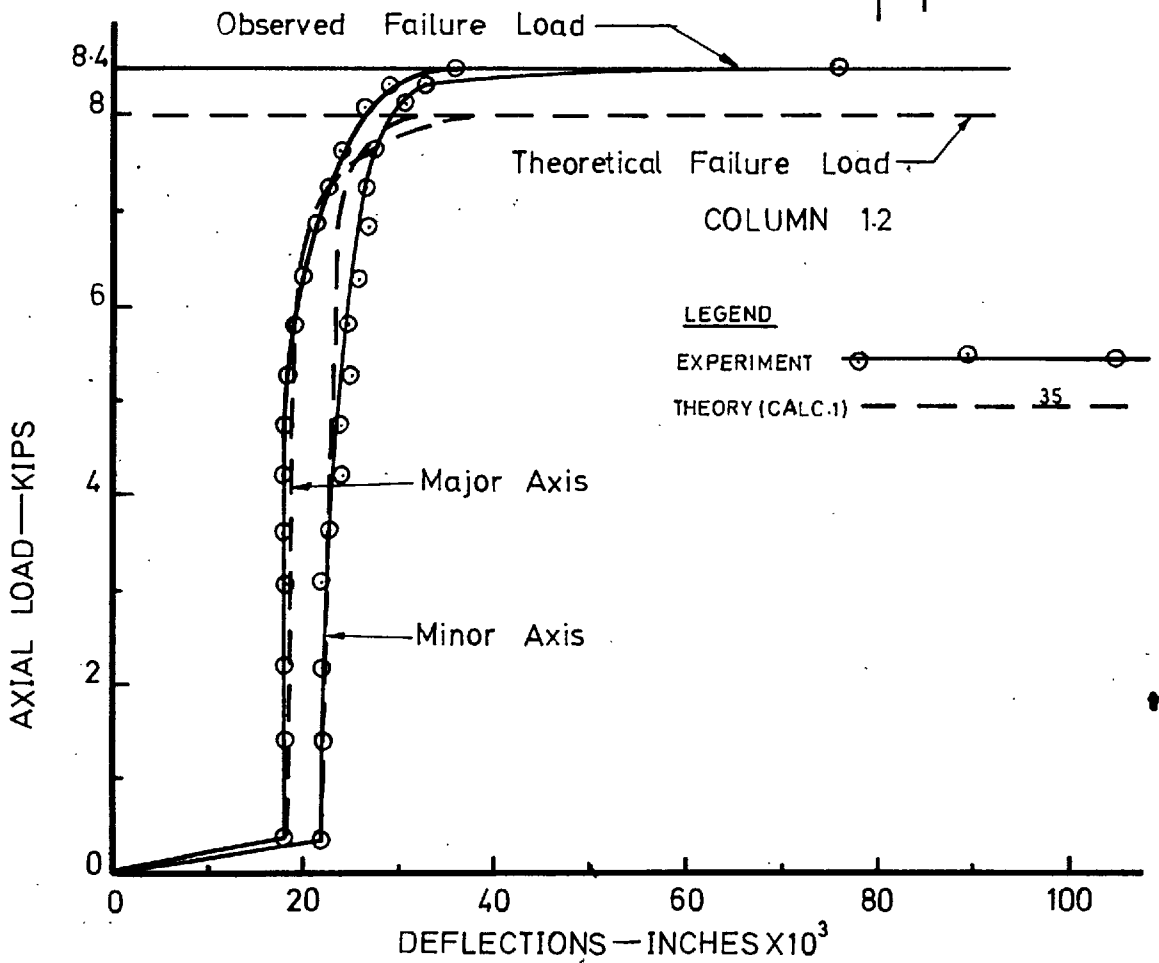
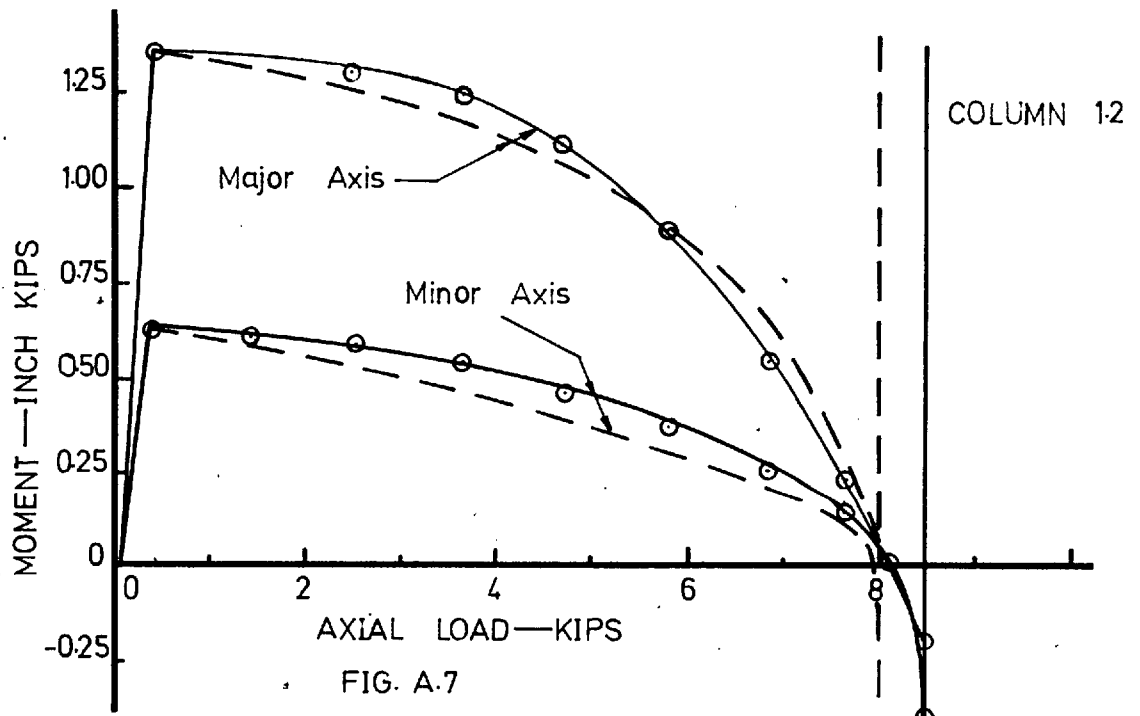
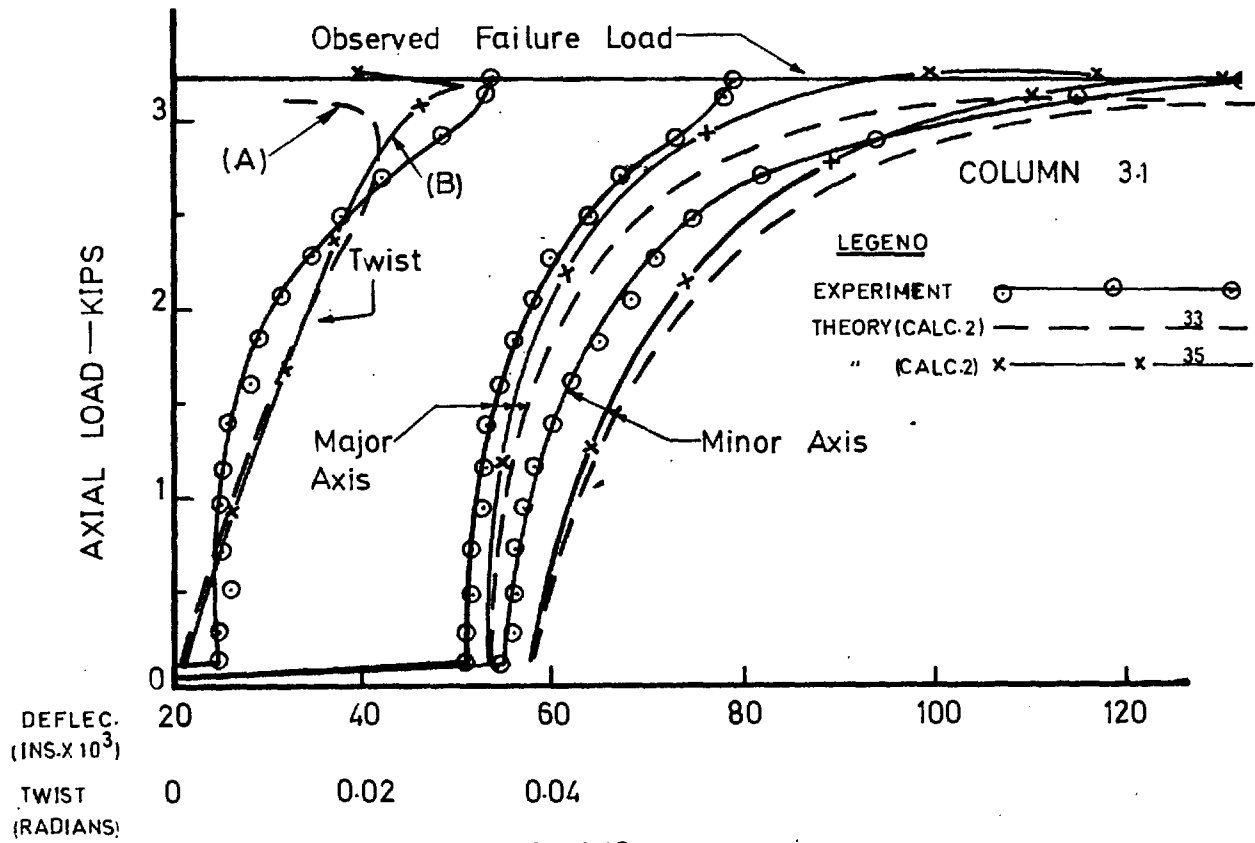
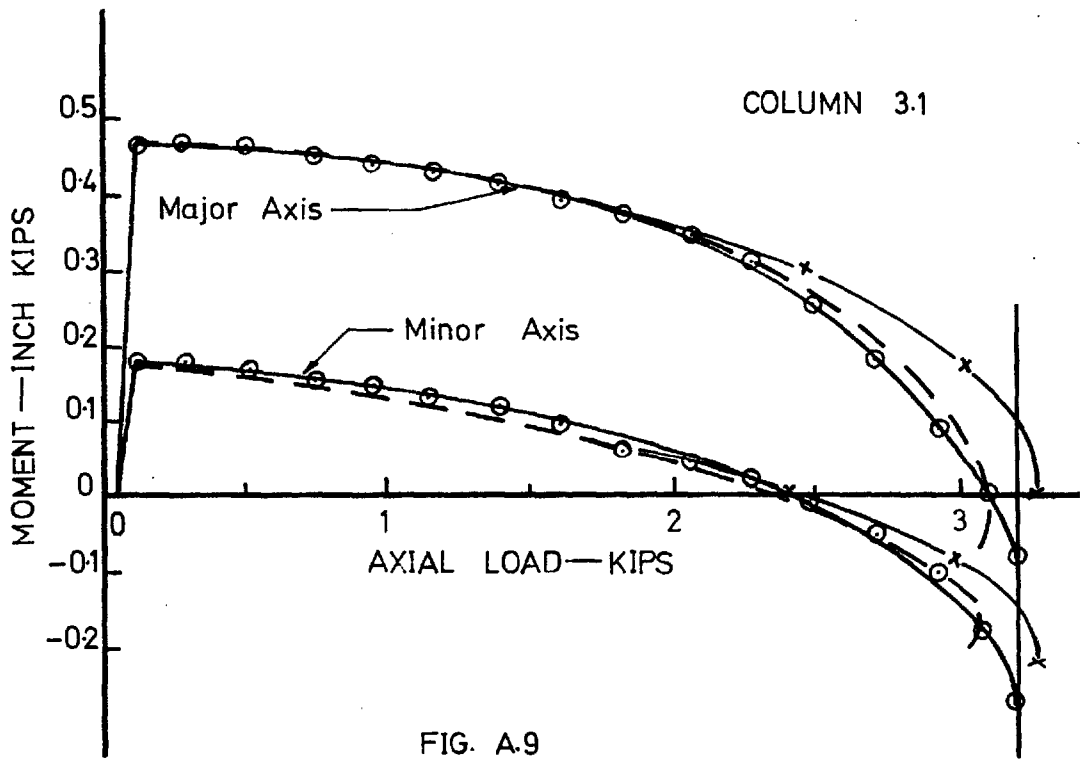


FIG. A.8



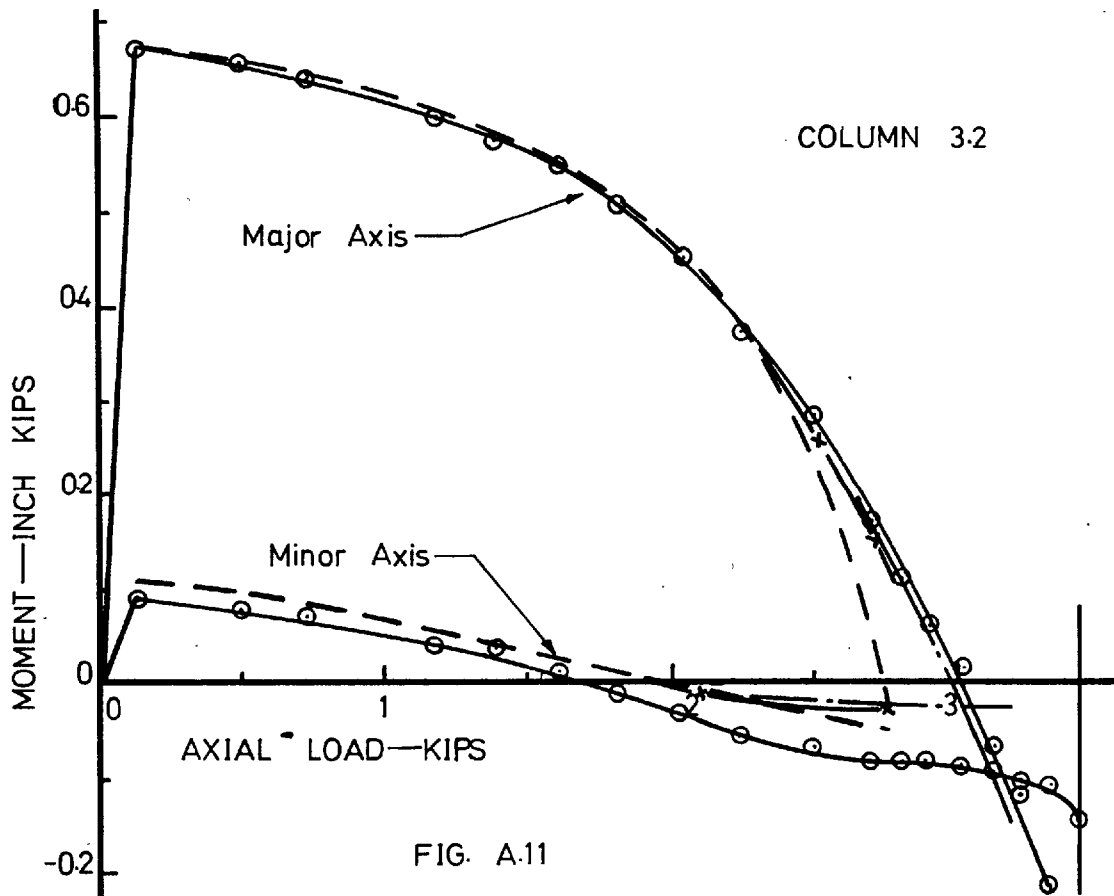


FIG. A-11

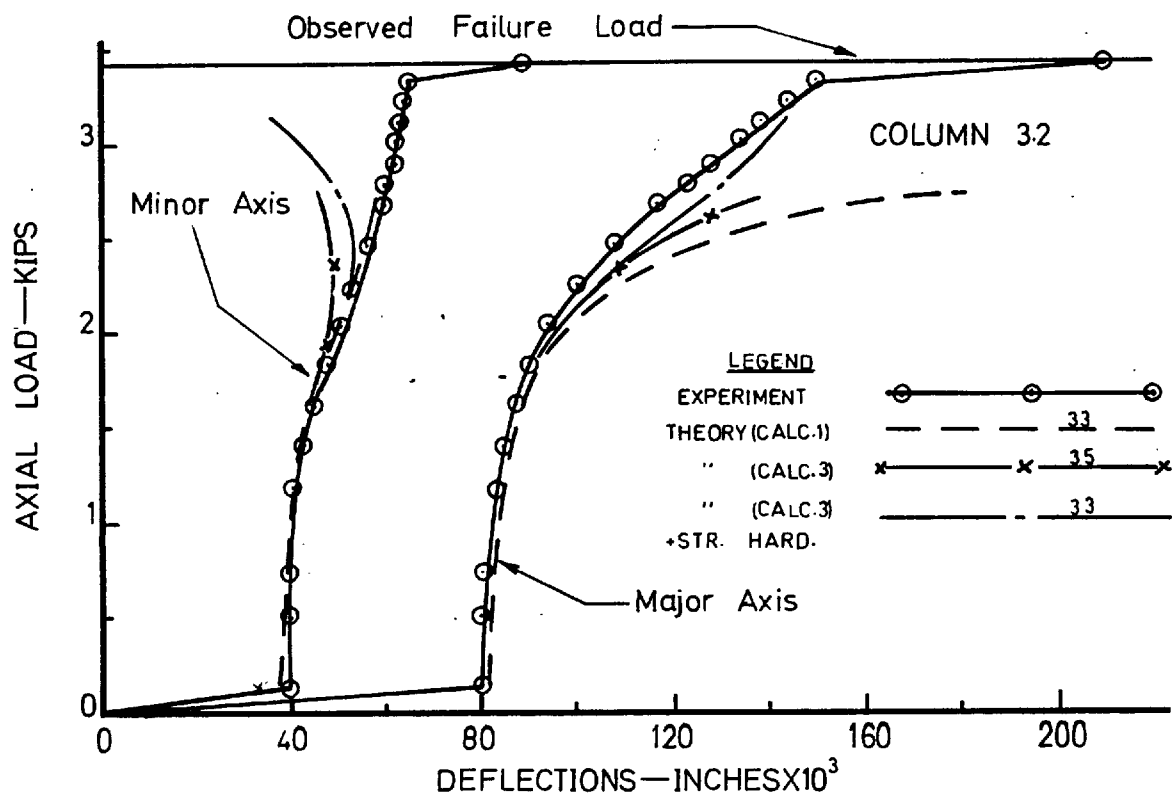


FIG. A-12

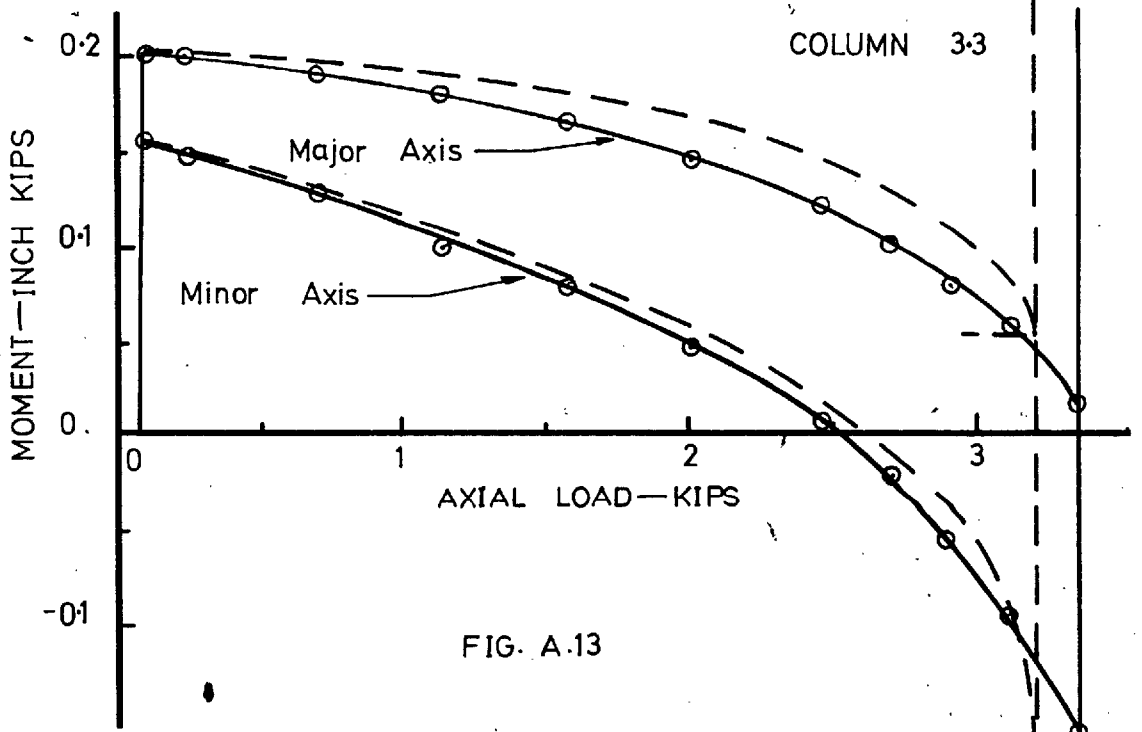


FIG. A.13

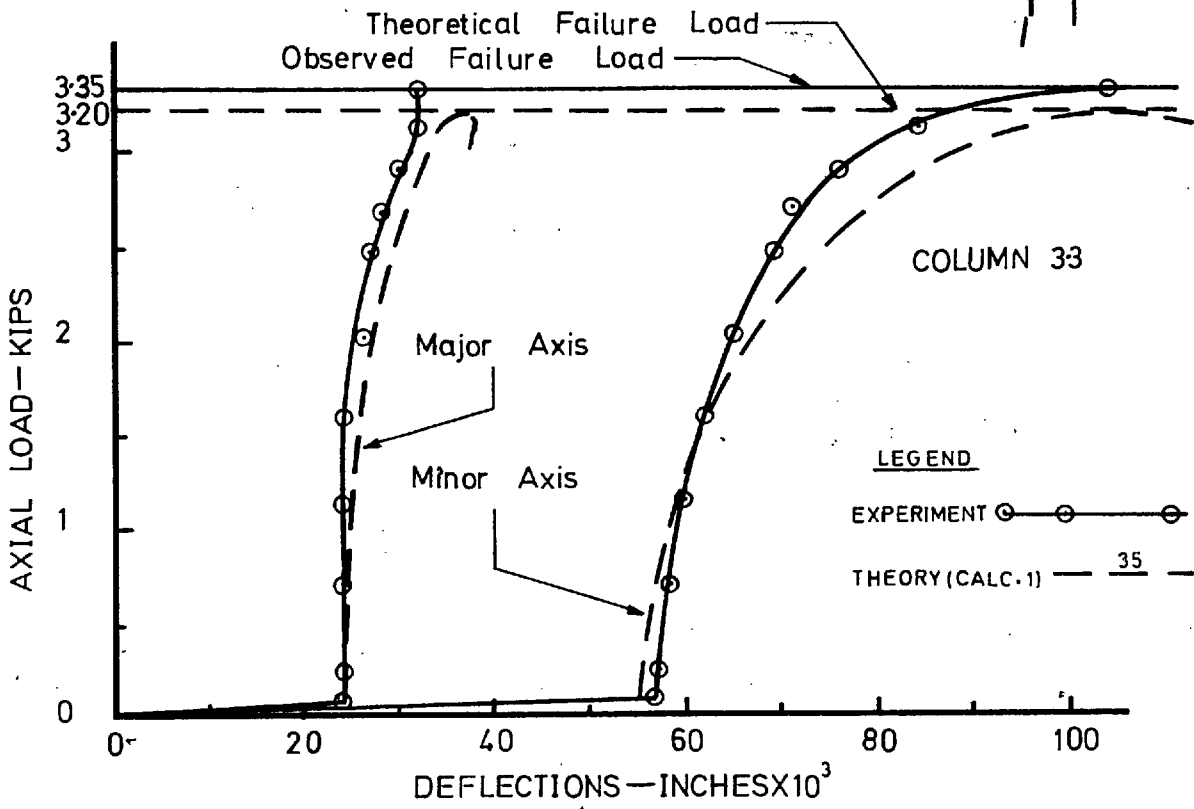


FIG. A.14

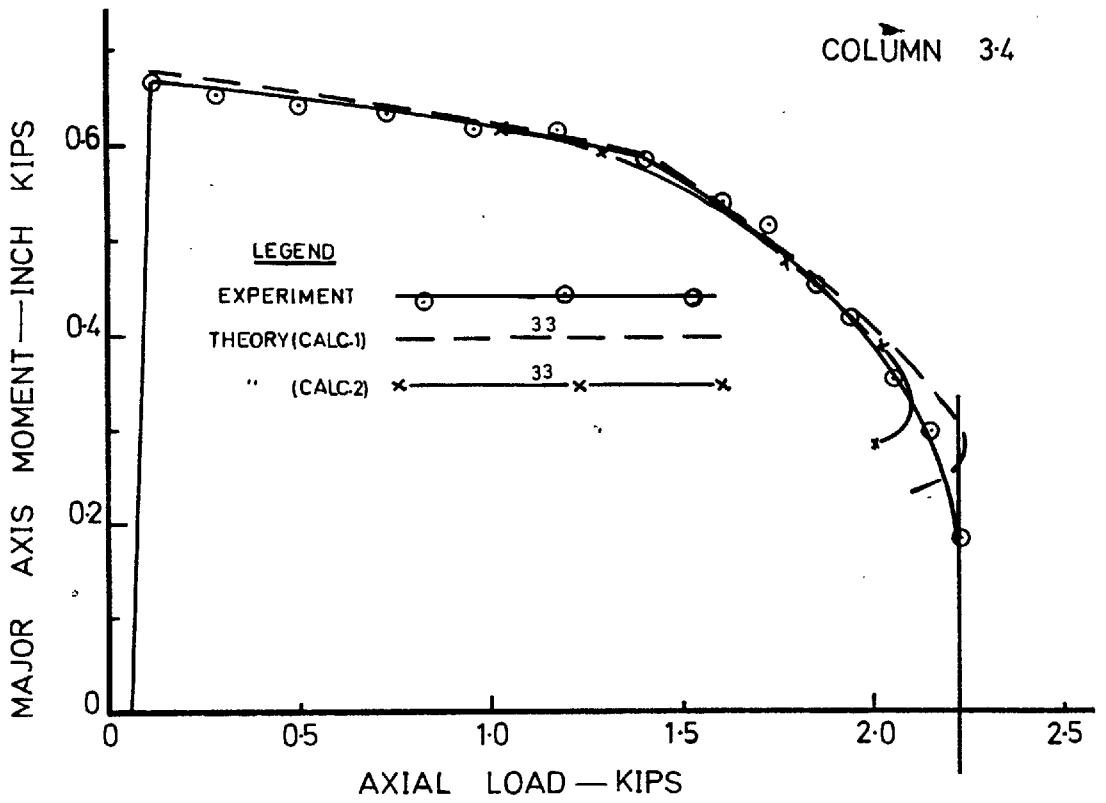


FIG. A-15(a)

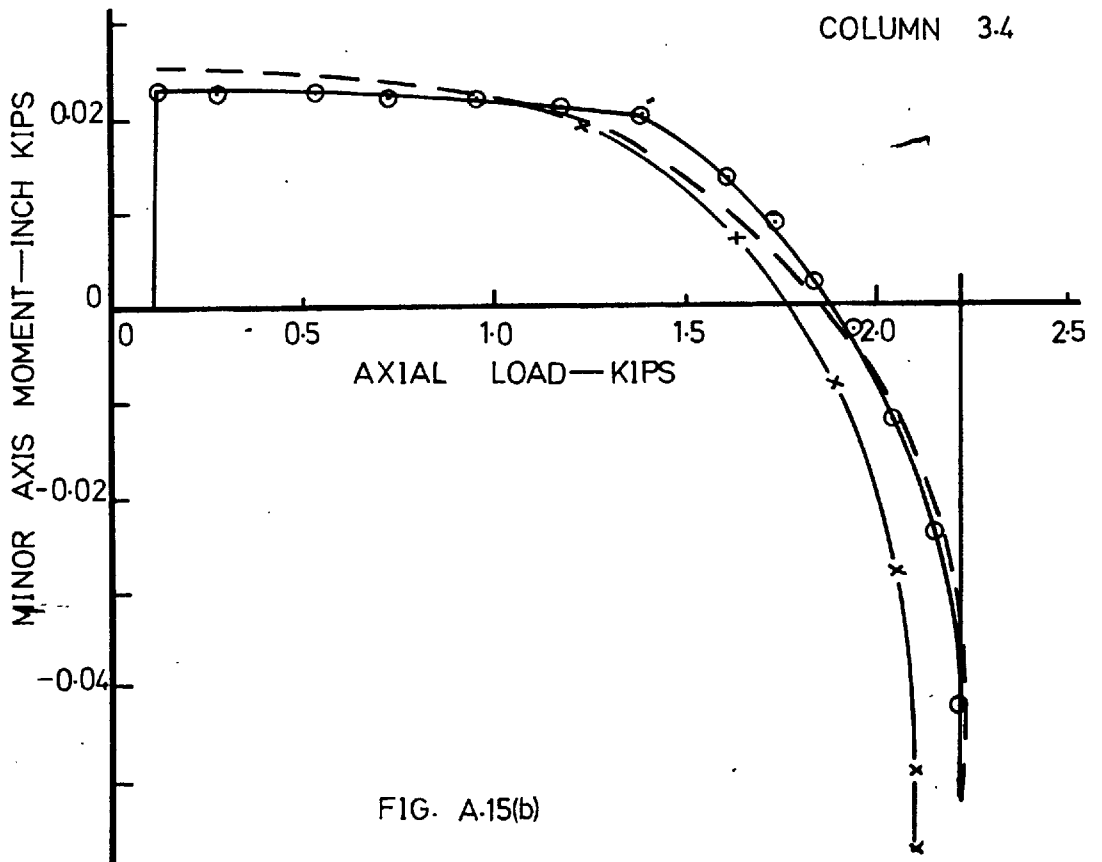


FIG. A-15(b)

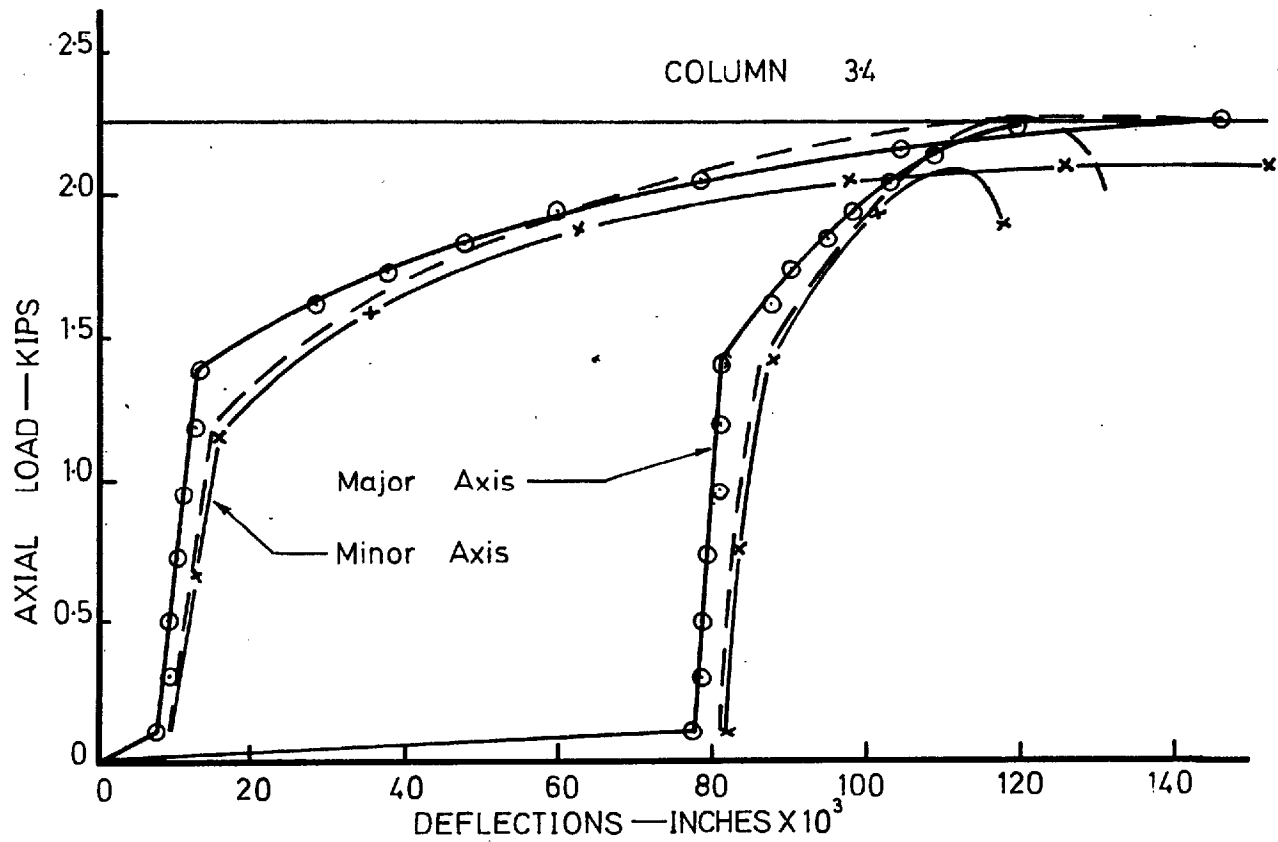


FIG. A.16(a)

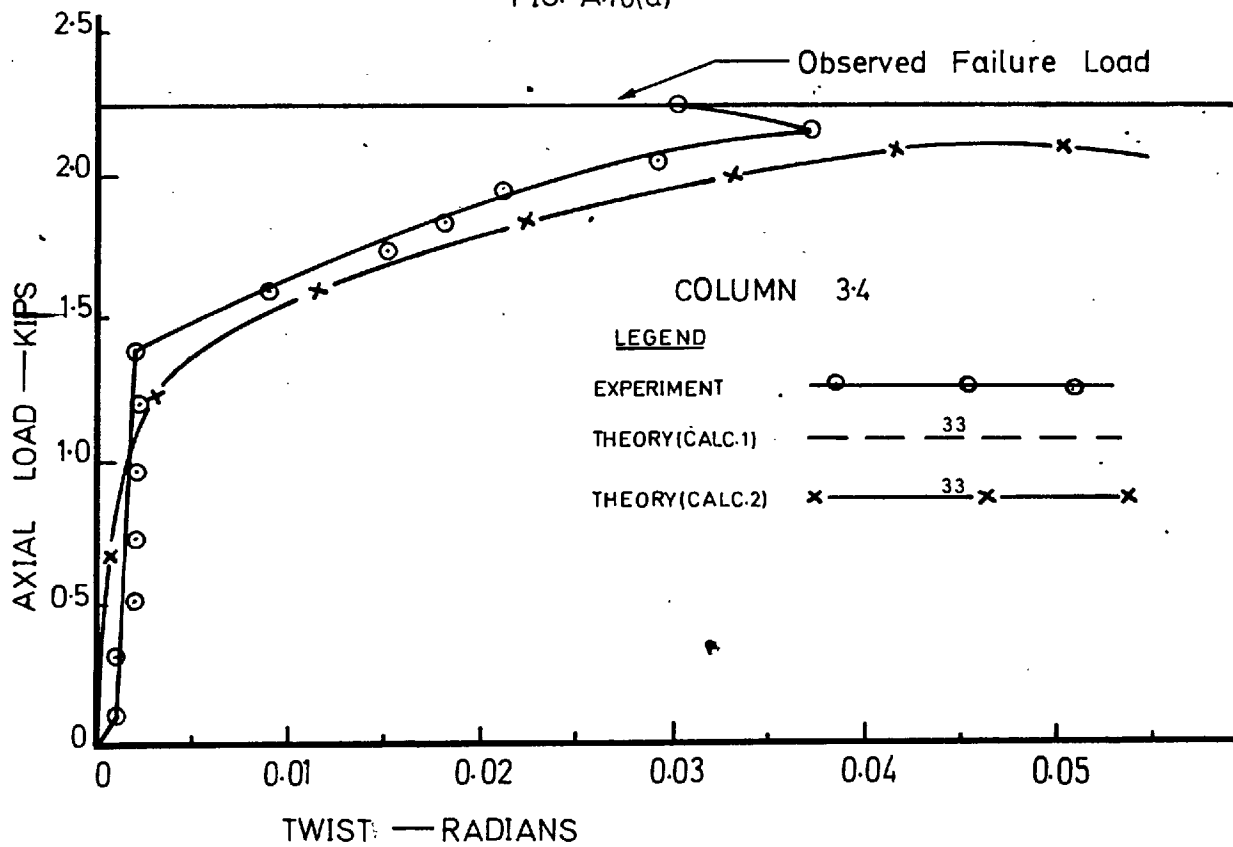


FIG. A.16(b)

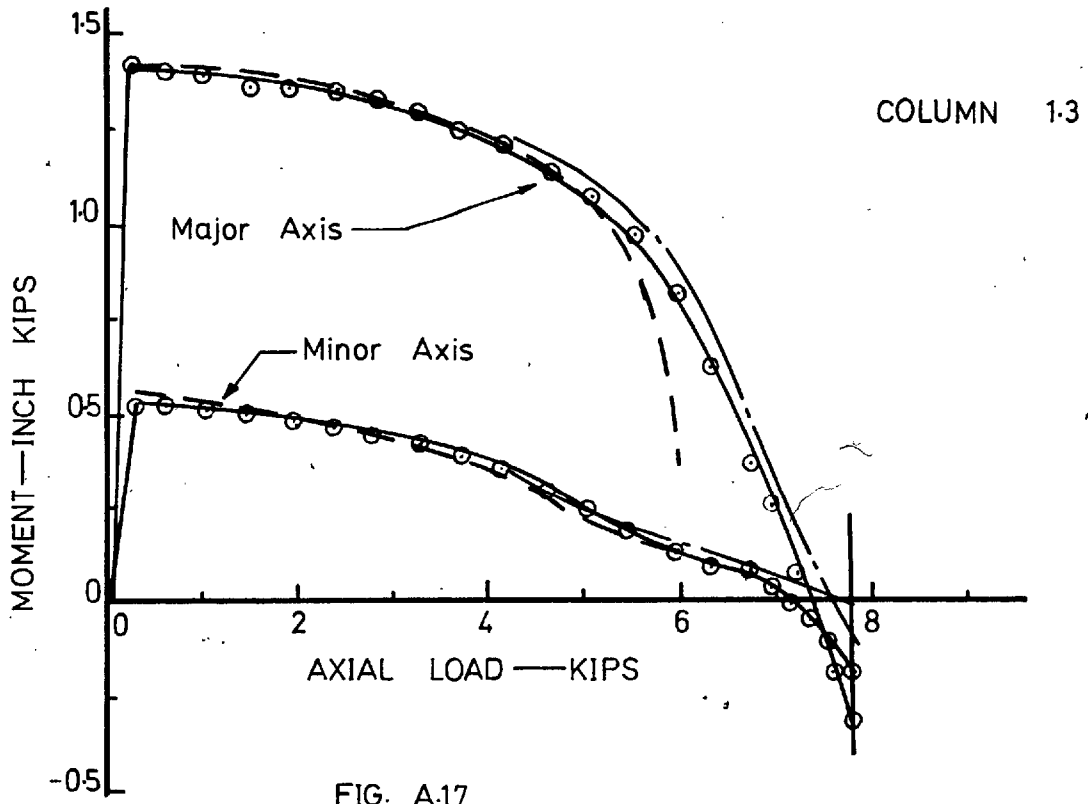


FIG. A.17

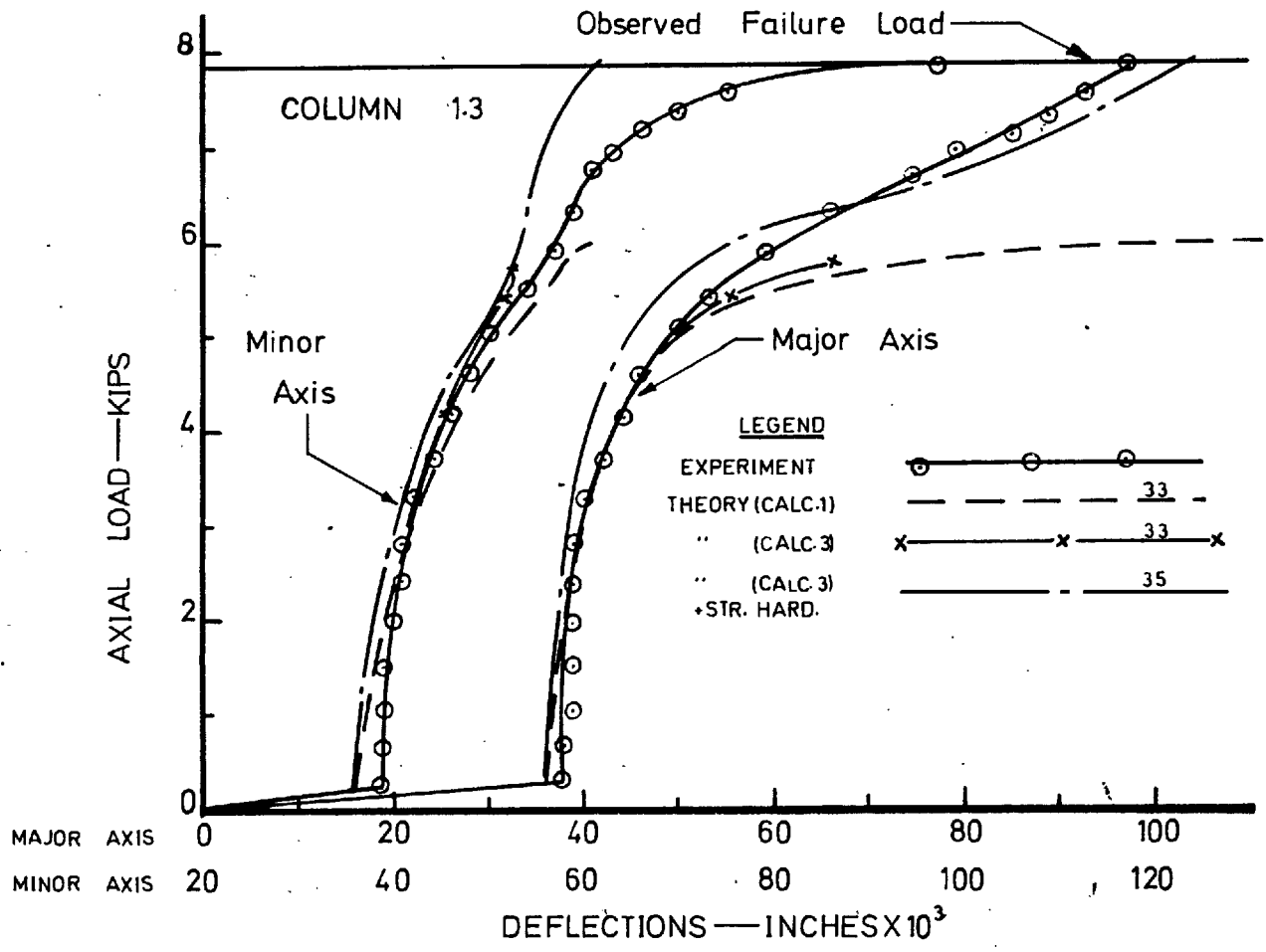


FIG. A.18

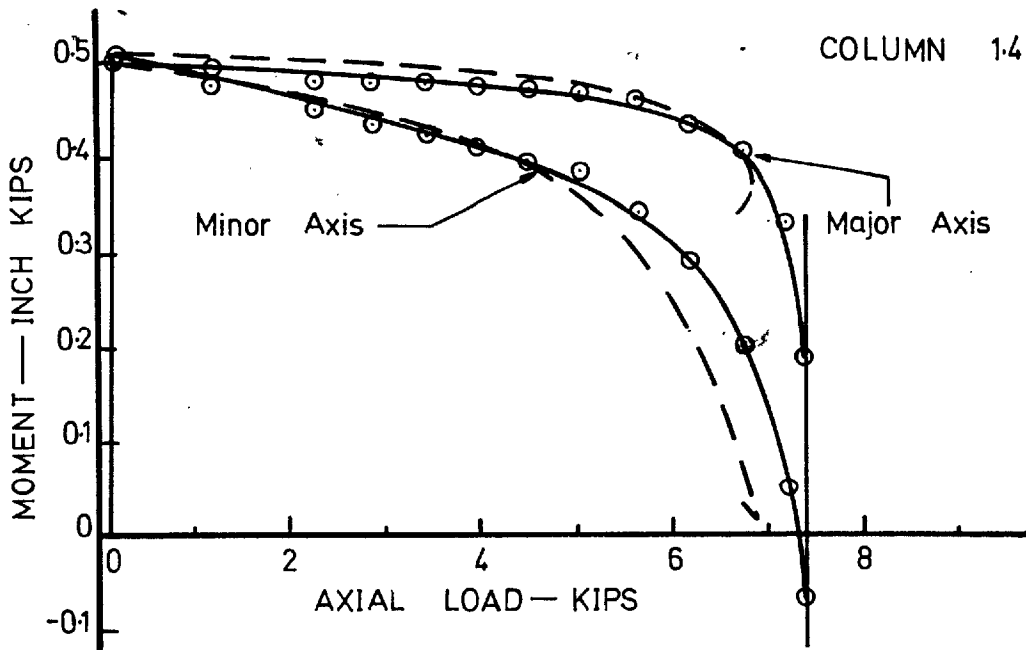


FIG. A.19

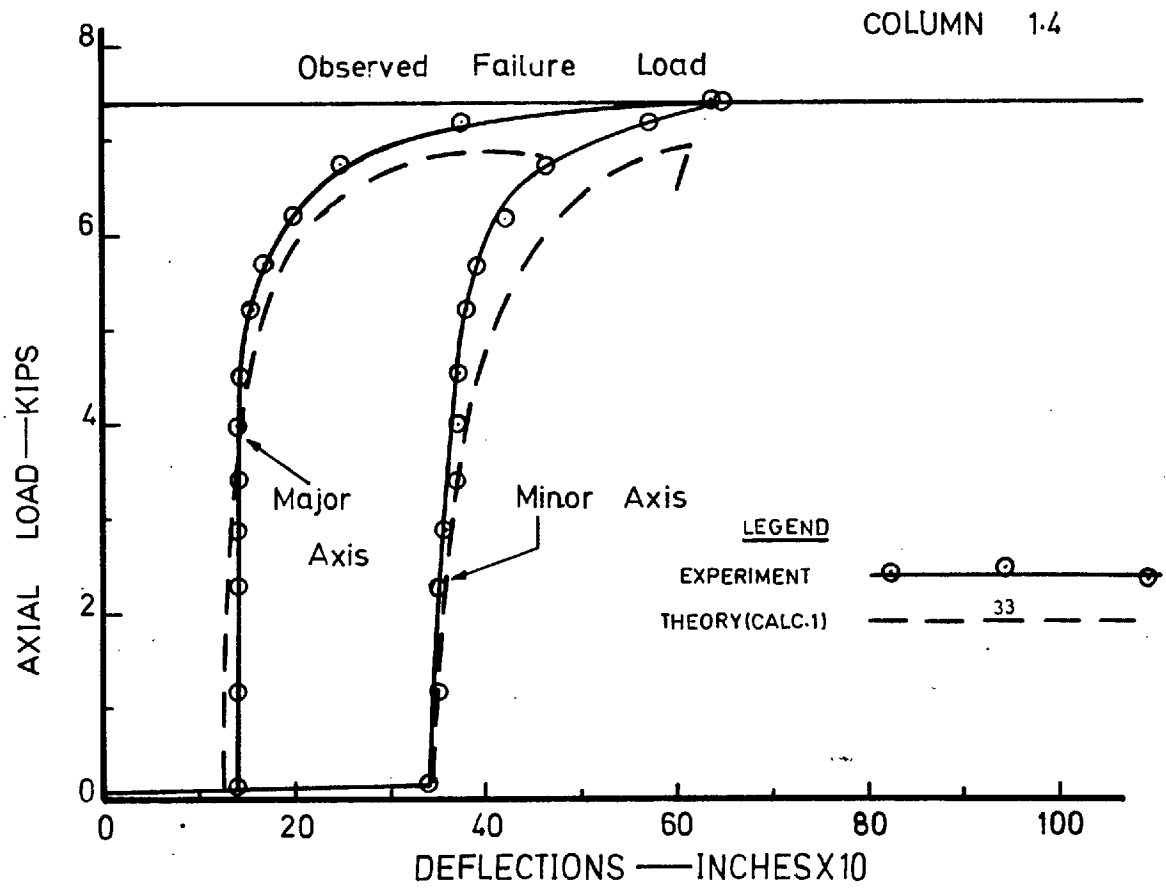


FIG. A.20